Table of Contents

Agenda

Monday, 09.10.2017(Day 1)(1st floor conference hall, Mongolia-Japan Center)	
	Responsible: N.Otsuka
10^{00}-16^{00}	Compilation

Tuesday, 10.10.2017 (Day 2)(1st floor conference hall, Mongolia-Japan Center)	
	Responsible: N.Otsuka
10^{00}-16^{00}	Compilation

Wednesday, 11.10.2017(Day 3)(1st floor conference hall, Mongolia-Japan Center)		
9^{00}-9^{30}	Registration	
9^{30}-9^{40}	Opening speech	Ts.Enkhbat
		Chairman: S.Davaa
9^{40}- 9^{55}	**Ts. Enkhbat (NRC)**: Research activities at Nuclear Research Center	
10^{00}-10^{25}	**Naohiko Otsuka (IAEA)**: Measurement of neutron capture thermal cross section and resonance integral of gallium-71 with an Am-Be neutron source	
10^{25}-10^{50}	**Sung-Chul Yang (KAERI)**: EXFOR Compilation and Nuclear Data Measurement at KAERI/NDC	
10^{50}-11^{15}	**Vidya Devi (IET-Bhaddal)**: Recent EXFOR compilation status in India and estimation of uncertainty propagation in efficiency	
11^{15}-11^{30}	Coffee break	

11^{35}-12^{00}	**Yongli Jin (CIAE)**: "NDPlot: A Plotting Software for Nuclear Data"
12^{00}-12^{25}	**Jimin Wang (CIAE)**: Recent EXFOR compilation in CNDC
12^{25}-12^{50}	**Xi Tao (CIAE)**: The evaluations of gamma induced Cr-52
13^{00}-15^{00}	Lunch

Chairman: Jimin Wang

15^{00}-15^{20}	**T.K. Zholdybayev (INP)**: Interaction of ^{3}He and ^{4}He ions of energy 29 and 50 MeV with ^{27}Al and ^{59}Co
15^{20}-15^{40}	**M. Odsuren (NUM)**: Virtual State of the Two-Body System
16^{00}-17^{00}	Mongolian national spectacle
17^{30}	Welcome Dinner

Thursday, 12.10.2017 (Day 4)(1st floor conference hall, Mongolia-Japan Center)

Chairman:M. Kimura

10^{00}- 10^{25}	**D. Ichinkhorloo (Hokkaido U.)**: Analysis of the ^{16}O(n,pn)^{15}O reaction using the CDCC method
10^{25}-10^{50}	**M. Aikawa (Hokkaido U.)**: Activation cross sections of deuteron-induced reactions on natural palladium for ^{103}Ag production
10^{50}-11^{10}	**Ch. Saikhanbayar (NRC)**: Some Possibilities of Radioisotope Production in Low Energy Accelerators and Small Sized Reactors
11^{10}-11^{25}	Coffee break

Chairman: Sung-Chul Yang

11^{25}-11^{50}	**M. Kimura**: The recent activities of JCPRG
11^{50}-12^{15}	**A.D. Duisenbay (KazNU)**: Dynamics of two-cluster systems and structure of light nuclei
12^{15}-12^{35}	**Ts. Zolbadral (NRC)**: Analysis of (n,α) reaction total cross-sections at 14.8 MeV using the exciton model
13^{00}-15^{00}	Lunch

Chairman: M.Aikawa

15^{00}-15^{20}	**B. Batchimeg (NRC)**: Alpha-particle Formation Probability in the (n,α) Reaction Induced by Fast Neutrons
15^{20}-15^{35}	**B. Regzedmaa (NUM)**: Systematical Analysis of the Photonuclear Reaction Data

15^{35}-15^{50}	**D. Dolzodmaa (NUM)**: Resonance states in the simple schematic model

<div align="right">Chairman: S.Davaa</div>

15^{50}-16^{20}	Concluding Remark
16^{20}-17^{00}	**N. Otsuka (IAEA)**: Lecture
17^{30}	Dinner

Friday, 13.10.2017 (Day 5)(main building of NUM)

<div align="right">Moderator: S.Davaa</div>

10^{00}-12^{00}	Closing session: round table discussion (13th Century Complex)
13^{00}-17^{00}	Sightseeing (Tsonjin Boldog)
18^{00}	Dinner

^{71}Ga(n$_{th}$,γ)^{72}Ga Cross Section Measurement Using Am-Be Source

Priyada Panikkath[1], P. Mohanakrishnan[1], Naohiko Otuka[2]

[1]*Manipal Centre for Natural Sciences, Manipal Academy of Higher Education, Manipal,Karnataka-576104, India*
[2]*Nuclear Data Section, International Atomic Energy Agency, A-1400 Wien, Austria*

The thermal neutron cross section is an important constant in the low-energy neutron induced reaction data field. Energy dependent experimental and theoretical neutron-induced reaction cross section are often normalized to the thermal neutron cross section. A few thermal neutron cross sections such as ^{235}U(n$_{th}$,f) cross section are extremely important, and they are included in the IAEA Neutron Cross-Section Standards [1]. Mughabghab's comprehensive compilation of thermal neutron cross sections [2] is also widely known.

We have reported the neutron capture thermal cross sections and resonance integrals of ^{138}Ba, ^{141}Pr, ^{139}La and ^{140}Ce measured with an Am-Be neutron source (4×10^7 neutrons/sec) installed in the Neutron Physics Laboratory of Manipal Centre for Natural Science, Manipal University [3-4]. The neutron source is kept inside a concrete bunker which moderates fast neutrons from the Am-Be neutron source.

In the literature, the epithermal neutron spectrum is often assumed to be proportional to 1/E in determination of the resonance integral measured in neutron fields characterized by broad neutron spectra. However Moens et al. [5] established a method to correct the resonance integral for deviation of the ideal spectrum from more realistic 1/E$^{1+\alpha}$spectrum (α≠0), and we have adopted the formalism as done by the Turkey group [6]. The neutron spectrum of our irradiation field was estimated by the multiple foil activation and unfolding by SAND-II with a prior neutron spectrum calculated by MCNP. It concluded that the epithermal neutron spectrum of our neutron irradiation field is characterized by 1/E$^{1+\alpha}$ with α=-0.148±0.007 [1].

The thermal cross section of ^{71}Ga(n,γ)^{72}Ga have been already studied by the Turkey group and various other experimental works. Majority of them were measured under neutron fields having broad neutron spectra (e.g., reactor neutrons). On the other hand Koester et al. [5] measured the cross section by using neutrons filtered by a Christiansen filter (mean neutron energy 0.56±0.01 meV), and obtained the thermal neutron cross section extrapolated from the directly measured cross section, which is about 20% lower than the majority of the measured thermal cross sections. Among evaluated data libraries, the ENDF/B-VII.1 library [6] adopts the thermal cross sections recommended based on those obtained with broad neutron spectra while the

JENDL-4.0 library [7] adopts Koester's thermal cross section. Under this situation, we decided to measure the thermal cross section by using our facility.

The experimental technique and data reduction formalism of our present study are basically same as our previous works [1,2]. In our works, we always use dual monitor foils for two monitor reactions ^{55}Mn(n,γ)^{56}Mn and ^{197}Au(n,γ)^{198}Au. This is helpful to exclude bias in neutron flux determination. Two thermal cross sections or resonance integrals of our interest by using the two neutron flux values determined with the two monitor reaction rates, and their weighted mean can be adopted as our final value. Some parameters adopted in our cross section and resonance integral derivation (e.g., the number of γ-ray emitted from ^{72}Ga) are fully correlated between two values in our present work, and therefore we have to use the off-diagonal weighted mean instead of the conventional weighted mean [7] to avoid underestimation of the uncertainty in the weighted mean value [8]. In order to obtain the reasonable mean weighted value for our thermal cross section and resonance integral, we are performing a detailed covariance analysis of our measurement result.

References

[1]. A.D. Carlson et al., Nucl. Data Sheets **110** (2009) 3215.
[2]. S.F. Mughabghab, "Atlas of neutron resonance - Resonance parameters and thermal cross sections Z=1-100", Elsevier, 2006.
[3]. PriyadaPanikkath and P. Mohanakrishnan, Eur. Phys. J. A **52** (2016) 276.
[4]. PriyadaPanikkath and P. Mohanakrishnan, Eur. Phys. J. A **53** (2017) 46.
[5]. L. Moens et al., J. Radioanal. Chem. **52** (1979) 379.
[6]. M. Karadag et al., Nucl. Instrum. Meth. A **501** (2003) 524.
[7]. M.B. Chadwick et al., Nucl. Data Sheets **112** (2011) 2887.
[8]. K. Shibata et al., J. Nucl. Sci. Technol. **48** (2011) 1.
[9]. W, Mannhart, INDC(NDS)-0558 Rev., International Atomic Energy Agency, 2013.
[10]. N. Otuka and D.L. Smith, Nucl. Data Sheets **120** (2014) 281.

Activity of Hokkaido University Nuclear Reaction Data Centre (JCPRG)

M. Kimura, S. Ebata, D. Ichinkhorloo, A. Sarsembaeva, N. Ukon and S. Jagjit

[1]*Faculty of Science, Hokkaido University, Sapporo 060-0810, Japan*

Nuclear reaction data are necessary and are used for many application fields, which are available through the EXFOR database maintained by the International Network of Nuclear Reaction Data Centres (NRDC). As a member of the NRDC, Nuclear Reaction Data Centre (JCPRG) compiles charged-particle induced reaction data and contributes about 10 percent of the EXFOR database. In this paper, we report our recent nuclear data activity and research topics, including Asian collaboration.

1. Introduction

Nuclear data are available for several fields, not only nuclear physics and astrophysics but also application fields, such as nuclear engineering and medicine. The importance of the nuclear database is increasing while the recent demand is expanding in the kind of reaction and in the energy. Especially the demands in Asian region can be expected and the international cooperation among Asian countries will become more important. Our group (Nuclear Reaction Data Centre: JCPRG) plays the nuclear data activity as a member of them.

There is an international nuclear database consisting of scientific experimental nuclear reaction data, which is the EXFOR database maintained by the International Network of Nuclear Reaction Data Centres (NRDC) under the auspices of the International Atomic Energy Agency (IAEA) [1]. In these years, Asian centers in NRDC and others have organize a workshop. The workshop is called AASPP and has been held 7 times this year in which the worth information on compilation and related activities in each institute is sharing. In this paper, we report the recent activities in the Hokkaido University JCPRG.

2. JCPRG activity

The member of JCPRG is composed of two staffs and four postdoctoral researchers. Our nuclear data activity has mainly four contents as follows:

1. *Compilation,*
2. *Application,*
3. *Experiment,*
4. *Evaluation.*

2.1. *Compilation*

JCPRG compiles charged-particle induced nuclear reaction data obtained in Japanese institutes. The nuclear data which should be compiled are published in papers surveyed in peer-reviewed journals. JCPRG individually performs an article-survey also in addition to the NRDC survey. We assign entry numbers with E, J, and K which are charged-particle, meson, and photon induced reactions, respectively. We also maintain entries with R, which was compiled by a former member of the NRDC and RIKEN. JCPRG contributes about 10 percent of the EXFOR database.

This year, we transmitted 94 new and 13 revised/deleted entries as 12 trans-files (E095-E103, K015,016, R028) to the open area of Nuclear Data Section in IAEA.

2.2. *Application*

JCPRG activity on nuclear data study is not only the compilation. We study the application and leverage of the nuclear data. In these years, we study the nuclear transmutation to dispose of radiative material, such as nuclear waste. The nuclear data related to the material is essential for the transmutation technology. However it has restrictions to measure the data, indeed they are very little in the EXFOR database. We suggest the way to obtain the data (thick-target yield and interaction cross section) of radiative material using inverse kinematics [2].

We have started development of a new editor for the compilation specialized for EXFOR outputs. The developing editor called ForEX (**For EX**FOR) is represented in Java programing language for the operation-system independent software. The current status of the editor is reported by Sarsembaeva.

2.3. *Experiment*

The members of JCPRG perform the experiments to measure the production cross section of radio isotopes for RI medicine. One of the experiments was devoted to obtain the excitation function of the $^{nat}Pd(\alpha,x)^{103}Ag$ reaction for the production of a medical RI ^{103}Ag, which is performed by Ukon. The excitation function of production cross section 169Yb was measured through the $^{169}Tm(d,2n)^{169}Yb$ reaction by master course student [3].

2.4. *Evaluation*

We perform theoretical calculations to evaluate the experimental reaction data based on the nuclear physics. The theoretical evaluation can provide us very useful information for the reactions and structures which have not been obtained in experiments.

In our evaluation activities, two kinds of the calculation are mainly performed. For reaction model, the continuum discretized coupled channel (CDCC) is employed to investigate elastic and inelastic scattering cross sections for ^{6,7}Li. The ground state properties in the nuclear chart are investigated using the systematic calculations by the mean field model. These studies are performed by Ichinkhorloo and Ebata, respectively.

3. Asian collaboration

As one of the purposes, JCPRG promotes nuclear data activity among Asian countries. The activity was supported by the 'R&D' Platform Formation of Nuclear Reaction Data in Asian Countries (2010-2013), the Asia-Africa Science Platform Program (AASPP), the Japan Society for the Promotion of Science from April 2010 to March 2013. In this respect, AASPP workshops were annually held in Japan, China, and Korea, from 2010 to 2012. At the end of the support, we continued the workshops in Kazakhstan, India, Japan and China, from 2013 to 2016. The plan for the next workshop, in 2017, is that it will be held in Mongolia.

One of the topics in the workshop is sharing information of compilation among Asian institutes and countries. In the NRDC, there are five Asian institutes; China Nuclear Data Centre (CNDC), China, Bhabha Atomic Research Centre (BARC), India, Hokkaido University Nuclear Reaction Data Centre (JCPRG) and JAEA Nuclear Data Center, Japan, and Korea Nuclear Data Center (KNDC), Korea. The four centres are in charge of compilation of domestic nuclear reaction data, and maintain the database with helps among Asian countries.

4. Summary

Compilation of nuclear reaction data is necessary for not only academic fields but also application fields. JCPRG contributes the compilation as a member of the NRDC. Related to such compilation activity, we conduct and promote research on nuclear data under international and Asian collaboration.

[1]. N. Otuka, et al., Nucl. Data Sheets 120, (2014), 272.
[2]. M. Aikawa, S. Ebata and S. Imai, Nucl. Instr. Meth. B **383**, (2016), 156; Nucl. Instr. Meth. B **353**, (2015), 1.
[3]. M. Saito, et al, submitted to Appl. Radiat. Isot.

Activation Cross Sections of Deuteron-Induced Reactions on Natural Palladium for 103Ag Production

N. Ukon[1,*], M. Aikawa[1], Y. Komori[2], H. Haba[2]

[1]*Faculty of Science, Hokkaido University Sapporo 060-0810, Japan*
[2]*Nishina Center for Accelerator-Based Science, RIKEN, Wako 351-0198, Japan*

Cross sections to produce medical radioactive isotopes (RI) are one of the important nuclear data for therapy and diagnostics in nuclear medicine. The data are fundamental information for production of the required RI with less by-products. Palladium-103 ($T_{1/2}$ = 16.991 d) is a medical RI available for brachytherapy [1]. One possible way to obtain ^{103}Pd with less by-products is a generation of ^{103}Pd from its parent, ^{103}Ag ($T_{1/2}$ = 65.7 min). Therefore, the production cross sections of ^{103}Ag are worthy investigated. Among a variety of reactions to produce ^{103}Ag, the deuteron-induced reaction on ^{nat}Pd was found in the EXFOR database [2]. However, the energy region of the previous studies [3-5] is up to 20.3 MeV and the data in the higher energy region is required. In this paper, we report a preliminary result of an experiment to obtain the excitation function of the ^{nat}Pd(d,x)^{103}Ag reaction up to 24 MeV.

The experiment was performed at the RIKEN AVF cyclotron by using the stacked foil technique and the activation method. The target consisting of ^{nat}Pd foils (9.80 mg/cm^2 thickness, 99.95% purity, Nilaco Corp., Japan), ^{nat}Ti monitor foils (2.25 mg/cm^2, 99.6%, Nilaco Corp., Japan) and ^{nat}Zn foils (17.95 mg/cm^2, >99.9%, Nilaco Corp., Japan) was irradiated by a 23.95 MeV deuteron beam for 20 min. The incident energy is measured by the TOF method [6]. The energy degraded in the foils were estimated by the polynomial approximation of the stopping power data [7]. The average beam intensity of 174 nA was measured by a Faraday cup. The γ-rays from the irradiated foils were measured by HPGe detectors. Nuclear data such as half-lives of RI, energy and ratios of emitted gammas were derived from the NuDat2 database [8].

---

[*]Present address: Advanced Clinical Research Center, Fukushima Global Medical Science Center, Fukushima Medical University, Fukushima 960-1295, Japan

Table 1: Nuclear data of reaction products

Reaction product	$T_{1/2}$	Decay mode (%)	E_γ (keV)	I_γ (%)	Contributing reactions	Q-value (MeV)
^{48}V	15.9735d	ε (100)	983.53	99.98		
^{103}Ag	65.7 min	ε (100)	118.7	31.2	^{102}Pd(d,n)	1.9
			148.2	28.3	^{104}Pd(d,3n)	-15.7
			266.9	13.3		

The cross sections of the ^{nat}Ti(d,x)^{48}V monitor reaction were measured by using the 983.53 keV (99.98%) γ-lines from the decay of ^{48}V($T_{1/2}$ = 15.9735 d). The measurements were performed after long cooling times (~50 d) to neglect the contribution from the ^{48}Sc decay ($T_{1/2}$ = 43.67 h). The beam intensity was normalized to fit the derived excitation function to the recommended values [9] (Fig. 1).

The 118.74 keV γ-rays (31.2%) from the decay of ^{103}Ag in the irradiated Pd foils were measured to derive the excitation function of the ^{nat}Pd(d,x)^{103}Ag reaction. Its preliminary result is shown in Fig. 2 with the data of the previous study [3] and the theoretical calculation TENDL2015 [10]. The result is in good agreement with the previous data [3] up to 20.3 MeV. However, the theoretical calculation overestimates the ^{104}Pd(d,3n)^{103}Ag reaction above 17 MeV.
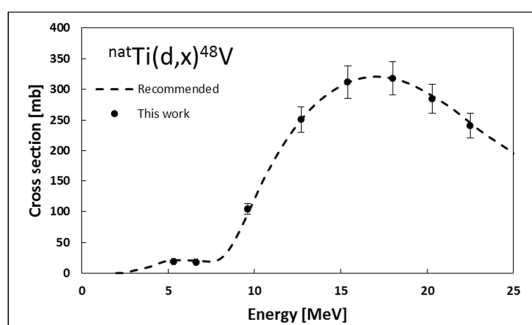
Fig. 1. The excitation function of the ^{nat}Ti(d,x)^{48}V monitor reaction.
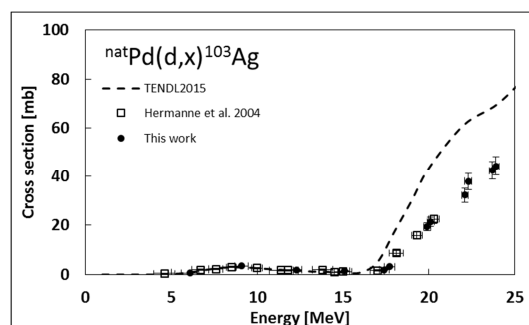
Fig. 2. The excitation function of the ^{nat}Pd(d,x)^{103}Ag reaction

In summary, we have measured the excitation function of the $^{nat}Pd(d,x)^{103}Ag$ reaction. The preliminary result shows a good agreement with the earlier study [2] and new points at a higher energy region up to 24 MeV. The data is being analyzed in detail and will be submitted in a scientific journal soon.

Acknowledgements

References

[1]. S. Nag, D. Beyer, J. Friedland, P. Grimm, R. Nath, American Brachytherapy Society (ABS) recommendations for transperineal permanent brachytherapy of prostate cancer, Int. J. Radiat. Oncol. Biol. Phys. 44 (1999) 789.

[2]. N. Otuka, E. Dupont, V. Semkova, B. Pritychenko, A.I. Blokhin, M. Aikawa, S. Babykina, M. Bossant, G. Chen, S. Dunaeva, R.A. Forrest, T. Fukahori, N. Furutachi, S. Ganesan, Z. Ge, O.O. Gritzay, M. Herman, S. Hlavac, K. Kato, B. Lalremruata, Y.O. Lee, A. Makinaga, K. Matsumoto, M. Mikhaylyukova, G. Pikulina, V.G. Pronyaev, A. Saxena, O. Schwerer, S.P. Simakov, N. Soppera, R. Suzuki, S. Takács, X. Tao, S. Taova, F. Tárkányi, V.V. Varlamov, J. Wang, S.C. Yang, V. Zerkin, Y. Zhuang, Towards a more complete and accurate experimental nuclear reaction data library (EXFOR): international collaboration between nuclear reaction data centres (NRDC), Nucl. Data Sheets 120 (2014) 272.

[3]. A. Hermanne, S. Takács, F. Tárkányi, R. Bolbos, Cross section measurements of proton and deuteron induced formation of ^{103}Ag in natural palladium Radiochim. Acta 92 (2004) 215.

[4]. F. Ditrói, F. Tárkányi, S. Takács, A. Hermanne, A.V. Ignatyuk, M. Baba, Activation cross-sections of deuteron induced reactions on natural palladium, Nucl. Instrum. Meth. B 270 (2012) 61.

[5]. F. Ditrói, F. Tárkányi, S. Takács, A. Hermanne, A.V. Ignatyuk, Measurement of activation cross-section of long-lived products in deuteron induced nuclear reactions on palladium in the 30-50 MeV energy range, Applied Radiation and Isotopes 128(2017)297.

[6]. T. Watanabe, M. Fujimaki, N.Fukunishi, H. Imao,O. Kamigaito, M.Kase, M. Komiyama, N. Sakamoto, K. Suda, M. Wakasugi, K. Yamada, Beam energy and longitudinal beam profile measurement system at RIBF, Proceedings 5th

International Part. Accel. Conference (IPAC2014), (2014) 3566.

[7]. SRIM: the Stopping and Range of Ions in Matter, available online ⟨http://www.srim.org⟩.

[8]. NuDat 2.7β, National Nuclear Data Center database, available online ⟨http://www.nndc.bnl.gov/nudat2/⟩.

[9]. F. Tárkányi, S.Takács, K. Gul, A.Hermanne, M.G. Mustafa, M. Nortier, P. Oblozinsky, S.M. Qaim, B. Scholten, Y.N. Shubin, Z.Youxiang, Charged particle cross section database for medical radioisotope production: diagnostic radioisotopes and monitor reactions, IAEA-TECDOC 1211. Updated web-version at ⟨http://www-nds. iaea.org/medical/⟩.

[10]. TENDL-2015: TALYS-based evaluated nuclear data library, available online ⟨https://tendl.web.psi.ch/tendl_2015/tendl2015.html⟩.

Virtual State in the Complex Scaling Method

M. Odsuren[1], Y.Kikuchi[2], T. Myo[3,4], G. Khuukhenkhuu[1], H. Masui[5], K. Katō[6]

[1]*School of Engineering and Applied Sciences and Nuclear Research Center, National University of Mongolia, Ulaanbaatar 210646, Mongolia*
[2]*Department of Physics, Osaka City University, Osaka 558-8585, Japan*
[3]*General Education, Faculty of Engineering, Osaka Institute of Technology, Osaka 535-8585, Japan*
[4]*Research Center for Nuclear Physics (RCNP), Osaka University, Ibaraki 567-0047, Japan*
[5]*Information Processing Center, Kitami Institute of Technology, Kitami 090-8507, Japan*
[6]*Nuclear Reaction Data Centre, Faculty of Science, Hokkaido University, Sapporo 060-0810, Japan*

The sharp peak observed just above the ^{8}Be+n threshold in the photodisintegration cross section of ^{9}Be is interpreted due to a virtual state but not resonant state through the calculations of $\alpha+\alpha+n$ three-body model. To obtain a deeper understanding of the virtual-state characterization, we calculate the phase shifts and the photodisintegration cross section using a simple schematic two-body model and the complex scaling method.

1. Introduction

The first 1/2$^+$ unbound state of ^{9}Be is calculated applying the complex scaling method (CSM) [1, 2] to the $\alpha+\alpha+n$ three-cluster model [3]. The results indicate that there is no sharp resonant state corresponding to the distinguished sharp peak observed just above the ^{8}Be+n threshold in the photodisintegration cross section of ^{9}Be. However, the recent experimental cross section data [4, 5] can be well explained by using the $\alpha+\alpha+n$ calculation. In our previous work, we concluded that the first excited 1/2$^+$state in ^{9}Be is a ^{8}Be+n virtual state but not a resonant one [3].

Recently, we discussed the virtual state in detail, calculating the photodisintegration cross section corresponding to the existence of a virtual state applying the CSM to the two-body model [6]. We show that when a virtual state approaches the zero energy near the physical scattering region, it has a strong influence on the scattering observables (the phase shift, the scattering length). Those quantities are calculated by using the continuum level density obtained in the CSM. We investigate the behavior

of scattering observables in relation to the existence of the virtual state located near the threshold by adjusting different potential strengths.

2. Complex scaled two-body model

To understand the photodisintegration of ^{9}Be, we investigate the simple two-body model corresponding to the ^{8}Be+n structure in ^{9}Be. In this model, both clusters are assumed to have
no-spin and the relative motion between clusters is described by the following Schrödinger
equation:

$$H\psi_{J^\pi}^\nu = E_\nu \psi_{J^\pi}^\nu, \tag{1}$$

where J^π is spin and parity, and ν is the state index. The Hamiltonian is given as

$$H = -\frac{\hbar^2}{2\mu}\nabla^2 + V(r), \tag{2}$$

where we assume a simple Gaussian potential

$$V(r) = V_1 \exp(-ar^2). \tag{3}$$

For simplicity, we put $\frac{\hbar^2}{2\mu} = 1$ (MeV fm^2) and $a = 0.16$ fm^{-2}. The potential depth V_1 is taken to reproduce one bound state of the s-and p-waves. The first s-wave bound state is treated as the Pauli-forbidden state considering the ^{9}Be structure, and then the bound p-wave solution is the ground state corresponding to the 3/2$^-$ state of ^{9}Be which is shown in Fig.1. We calculate the electric dipole ($E1$) transition from the ground state to the excited unbound states. Here, we briefly explain CSM applied to the wave function with the basis expansion method. In the CSM, the relative coordinate r is transformed as

$$U(\theta): \qquad r \rightarrow re^{i\theta}, \tag{4}$$

where $U(\theta)$ is a complex scaling operator depending on a scaling parameter θ. The complex-scaled Hamiltonian H^θ and wave function $\psi_{J^\pi}^\nu(\theta)$ are defined as $U(\theta)HU^{-1}(\theta)$ and $U(\theta)\psi_{J^\pi}^\nu$, respectively, and see Ref. [2] for details. Applying this transformation to Eq. (1), we obtain the complex-scaled Schrödinger equation:

$$H^\theta \psi_{J^\pi}^\nu(\theta) = E_\nu^\theta \psi_{J^\pi}^\nu(\theta). \tag{5}$$

Applying the L^2 basis function method, the wave function is expanded as

$$\psi_{J^\pi}^v(\theta) = \sum_{n=1}^N c_n^{J^\pi v}(\theta)\phi_n(r),\tag{6}$$

where $\{\phi_n(r)\}$ is an appropriate basis function set. The expansion coefficients $c_n^{J^\pi v}(\theta)$ and the complex energy eigenvalues E_v^θ are obtained by solving the complex-scaled eigenvalue problem.

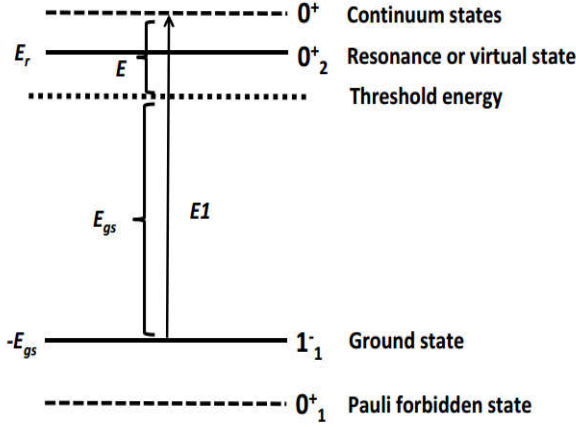

Fig. 1. The energy level diagram of the two-body potential model simulating ^{9}Be. The dotted line represents the threshold energy.

The scattering phase shifts $\delta^{J^\pi}(E)$ for the Hamiltonian Eq. (2) can be easily calculated
using the solutions of the complex-scaled Schrödinger Eq. (5) with and without the interaction, which evaluate the continuum level density [3]. From Eq. (11) in Ref. [3], we have

$$\delta^{J^\pi}(E) = N_b\pi + \sum_{r=1}^{N_r^\theta}\left\{-\cot^{-1}\left(\frac{E-E_r^{res}}{\Gamma_r/2}\right)\right\} + \sum_{r=c}^{N_c^\theta}\left\{-\cot^{-1}\left(\frac{E-\epsilon_c^r}{\epsilon_c^i}\right)\right\}$$
$$- \sum_{k=1}^{N}\left\{-\cot^{-1}\left(\frac{E-\epsilon_c^{0r}}{\epsilon_c^{0i}}\right)\right\},\tag{7}$$

where the eigenvalues E_v^θ are classified into the bound states with the number of N_b, resonant states with N_r^θ and N_c^θ complex-scaled continuum states for a given θ where $N = N_b + N_r^\theta + N_c^\theta$. The number N of the eigenvalues of the free Hamiltonian given by the only kinetic energy operator are expressed as $\epsilon_c^{0r} - i\epsilon_c^{0i}(k = 1,\cdots,N)$.

The photodisintegration cross section due to the electric dipole transition from the ground state $J_{gs}^{\pi} = 1^-$ to the continuum $J_f^{\pi} = 0^+$ states is expressed as

$$\sigma_{E1}\left(E_{\gamma}\right) = \frac{16\pi^2}{9}\left(\frac{E_{\gamma}}{\hbar c}\right)\frac{dB\left(E1,E_{\gamma}\right)}{dE_{\gamma}}, \qquad (8)$$

where the transition strength is calculated by using the solutions of the CSM

$$\frac{dB\left(E1, E_{\gamma}\right)}{dE_{\gamma}} = -\frac{1}{\pi}\frac{1}{2J_{gs}+1}Im\left[\sum_{v=1}^{N}\langle\tilde{\psi}_{J_{gs}^{\pi}}^{gs}(\theta)\left|\widehat{O}^{\theta+}(E1)\right|\psi_{J_f^{\pi}}^{v}(\theta)\rangle\right.$$

$$\left. x\frac{1}{E - E_v^{\theta}}\langle\tilde{\psi}_{J_f^{\pi}}^{v}(\theta)\left|\widehat{O}^{\theta}(E1)\right|\psi_{J_{gs}^{\pi}}^{gs}(\theta)\rangle\right],$$

$$(9)$$

where J_{gs} and $\psi_{gs}(\theta)$ are the total spin and the wave function of the ground state, respectively, and $\widehat{O}(E1)$ is an electric dipole transition operator. The energy E is related to E_{γ} as $E = E_{\gamma} - E_{gs}$, where E_{gs} is the binding energy of the ground state measured from the threshold.

3. Results and Discussions

Using the calculated eigenvalues including the continuum states for V_1=-1.42 MeV, we calculate the photodisintegration cross section due to the $E1$ transition. The result is shown in Fig. 2. It is seen that the peak is obtained at a lower energy region with the similar shape as observed in the ^{9}Be($1/2^+$) state (shown in Fig. 1 of Ref. [3]).

To understand the virtual-state contribution to the cross section in the CSM calculation more clearly, we calculate the continuum level density of the $J^{\pi}=0^+$ state, using Eq. (10) of Ref. [6] with different potential strengths V_1=-1.42 MeV and -1.43 MeV, which correspond to virtual-state and bound-state cases, respectively. In Fig. 3, we show the calculated continuum level density. The results show a very similar behavior for V_1= -1.42 MeV and -1.43 MeV, and the difference seems very small except for a small energy region.

To see a difference between the calculated continuum level densities for V_1= -1.42 MeV and -1.43 MeV, we calculate the phase shifts by using Eq. (7). The results are presented in Fig. 4, and we can see a large difference in the low-energy region. In the case of V_1=-1.43 MeV, there is one bound state except for the lowest bound state assigned to the Pauli forbidden state, and then the phase shift starts from π at E=0 MeV because of the Levinson theorem and decreases with energy. On the other hand,

in the case of V_1=-1.42 MeV, the phase shift starts from zero and increases up to about $\pi/3$ but not $\pi/2$ unlike a resonance. This phase shift behavior supports the appearance of the virtual state. In the case of V_1=-1.43 MeV, the phase shift decreases passing across $\pi/2$ from above, and an enhancement of the cross section due to $\delta=\pi/2$ is often called an echo.

Furthermore, we calculate the scattering length from the obtained s-wave phase shift using the relation

$$a_s = -\lim_{k\to 0}\tan\delta_\theta^N(E)/k,$$

where is $k = \sqrt{2\mu E}/\hbar$ a momentum. For different potential strengths in the range of $-1.43 < V_1 < -1.42$ MeV, the calculated scattering lengths a_s are shown in Fig. 5. We find a sudden change of a_s in the range of $-1.43 < V_1 < -1.42$ MeV. While a_s is positive for the potential strength ($V_1 \leq -1.43$ MeV) reproducing a bound 0_2^+ state, a_s is negative for $V_1 \geq -1.42$ MeV. And at $V_1 = -1.42$ MeV, it is seen that a_s has a large negative value, which also indicates the existence of the virtual state.
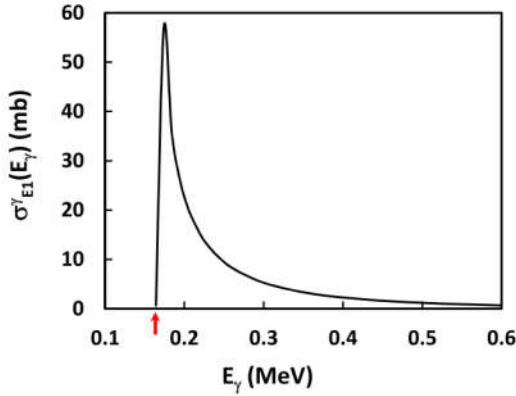

Fig. 2. Photodisintegration cross sections due to the $E1$ transition calculated with the two-body potential model with the strength V_1=-1.42 MeV. The arrow indicates the threshold energy which is shown in the Fig.1 as a dotted line.
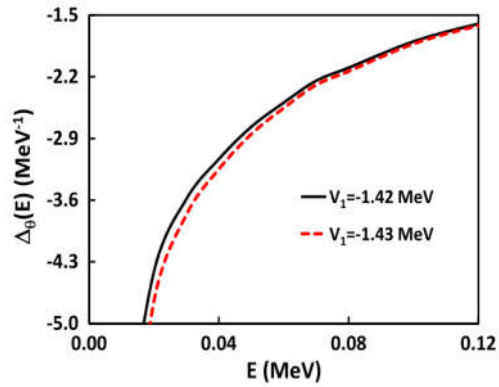
Fig. 3. Calculated continuum level density $\Delta_\theta^N(E)$ at the strengths of V_1=-1.42 MeV and -1.43 MeV. The black solid and red dashed curves are the results at V_1=-1.42 MeV and -1.43 MeV, respectively
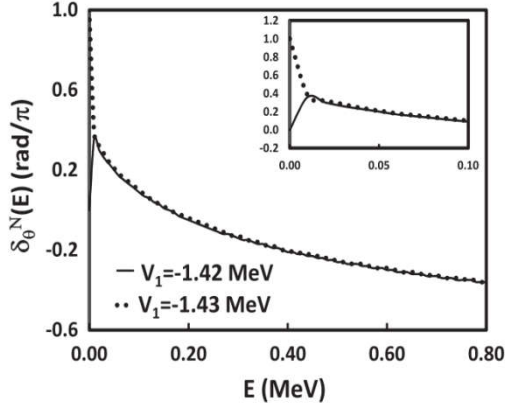
Fig. 4. Calculated phase shifts of the 0^+ state for V_1=-1.42 MeV and -1.43 MeV. The solid and open solid curves are phase shifts calculated at V_1=-1.42 MeV and -1.43 MeV, respectively. The scale of the graph was magnified in the inset.
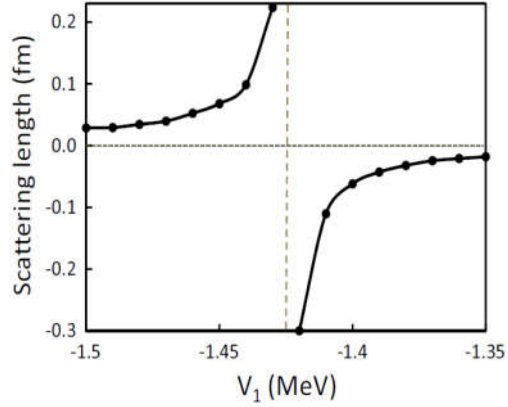
Fig. 5. Scattering length of the 0+ state calculated for V_1 =-1.42 MeV and −1.5 MeV in the CSM. The horizontal dotted line indicates $a_S = 0$ and the vertical broken line shows a border where the a_S changes sign.

From the result of phase shifts which are calculated using the complex-scaled energy eigenvalues, we confirm that the virtual state is included in the continuum solutions of the CSM though it is not an isolated solution. We try to extract a more detailed information on the virtual state, such as the pole position, from the CSM solutions.

The continuum level density $\Delta_\theta^N(E)$ given by Eq. (10) of Ref. [6] depends on the potential strength V_1 and we express this quantity as $\Delta_\theta^N(E; V_1)$ for convenience. The quantity $\Delta_\theta^N(E; V_1)$ of J^π=0^+ states is expected to have a contribution from the virtual state in the case of V_1 =-1.42 MeV, which disappears in the case of V_1 = -1.43 MeV. In the case of V_1 = -1.43 MeV, a bound 0^+ state appears instead of the virtual state, and then the continuum level density is expressed as

$$\Delta_\theta^N(E;\ -1.43\ \text{MeV}) = \Delta_b^2(E) + \Delta_c^{N-2}(E;\ -1.43\ \text{MeV}) \qquad (10)$$

where Δ_b^2 and Δ_c^{N-2} are the contribution from two bound states and the residual continuum states, respectively. In this case, there are two bound 0^+ states including the Pauli forbidden state, and then the contribution from continuum states is calculated by using the solutions with the number of $N-2$ on the 2θ line in the complex energy plane because of no resonances. Similarly, in the case of V_1 =-1.42 MeV, we have the relation

24

$$\Delta_\theta^N(E; -1.42 \text{ MeV}) = \Delta_b^1(E) + \Delta_c^{N-1}(E; -1.42 \text{ MeV}) \tag{11}$$

where the bound 0^+ state is the Pauli forbidden state alone.

We calculate a difference between Eq. (10) and (11)

$$\Delta_\theta^{vir}(E) = \Delta_c^{N-1}(E; -1.42 \text{ MeV}) - \Delta_c^{N-2}(E; -1.43 \text{ MeV}). \tag{12}$$

From this quantity, it is expected to extract the effect of the virtual state on the continuum level density. The difference is displayed in Fig. 6, which shows the sharp peak near the zero energy. Here we assume that $\Delta_c^{N-1}(E; -1.42 \text{ MeV})$ consists of two types of contributions; one is a virtual-state contribution and another is a background. The background contribution is also assumed to have a weak dependence of the strength of V_1. Then the background contributions are considered to be almost the same in both cases of V_1 -1.42 MeV and -1.43 MeV. When the background is expressed by $\Delta_c^{N-2}(E; -1.43 \text{ MeV})$ approximately, we can consider that $\Delta_\theta^{vir}(E)$ corresponds tothe virtual-state contribution of the continuum level density.

Since the phase shift is obtained by integrating the continuum level density, the phase shift of the virtual state is given as

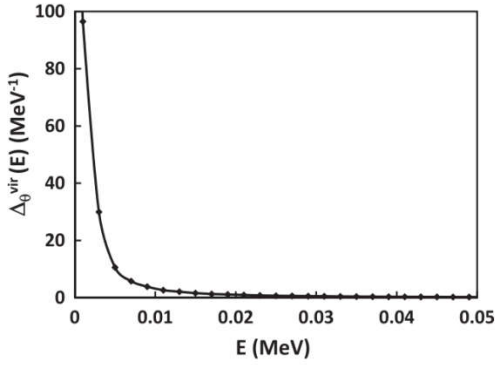$$\delta^{vir}(E) = \pi \int_0^E \Delta^{vir}(E') dE'. \tag{13}$$

Fig. 6. The difference between the continuum level densities for V_1=-1.42 MeV and -1.43 MeV. Ideally, the continuum level density calculated by the virtual state $\Delta_\theta^{vir}(E)$.
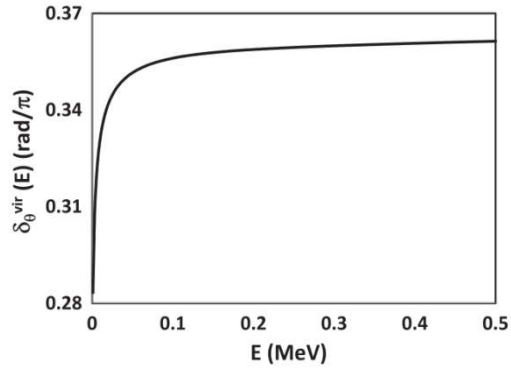
Fig. 7. The phase shift of the virtual state, calculated from the virtual-state continuum level density $\Delta_\theta^{vir}(E)$.

Using the result of $\Delta^{vir}(E)$ shown in Fig. 6, we obtained the corresponding phase shift as shown in Fig. 7. This result indicates a characteristic behavior of the phase shift of the virtual state. The phase shift of the virtual state is described as an increasing function of energy but does not reach $\pi/2$. The phase shift given in Fig. 4 is understood as a summation of phase shifts of the virtual state and the background states. The background phase shift seems to behave like a monotonic decreasing function of energy, similarly to hard-sphere scattering, as seen from Fig. 4.

4. Summary

In this report, much interest focused on the *s*-wave virtual state because it was discussed as an origin of the peak of the photodisintegration cross section in ^{9}Be in the previous work [3]. Moreover, another aim of this work is to show that the virtual state can be successfully described in the CSM, which has been believed to be not able to treat such a state.

In the CSM, the virtual state cannot be obtained as an isolated solution, but the continuum solutions are considered to include the effect of the virtual state. We tried to extract the information of the virtual-state pole in terms of the continuum solutions in the CSM.

Reference

[1] Y. K. Ho, Phys. Rep. **99**, (1983), 1
[2] T. Myo, Y. Kikuchi, H. Masui, and K. Katō, Prog. Part. Nucl. Phys. **79**, (2014), 1
[3] M. Odsuren, Y. Kikuchi, T. Myo, M. Aikawa, K. Katō, Phys. Rev. C **92**, (2015), 014322
[4] C. W. Arnold, T. B. Clegg, C. Iliadis, H. J. Karwowski, G. C. Rich, J. R. Tompkins, C. R. Howell, Phys. Rev. C **85**, (2012), 044605
[5] H. Utsunomiya, S. Katayama, I. Gheorghe, S. Imai, H. Yamaguchi, D. Kahl, Y. Sakaguchi, T. Shima, K. Takahisa, S. Miyamoto, Phys. Rev. C **92**, (2015), 064323
[6] M. Odsuren, Y. Kikuchi, T. Myo, G.Khuukhenkhuu, H.Masui, K. Katō, Phys. Rev. C **95**, (2017), 064305
[7] H. Masui, S. Aoyama, T. Myo, K. Katō, K. Ikeda, Nucl. Phys. A 673, (2000), 207

Interaction of ^{4}He and ^{3}He Ions of Energy 29 and 50 MeV With ^{27}Al and ^{59}Co

T.K. Zholdybayev[1], N. Kenzhebayev[2], B.M. Sadykov[1]

[1]*Institute of Nuclear Physics, 050032 Almaty, Kazakhstan*
[2]*Al Farabi Kazakh State University, 050040 Almaty, Kazakhstan*

At present, the world is facing the problem of energy production in the scale necessary to ensure sustainable economic growth without disrupting the ecological balance. At the same time, one should take into account the accumulation of carbon dioxide in the atmosphere in a large amount as a result of the generation of energy from organic materials, leading to a change in the climate on the planet. In this situation, the world is searching for alternative ways to develop nuclear energy, which can solve such problems as improving the level of security, reducing the amount of spent nuclear fuel and eliminating the uncontrolled proliferation of nuclear weapons.

In the middle of the last century, the idea of creating a nuclear power system was put forward, implemented to date as the Accelerator Driven System (ADS)[1], consisting of a proton accelerator (deuterons) with an energy of 0.8-1.5 GeV and a current of 30-100 mA, a neutron-producing targets with a power of 30-100 MW and a subcritical reactor (blanket) with a thermal neutron flux (1-5) 10^{15} cm^{-2} s^{-1}. In addition to receiving energy, the system allows the transmutation of long-lived radioactive waste from the nuclear industry.

According to the physical scenario of the ADS operation (Fig. 1), high-energy protons during the passage of the target assembly generate not only a neutron flux, but also a spectrum of more complex nuclides of hydrogen and helium that act as initiating reaction agents with the emission of secondary neutrons. The range of nucleon composition and excitation energies in the ADS system is much wider than in traditional reactors. New additional data are needed on nuclear reactions with hydrogen and helium nuclides occurring in target, fuel assemblies, and structural materials.

It is physically and economically impossible to measure all the necessary cross sections of nuclear reactions in such a wide range of energies and masses. In this situation, the development of nuclear models that have sufficient predictive power

plays an important role. On the basis of such models, computer programs have been developed that can calculate all possible channels of nuclear reactions and allow simulating estimated nuclear data in the energy range from 1 keV to 200 MeV. To clarify the model parameters and debug the work of programs, it is important to obtain new experimental data on the cross sections of nuclear reactions. Reviews on available experimental data in reactions with nucleons and heavier particles are presented in [2-4].
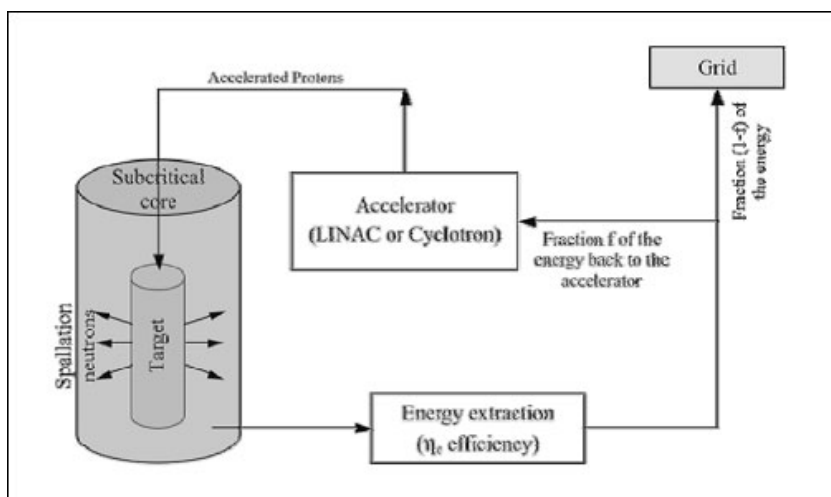

Fig. 1. Principle work scheme of ADS.

The experimental complex is located on the isochronous cyclotron U-150M of the Institute of Nuclear Physics (INP) of Kazakhstan. The scheme for transporting the beam of accelerated ions from the cyclotron chamber to the reaction chamber includes a quadrupole lens system, two bending magnets, two targeting magnets and a collimator system. The maximum angular uncertainty of the collimator is 24±. This ensured the linear dimensions of the beam on the target ~ 3 mm. The alignment of the position of the collimator and the scattering chamber with respect to the axis of the ion conductor was carried out by an optical method.

To determine the number of particles incident on the target, a Faraday cylinder-current integrator system was used. The error in determining the constant integrator did not exceed 1%.Based on the kinematic calculations, the working thicknesses of the detectors used are determined.

As the target, ^{27}Al and ^{59}Co are selected, as structural elements and elements of the target node of the ADS being designed. Enriched foils of these isotopes were prepared, the thickness and uniformity of which was determined by measuring the

energy loss of alpha particles from the ^{226}Ra isotope. The characteristics of the targets are given in Table.

The experimental spectra of nuclear reactions(^{3}He,xp),(^{3}He,xd)on the ^{59}Co nucleus and (^{4}He,xp),(^{4}He,xα) on the ^{27}Al nucleus have been obtained. The energy of the incident^{3}He ions was 50 MeV and^{4}He ions was 29 MeV. Measurements are made in the angular range of 30^{0} - 135^{0} in the laboratory coordinate system with a step of 15^{0}. The total systematic error of measured double-differential cross-sections did not exceed 10% and was mainly due to errors in the determination of the target thickness (<7%) and the solid angle of the spectrometer (1.3%). The beam energy of the accelerated particles was measured with an accuracy of 1%. The total statistical error varied from 5% to 20%.

Table 1. Characteristics of the target

Target	Thickness, (mg/cm^2)	Enrichment, (%)
^{27}Al	3,65	monoisotope
^{59}Co	2,3	monoisotope

The experimental results were analyzed using Griffin's model of exciton nuclear decay [5], which reflects the dynamics of the formation of an excited system and its transition to the equilibrium state. The Griffin model is essentially a statistical model in which the excited states of an intermediate system are described in terms of a single-particle model of shells; i.e., they are characterized by the number of excited particles (above the Fermi level) and holes (below the Fermi level). It is assumed that the system evolves through a sequence of more complicated configurations, and particle emission is possible at each phase of this evolution.

In the two-component exciton model [6]., the proton and neutron degrees of freedom are considered separately. It is assumed that the nucleus is characterized by the parameters p_π, h_π, p_ν and h_ν, where p and h denote partial and hole degrees, and π and ν are the proton and neutron degrees of freedom, respectively. The compound nucleus is formed with a partially-hole configuration, which takes into account only incoming nucleons as partial degrees of freedom and does not take into account hole

states. Such a configuration is denoted as $(p_\pi, h_\pi, p_v, h_v) = (Z_a, 0, N_a, 0)$, where a refers to the bombarding particle. The difference between the number of particles and holes during the transition to the equilibrium state remains constant. Calculations of the density of single-particle states are calculated separately for protons $g_{\pi 0}$ and neutrons g_{v0}:

$$g_{\pi 0} = \frac{Z}{K_g}, \tag{1}$$

$$g_{v0} = \frac{N}{K_g}, \tag{2}$$

where K_g is the normalization coefficient. Density of partially-hole states:

$$\omega_{ESM}(p, p_\pi, E) = \frac{\left(g_{\pi 0}\right)^{n_\pi} \left(g_{v0}\right)^{n_v} (E - A(p, p_\pi, E))^{n-1}}{p_\pi! h_\pi! p_v! h_v (n-1)!}, \tag{3}$$

where $A(p, p_\pi, E)$ is a correction that takes into account the Pauli exclusion principle. These densities are used to calculate the transition probabilities that transfer the core from one partial-hole configuration to another.

In view of the assumption that the residual two-particle interactions are small, the first order of perturbation theory can be used to determine the probability of inner nuclear transitions λ related to unit time:

$$\lambda = (2\pi / \hbar) \left\langle |M|^2 \right\rangle \omega, \tag{4}$$

where $|M|^2$ is the rms matrix element that determines the intensity of inner nuclear transitions, which means, transitions between states with different n, and ω is the density of final states that are actually achievable for a given transition. It is assumed that the matrix elements have the same formula and differ only in the normalizing coefficients K_{ij}:

$$|M_{ij}|^2 = K_{ij} A_a g_0^{-3} \left(\frac{E}{3A_a} + 20.9\right)^{-3}, \tag{5}$$

where A_a is the mass of the incident particle.

At any stage of the relaxation of the system, particles of type b can be emitted into a channel with energy ε. The rate of particle emission from this state is calculated by the

formula:

$$W_b(p, p_\pi, E, \varepsilon) = \frac{2s_b + 1}{\pi^2 h^3} \mu_b \varepsilon \sigma_b(\varepsilon) \frac{\omega(p_\pi - Z_b, h_\pi, p_\nu - N_b, h_\nu, U)}{\omega(p_\pi, h_\pi, p_\nu, h_\nu, E)}, \qquad (6)$$

where Z_b and N_b is the number of protons and neutrons of the emitted particle, S_b- its spin, and μ_b- its mass. The value $\sigma_b(\varepsilon)$ is the cross section for the inverse formation of the compound nucleus, U is the excitation energy.

Theoretical calculations were carried out within the framework of the computer code PRECO-2006 [7], optimized for the case under consideration.

The results of the calculations are given together with the experimental data in **Fig.2-5**.

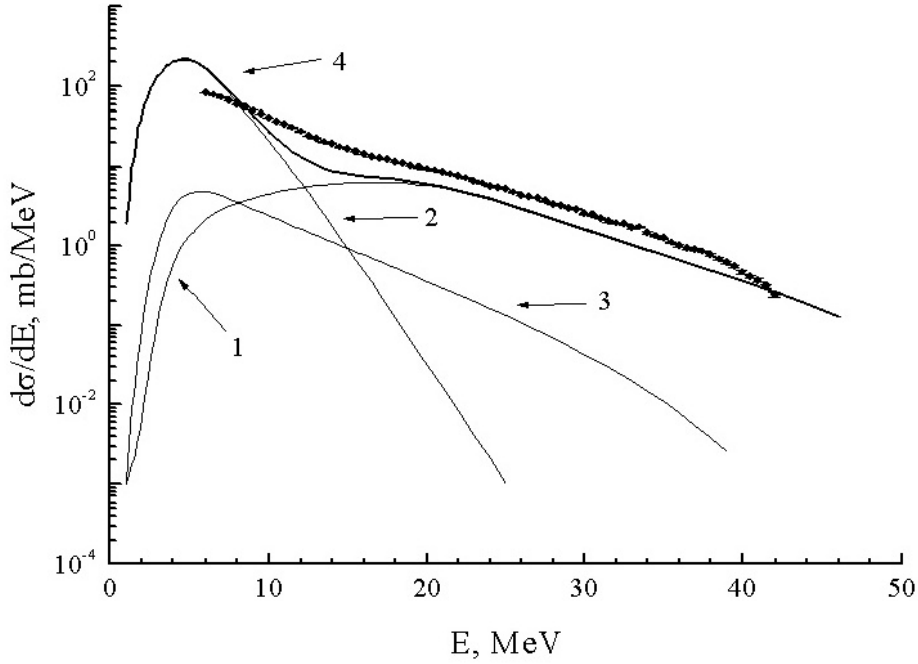**Fig. 2.** Comparison of the experimental integrated cross sections for ^{59}Co(^{3}He,xp) reactions with calculations within the exciton model. Symbols - experiment, 1-pre-equilibrium component, 2-equilibrium emission, 3-multiple pre-equilibrium emission, 4-total.

Fig. 3. Comparison of the experimental integrated cross sections for $^{59}Co(^{3}He,xd)$ reactions with calculations within the exciton model. Symbols - experiment, 1-pre-equilibrium component, 2-equilibrium emission, 3-total.

Fig. 4. Comparison of the experimental integrated cross sections for $^{27}Al(^{4}He,xp)$ reactions with calculations within the exciton model. Symbols - experiment, 1-pre-equilibrium component, 2-equilibrium emission, 3-total.
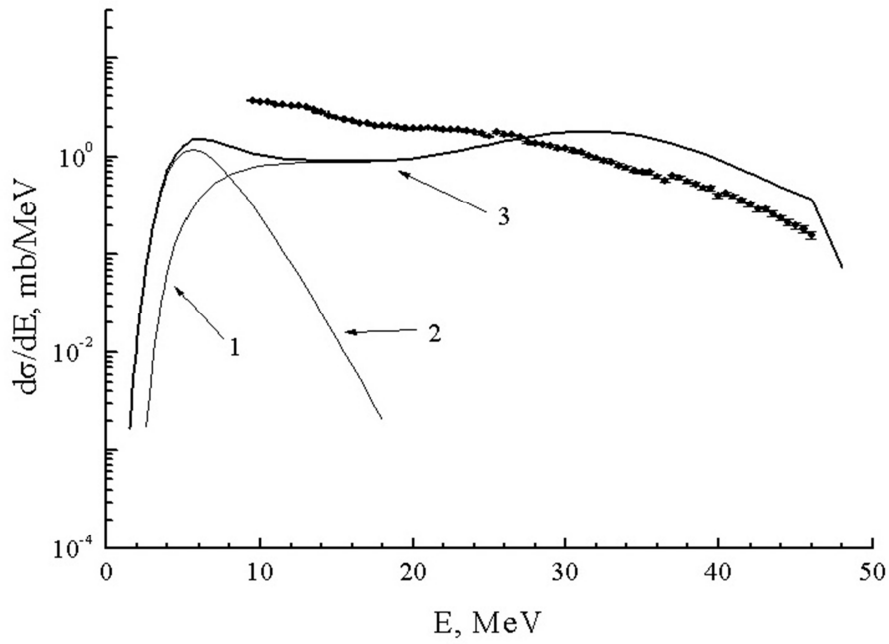
32

Fig. 5. Comparison of the experimental integral cross sections for $^{59}Co(^{4}He,xp)$ reactions with calculations within the exciton model Symbols − experiment, 1−pre-equilibrium component, 2−equilibrium emission, 3−total integrated cross section.
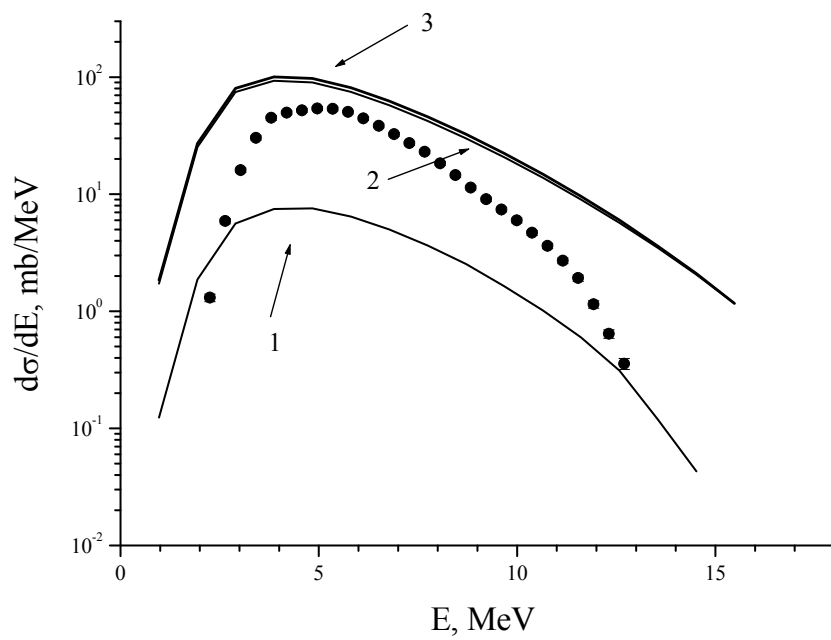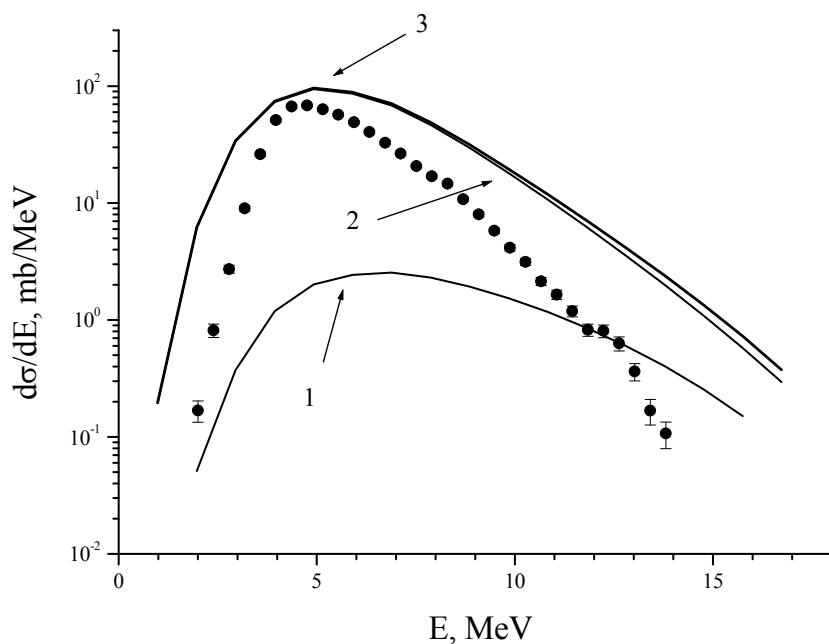
The obtained experimental results fill the missing values of the cross sections of the studied reactions and can be used in the development of new approaches to the theory of nuclear reactions, as well as in the construction of safe and non-waste hybrid nuclear power plants, calculations of the distributions of the primary knocked-out atoms in radiation material science.

References

[1] J.-P.Revol, Phys.-Usp. **46** (2003) 725.
[2] A.J.Koning, M.C. Duijvestijn,Nucl. Phys. **A744** (2004) 15
[3] C. Kalbach, Phys. Rev. **C71** (2005) 034606.
[4] P.E. Hodgson, E.Betak, Phys. Rep.**374**(2003) 1.
[5] J.J. Griffin, Phys. Rev. Lett. **17**(1966) 478.
[6] C. Kalbach, Phys. Rev. **C33**(1986) 818.
[7] Kalbach C. PRECO-2006: Exiton model preequilibrium nuclear reaction code with direct reaction. – Durham NC 27708–0308, 2007. – 184 p.

The Evaluations of Gamma-Induced Cr-52

Xi Tao[1], Jimin Wang[1], Ruirui Xu[1], Yuan Tian[1], Zhigang Ge[1], Chonghai Cai[2]

[1]*China Nuclear Data Center, China Institute of Atomic Energy, Beijing 102413, China*

[2] *Naikai University, Tianjin 300071, China*

Photonuclear data are important in radiation damage, reactor dosimetry, accelerator shielding etc. IAEA has started a new CRP (No.20466) from 2016 to 2019. Ruiui Xu, Xi Tao, Jimin Wang, Yuan Tian, Zhigang Ge, and Chonghai Cai have joined the CRP. In this new CRP, 12 nuclei need to be evaluated. Two theoretical codes, GLUNF and MEND-g, have been developed and used for calculating photonuclear data.

There are 4 stable isotopes for Chromium. Natural abundance of ^{52}Cr is the biggest. New evaluation of $\gamma+^{52}$Cr has been done in this work.

The absorption cross section evaluated by B.S.Ishkhanov [1] in 2002 is not equal to the sum of (γ,xn) [2] and [(γ,p)+(γ,n+p)] [3] cross sections. The theoretical ratios are used to separate (γ,xn) into (γ,n), (γ,n+p), and (γ,2n).

$$\sigma_{\exp}(\gamma, abs) \approx \sigma_{\exp}(\gamma, p) + \sigma_{\exp}(\gamma, n) + \sigma_{\exp}(\gamma, n+p) + \sigma_{\exp}(\gamma, 2n) \tag{1}$$

$$F_n = \frac{\sigma_{the}(\gamma, \mathrm{n})}{\sigma_{the}(\gamma, \mathrm{n}) + \sigma_{the}(\gamma, \mathrm{n+p}) + 2\sigma_{the}(\gamma, 2\mathrm{n})}$$

$$F_{np} = \frac{\sigma_{the}(\gamma, \mathrm{n+p})}{\sigma_{the}(\gamma, \mathrm{n}) + \sigma_{the}(\gamma, \mathrm{n+p}) + 2\sigma_{the}(\gamma, 2\mathrm{n})} \tag{2}$$

$$F_{2n} = \frac{\sigma_{the}(\gamma, 2\mathrm{n})}{\sigma_{the}(\gamma, \mathrm{n}) + \sigma_{the}(\gamma, \mathrm{n+p}) + 2\sigma_{the}(\gamma, 2\mathrm{n})}$$

$$
\begin{aligned}
\sigma(\gamma, n) &= F_n \cdot \sigma_{\exp}(\gamma, xn) \\
\sigma(\gamma, n+p) &= F_{np} \cdot \sigma_{\exp}(\gamma, xn) \\
\sigma(\gamma, 2n) &= F_{2n} \cdot \sigma_{\exp}(\gamma, xn)
\end{aligned}
\tag{3}
$$

Here, σ_{the} are the cross sections calculated by MEND-g with the default parameters.

The experimental data of [(γ,p)+(γ,n+p)] were also separated into (γ,p) and (γ,n+p) in the same way. The absorption cross section approximately equals to the sum of (γ,n), (γ,p), (γ,n+p), and (γ,2n) below 30 MeV. The absorption cross section calculated by Eq.1 was higher than the evaluation by B.S.Ishkhanov in 2002, see Fig.2.

There were 3 measurements of [89]Y, CEA/Saclay [4], Lawrence Livermore National Laboratory, Livermore [5], and Moscow State Univ., Nuclear Physics Inst., Moscow [6]. V.V.Varlamov [7] has evaluated the (γ,n) cross section in 2003. His evaluation agreed with Saclay's measurement, nevertheless was lower than the measurement of B.S.Ishkhanov. The [52]Cr(γ,n) measured by B.S.Ishkhanov (2nd author) was multiplied by factor=0.81, and then agreed with the evaluation, see Fig.3. Base on the corrected experimental data, the absorption cross section were equal to the evaluation by B.S.Ishkhanov in Fig.4.
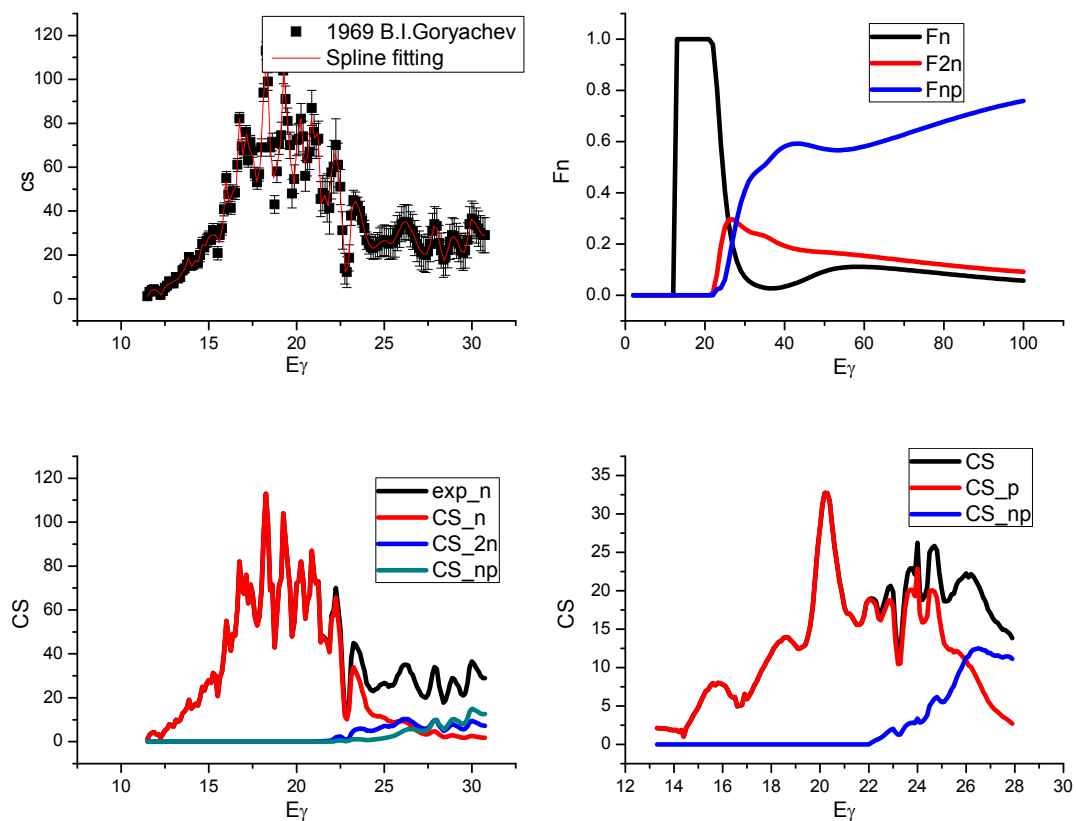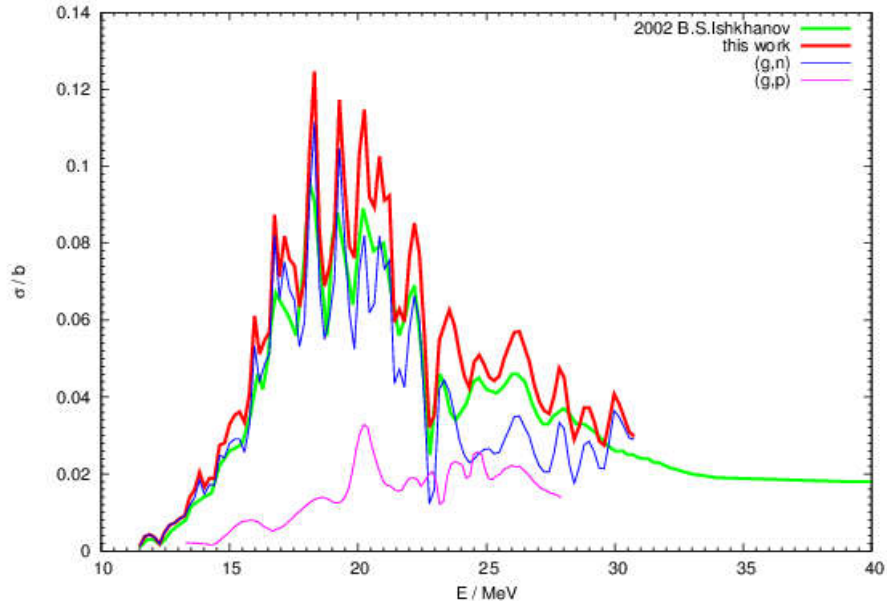

Fig. 1. Evaluation of (γ,xn) cross section

Fig. 2. The evaluation of absorption cross section
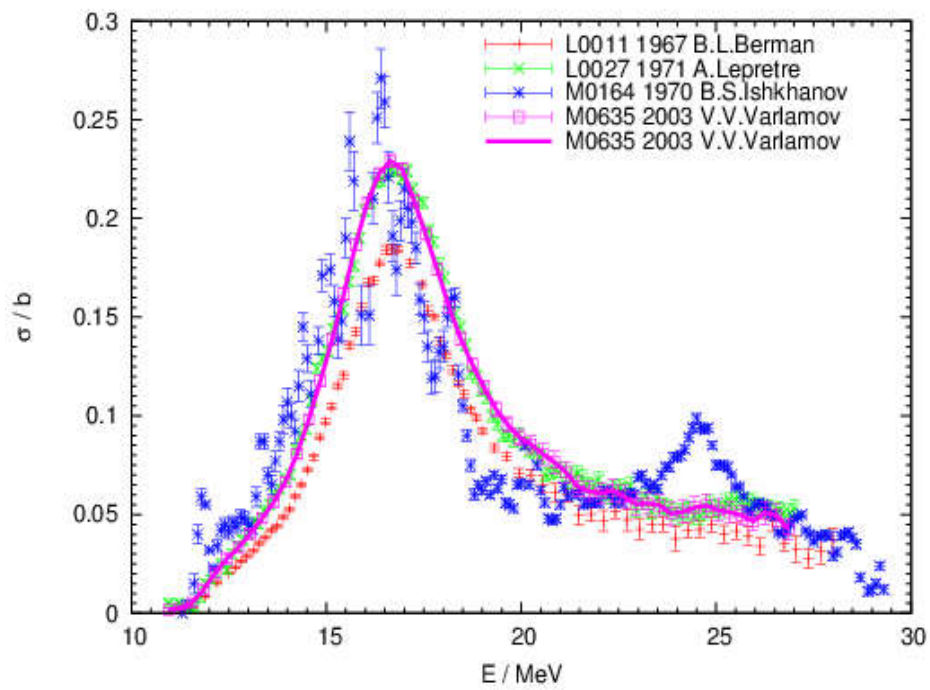
Fig. 3. The (γ,xn) cross section of ^{89}Y
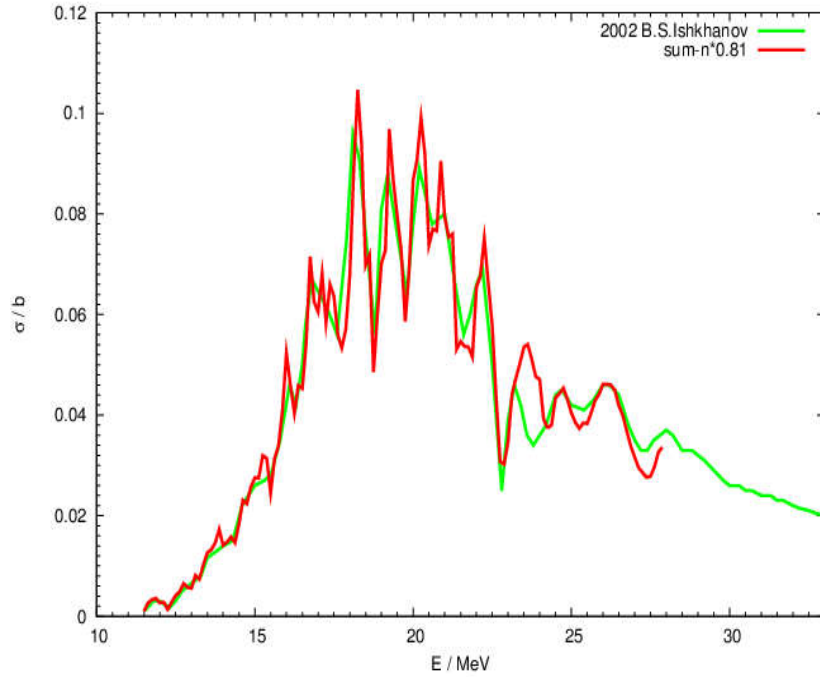
Fig. 4. The evaluation of absorption cross section

MEND-g is used for the theoretical calculation of $\gamma+^{52}Cr$. MEND-g is a theoretical code for calculating gamma induced reactions for medium heavy nucleus below 200MeV. It was compiled by Fortran language. The optical model, the preequilibrium process based on the exciton model, the evaporation model, and the Hauser-Feshbach theory with width-fluctuation correction are considered in MEND-g.

The absorption cross section was defined as input quantity. EGLO method is used to fit the experimental data in the peak energy range. In the high energy range, the (γ,abs) followed the experimental data. Near the threshold of (γ,n), the absorption cross section was cut down, see Fig.5. According to the evaluated absorption cross section, some channels were calculated by MEND-g, such as (γ,n), (γ,p), (γ,2n), (γ,3n), (γ,np) etc. The thresholds of considered reactions are listed in Table 1. The level density and pair parameters were adjusted by MINUT code. The sum of (γ,n), (γ,2n) and (γ,np) was in good agreement with the (γ,xn) experimental data in **Fig.6**. Below 30MeV, the proton outgoing cross section also agreed with the measurement by B.S.Ishkhanov in 1970, see Fig.7.

Table 1: The thresholds of considered reactions

Reaction Products	Q-value (keV)	Threshold (keV)
^{51}Cr+n	-12038.35 *0.92*	12039.846 *0.92*
^{51}V+p	-10503.37 *0.92*	10504.509 *0.92*
^{50}Cr+2n	-21299.01 *0.92*	21303.693 *0.92*
^{50}V+n+p	-21554.523 *0.92*	21559.318 *0.92*
^{50}Ti+2p	-18565.52 *0.36*	18569.078 *0.36*
^{49}Cr+3n	-34300.14 2.27	34312.28 2.27
^{49}V+2n+p	-30888.914 *0.895*	30898.764 *0.896*
^{49}Ti+n+2p	-29504.715 0.359	29513.701 0.359
^{49}Sc+3p	-30724.88 2.72	30734.63 2.72
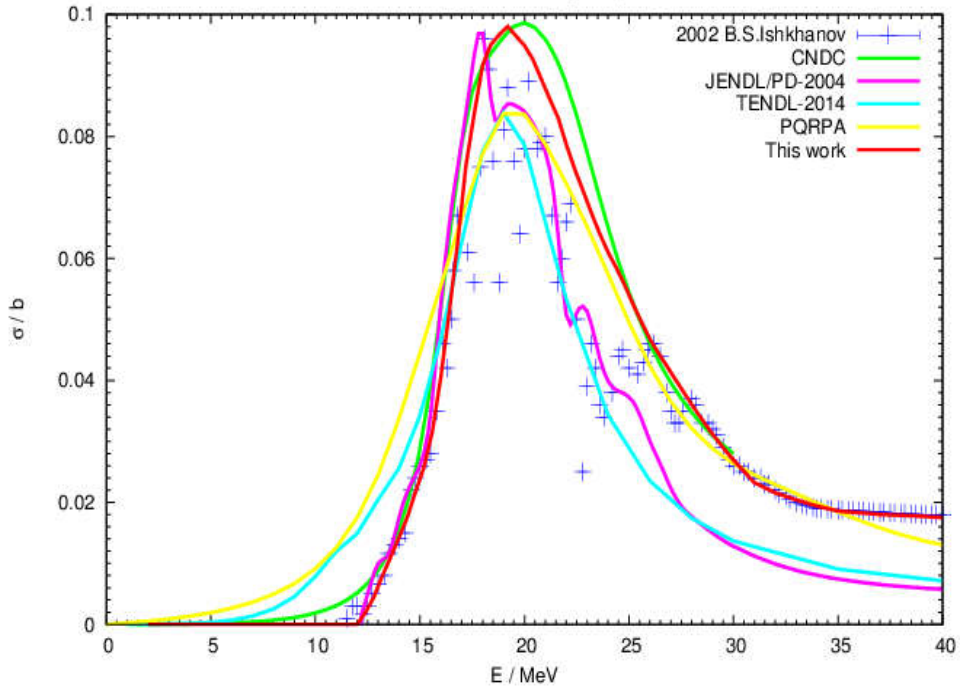
Fig. 5. The comparison of absorption cross sections
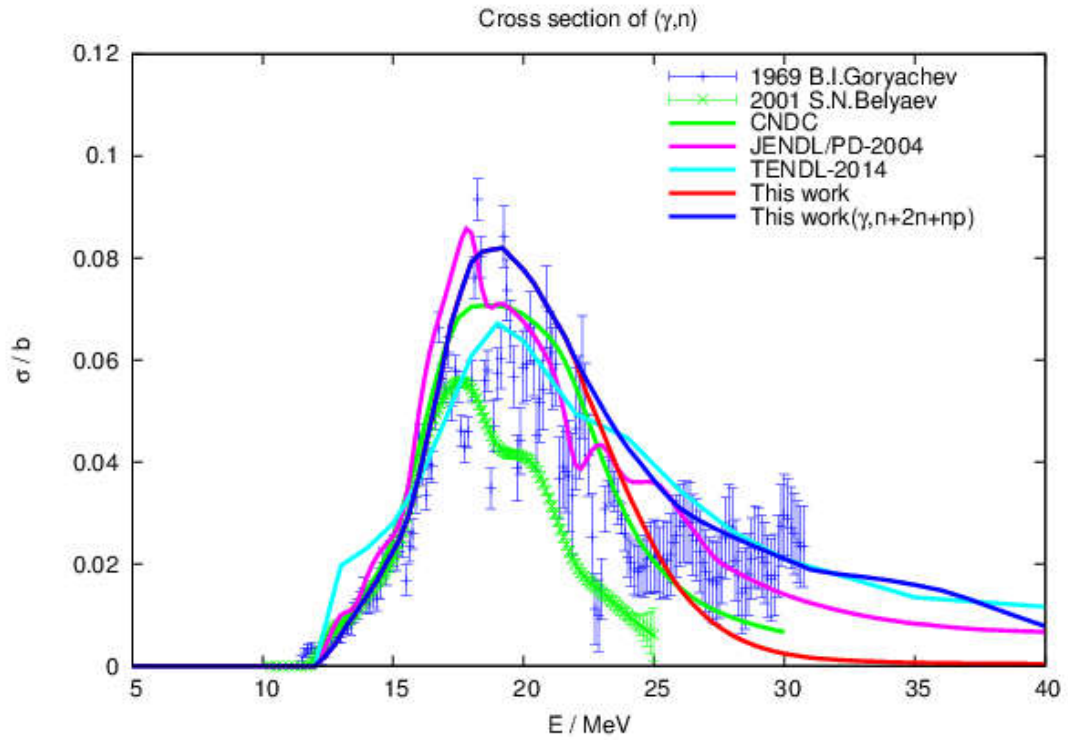
Fig. 6. (γ,n) cross section
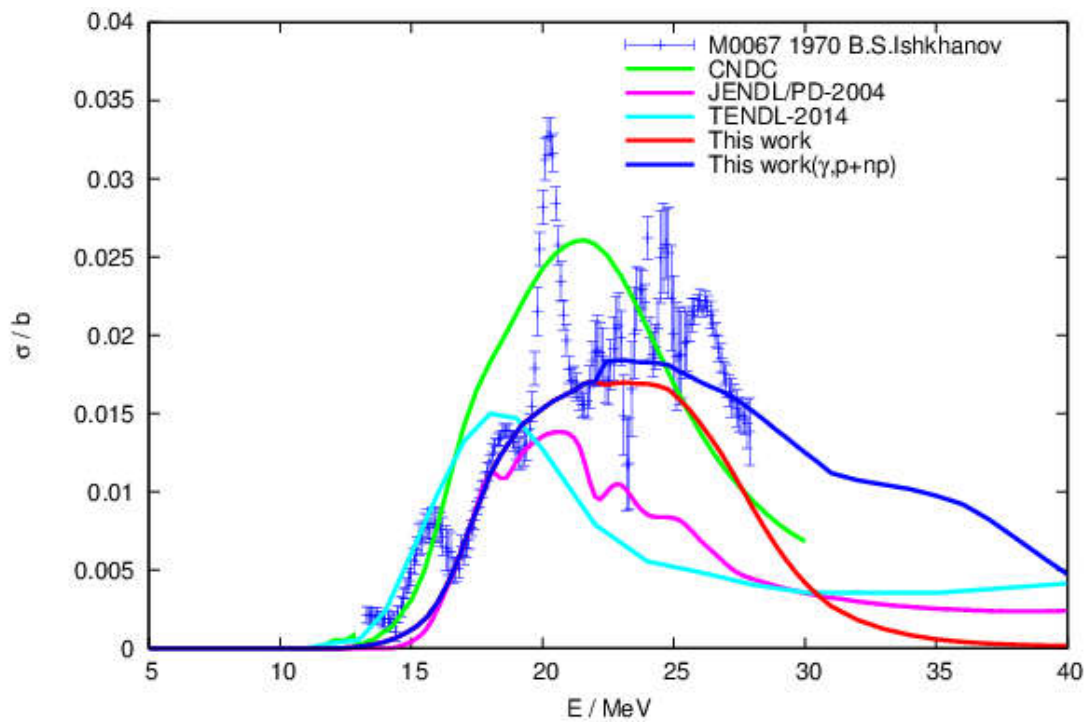
Fig. 7. (γ,p) cross section

The preliminary results of theoretical calculation for $\gamma + ^{52}Cr$ are in good

agreement with the experimental data. In future, the ^{52}Cr(γ,abs) cross section will be used for fitting by PSF (photon strength functions), and the parameters of PSF will be used to calculate the absorption cross sections of other isotopes, which have none experimental data. Based on the theoretical absorption cross sections, the calculation results of Cr isotopes will be given by MEND-g.

References

[1] B.S.Ishkhanov, et al. MSU-INP-2002-27/711 (2002). EXFOR M0648
[2] B.I.Goryachev ,et al. J,IZV,33, (1969), 1736. EXFOR M0093
[3] B.S.Ishkhanov, et al. J,YF,11,(3), (1970), 485. EXFOR M0067
[4] A.Lepretre, et al. NP/A,175,609 (1971). EXFOR L0027
[5] B.L.Berman, et al. PR,162, (1967), 1098. EXFOR L0011
[6] B.S.Ishkhanov, et al.IZV,34, (1970), 2232. EXFOR M0164
[7] V.V.Varlamov, et al. YK,2003,(1-2),48,200. EXFOR M0635

Overview of EXFOR Compilation Activity in Mongolia in 2016-2017

M.Odsuren[1] and N.Otuka[2]

[1]*Nuclear Research Center, and School of Engineering and Applied Sciences, National University of Mongolia, Mongolia*
[2]*Nuclear Data Section, IAEA, Vienna, Austria*

The Nuclear Research Center(NRC),National University of Mongolia– International Atomic Energy Agency (IAEA) collaboration built in 2014 for compilation of heavy-ion (A>12) induced reaction data measured in West European countries for the EXFOR library [1]. The NRC is the first nuclear research and educational institution in Mongolia, which carries out basic and applied research on low energy nuclear physics.

In the two years (2014-2015) since the launch of the NRC-IAEA collaboration, 17 EXFOR entries from articles published between 2009 and 2015 [2] were compiled and loaded into the EXFOR database. These entries included the data measured in West European countries. No Data Center offers compilation work on heavy-ion induced reaction measured in West European countries so far, thus, we started to collaborate on the compilation, in particular to improve completeness in the EXFOR library of West European countries. For the next two years (2016-2017), wecomplied18 EXFOR entries, which had been published between 2002 and 2017, as shown in **Table 1**. 10 of the total 18 entries contained heavy-ion induced reaction data measured at the LNL-INFN, Italy and the others contained data measured at the GANIL France, GSI Germany, CERN Geneva, and LNS-INFN, Italy, respectively.

To maintain good quality of the EXFOR library, one of authors (NO)always asks authors to provide the original numerical data. So far we have received numerical data for all cases, and it enables us to avoid compilation of digitized data.

Table 1: List of compiled articles

Entry number	First author	Journal volume, page and publication year+	Laboratory, country	Year of compil-ation	Status*
D0791	A.M.Stefanini	J,PR/C,92,064607, 2015	LNL, INFN, Italy	2016	in EXFOR
D0793	L.Pellegri	J,PR/C,92,014330, 2015	LNL, INFN, Italy	2016	in EXFOR
D0799	Y.X.Watanabe	J,PRL,115,172503,2015	GANIL, France	2016	in EXFOR
D0801	A.M.Stefanini	J,PL/B,728,639,2014	LNL, INFN, Italy	2016	in EXFOR
D0806	R.Kanungo	J,PR/C,84,061304(R),2011	GSI, Darmstadt, Germany	2016	in EXFOR
D0810	C.Scheidenberger	J,PR/C,70,014902,2004	CERN, Geneva	2016	in EXFOR
D0814	A.M.Stefanini	J,PR/C,65,034609,2002	LNL, INFN, Italy	2016	in EXFOR
D0815	A. Trzcinska	J,PR/C,93,054604,2016	Warsaw, Poland	2016	in EXFOR
D0823	M. Krzysiek	J,PR/C,93,044330,2016	LNL, INFN, Italy	2016	in EXFOR
D0825	E. Strano	J,PR/C,94,024622,2016	LNL, INFN, Italy	2016	in EXFOR
D0826	M.J.Ermamatov	J,PR/C,94,024610,2016	LNS, INFN, Italy	2016	in EXFOR
D0816	T. Mijatovic	J,PR/C,94,064616,2016	LNL, INFN, Italy	2017	in EXFOR
D0829	L. Manduci	J,PR/C,94,044611,2016	GANIL, France	2017	in EXFOR
D0838	M.Heine	J,PR/C,95,014613,2017	GSI, Darmstadt, Germany	2017	in EXFOR
D0840	D.Carbone	J,PR/C,95, 034603,2017	LNS, INFN, Italy	2017	in EXFOR
D0843	L.Corradi	J,PR/C,66,024606,2002	LNL, INFN, Italy	2017	in EXFOR
D0845	S.Szilner	J,PR/C,71, 044610,2005	LNL, INFN, Italy	2017	In EXFOR
D0848	A.M.Stefanini	J,PR/C,96, 014603,2017	LNL, INFN, Italy	2017	PRELIM

+PR/C: Phys. Rev. C, PRL: Phys. Rev. Lett, PL/B: Phys. Lett. B.

* "in EXFOR": The EXFOR entry is accessible through the EXFOR web retrieval systems."PRELIM": The EXFOR entry was created and under review by other centres.

[1] N.Otuka et al., "Towards a More Complete and Accurate Experimental Nuclear Reaction Data Library (EXFOR): International Collaboration Between Nuclear Reaction Data Centres (NRDC)", Nucl. Data Sheets **120**(2014), 272.

[2] M.Odsuren, N.Otuka, INDC(JP)-0200, International Atomic Energy Agency (2016), 57

NDPlot: A Plotting Software for Nuclear Data

Yongli Jin, Xi Tao, Jimin Wang, Zhigang Ge

China Nuclear Data Center, China Institute of Atomic Energy, Beijing 102413, China

The evaluators always desire to compare their evaluated nuclear data with experimental data. One of the most intuitive ways is plotting the data in a diagram. However, nuclear data is not easy to be plotted using common plotting software such as ORIGIN, GNUPLOT, etc. So, a more efficient plotting software for nuclear data needs to be developed.

NDPlot is not only a plotting tool for nuclear data, but also integrated application software. It has three properties as follows:

1. Convenience: It's online, and all the experimental data and evaluated data are converted to uniform units.

2. Traceability: Information can be stored in a project file, users can review it at any time, which includes: original data, coordinate system, annotations, memos, etc.

3. Reusability: You can save or continue the work at any time. Others also can use the file to continue or examine the work, even to edit the file.

The structure of NDPlot is Client-Server structure（Fig. 1）, the application server retrieves and handles the original ENDF and EXFOR data stored in the database, NDPlot client handles and plots the data. Programming language of NDPLot client is Perl [1], and GUI platform of NDPLot client is WxWindows [3]. A multi-document interface (MDI) is used in NDPlot, so it can have more than one window (Fig. 2). It can plot data with multi-windows., and can plot more than one reaction at a time with the batch plotting function.
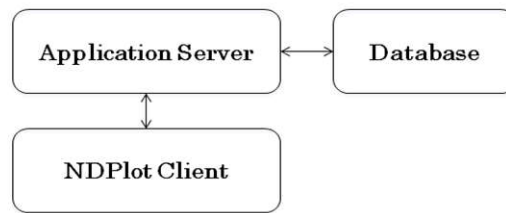
Fig. 1. Client-Server structure
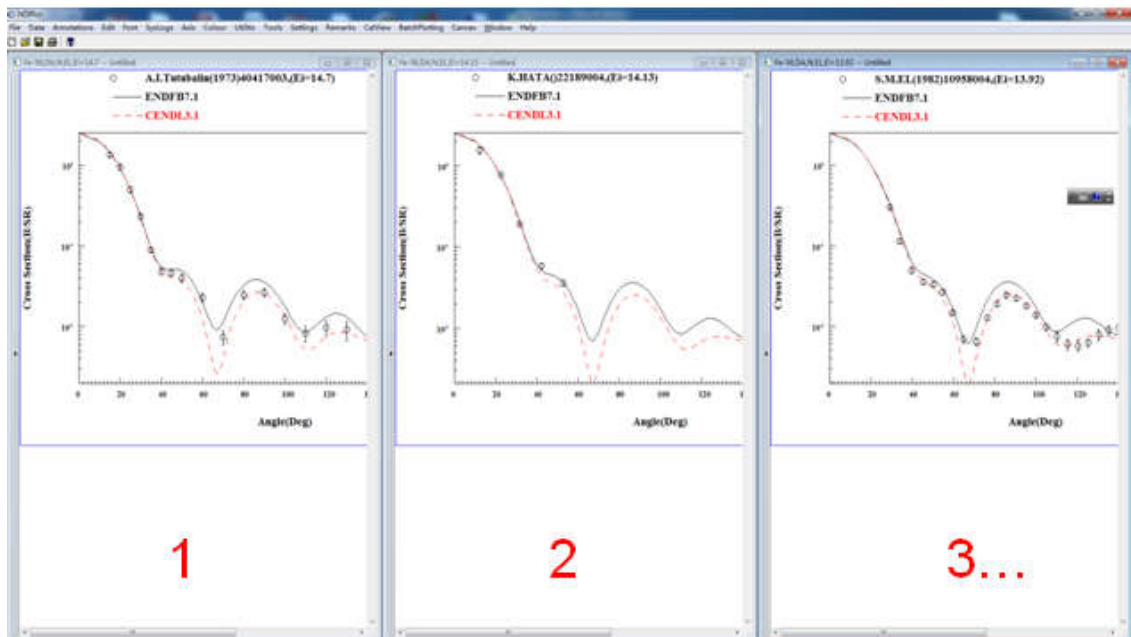
Fig. 2. Screenshot of NDPlot

Features of NDPlot as follows:

1. Treatments of CS, DA, DE, DAE etc.

2. Using EXFOR, ENDF, and user-defined format data (free format).

3. Saving project file.

4. Exporting figures as jpg, eps, pdf, etc.

5. Supporting Windows clipboard (inserting picture into MS Word, PowerPoint).

6. Online retrieve & transfer the exp. and eval. data from the database.

NDPlot can accept ENDF, EXFOR, PENDF [4, 5], free format, and NDPlot format data, and output graphs (jpeg, ps, pdf, etc.), NDPlot format and project file, see Fig.3.

The experimental data points can be plotted with x error bars and y error bars, the styles of the points, the curves and the axes can be determined by users. Users can change the axis ranges, curve and point's colors, size, etc., see Fig.4.
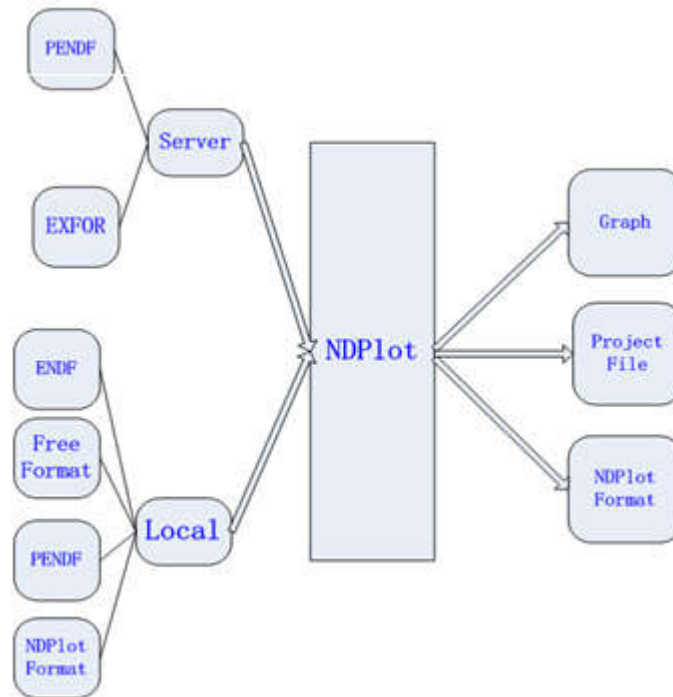
Fig. 3. Input and output of NDPlot
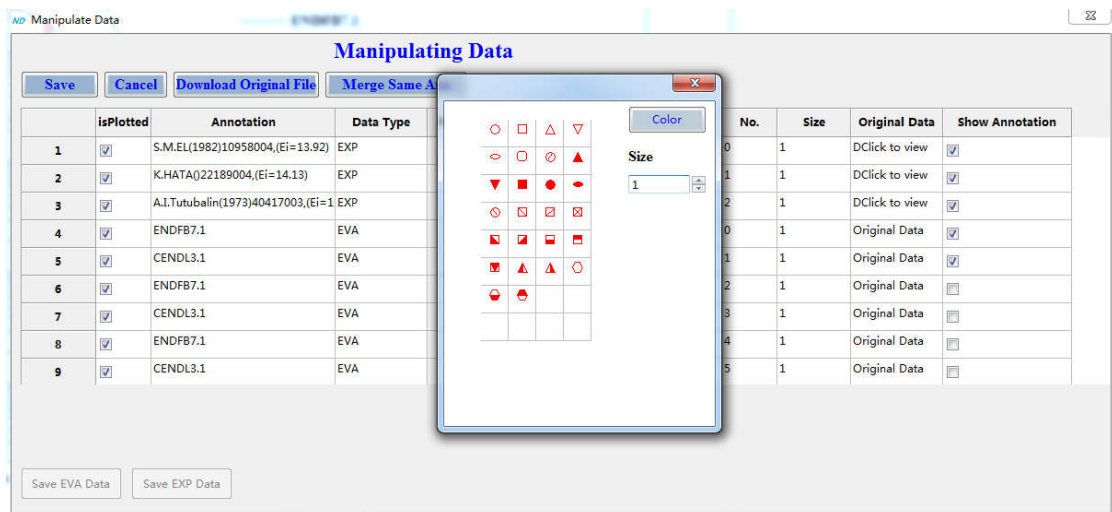
Fig. 4. Changing the point style

With batch plotting function, all the data can be plotted in one or multi-windows. If you plot all the data in one window, you can define a factor (for example 0.1) to differentiate the data, see from Fig. 5 to Fig. 6.
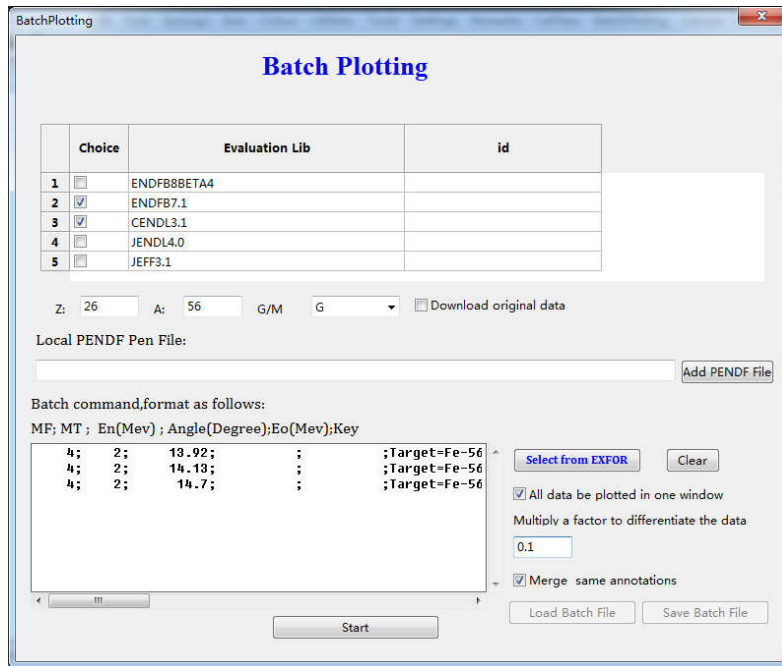
Fig. 5. Batch plotting function
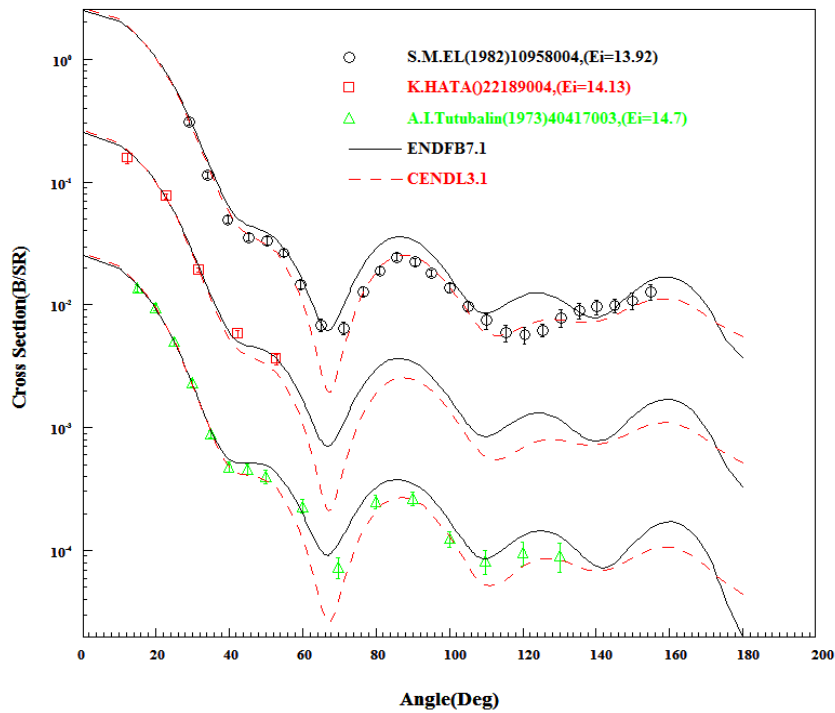
Fig. 6. Fe-56(n,el),DA,(13.92MeV,14.13MeV,14.7MeV)

All the ENDF data and EXFOR data can be stored in local project file or retrieved online. Users can check the data at any time (Fig. 7 and Fig.8).
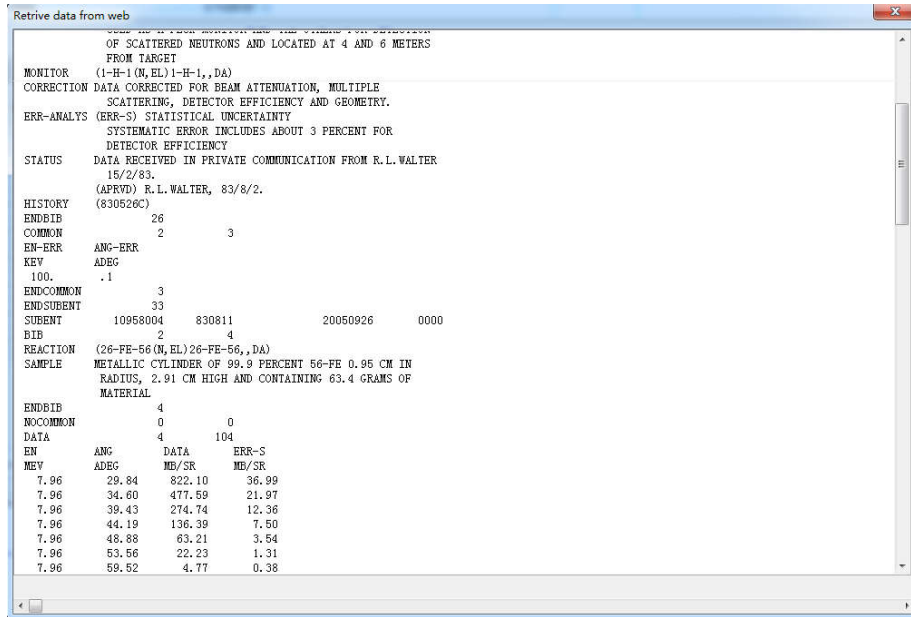
Fig. 7. Viewing the EXFOR data
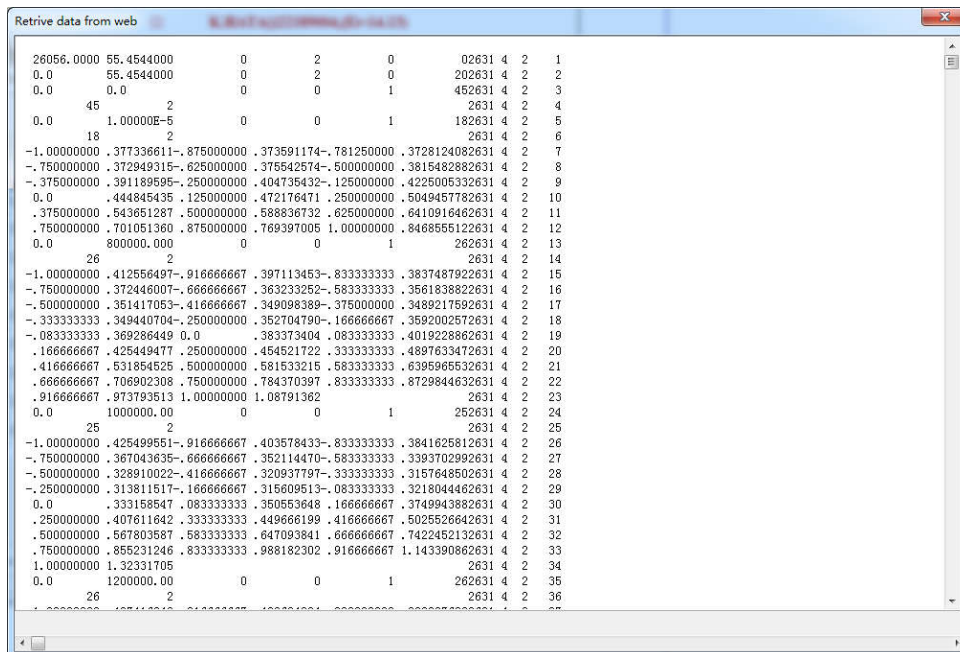
Fig. 8. Viewing the ENDF data

NDPlot is a high efficient plotting software for nuclear data. It is still under development yet. We will release it in 2018 and establish a NDPlot server on internet. Some functions need to be increased, such as the styles of the point and the curve to satisfy publishing, representation, and so on. More tests need to be done and the bugs must to be fixed.

References

[1] Larry Wall,Programming Perl, O'REILLY, 2012.
[2] Website: http://www-nds.iaea.org.
[3] Website:http://www.wxwidgets.org.
[4] Web site:https://www-nds.iaea.org/public/endf/prepro/.
[5] Web site:https://www-nds.iaea.org/public/endf/endver/.

EXFOR Compilation in CNDC

Jimin Wang, Xi Tao, Yongli Jin, Lile Liu, Zhigang Ge

China Nuclear Data Center, China Institute of Atomic Energy, Beijing, China, 102413

1. Introduction

There are two categories of nuclear data, namely nuclear reaction data and nuclear structure and decay data. The nuclear reaction data contain cross sections and other nuclear reaction quantities induced by neutron, charged-particle and photon beams. The nuclear structure and decay data contain half-life, abundance, intensities and decay energies, etc.

The main nuclear reaction databases include the Computer Index of Nuclear reaction Data (CINDA), Evaluated Nuclear Data File (ENDF), Evaluated Nuclear Structure Data File (ENSDF),and the Experimental Nuclear Reaction Data Library (EXFOR). CINDA contains bibliographic references to measurements, calculations, reviews, and evaluations of neutron cross-sections and other microscopic neutron data. ENDF contains recommended, evaluated cross sections, spectra, angular distributions, fission product yields, photo-atomic and thermal scattering law data, with emphasis on neutron induced reactions. ENSDF provides recommended unclear structure and decay information.

The EXFOR library has become the most comprehensive compilation of microscopic experimental nuclear reaction data [1]. It contains cross sections and other nuclear reaction quantities induced by neutron, charged-particle and photon beams.

Compilation is mandatory for all low and intermediate energy ($\leq$1GeV) neutron and light charged-particle (A$\leq$12) induced reaction data. Heavy-ion (A$\geq$13) and photon induced reaction data are also compiled on a voluntary basis.

Currently 13 data centers participate in the International Network of Nuclear Reaction Data Centers (NRDC) [2] and collaborate mainly for compilation and exchange of experimental data by using the common Exchange Format (EXFOR format) [3] under the auspices of the IAEA Nuclear Data Section (NDS).

2. EXFOR Compilation status

Since China joined IAEA in 1984 and China Nuclear Data Center (CNDC) joined NRDC in 1987, as one specialized center at NRDC, CNDC takes part in scanning Chinese journals and compiling EXFOR entries and collaborating with NRDC, which the experiments were carried out by Chinese researcher, the experiments were measured in China and measurements were published in Chinese journals, compilation of CINDA to microscopic neutron reaction data and related data published in Chinese.

CNDC is respond more than 11 Chinese journals now (**Table 1**), and IAEA NDS assigns EXFOR compilation task from other journals or proceedings, scans the literature and identify articles reporting experimental data, collects measured results and compiles these data and relevant information as EXFOR format.

Table 1: Main Chinese journals of responsibility for CNDC

Journal Name	Former title	Abb.	Language	First issue
Chinese Physics C		CPH/C	English	2007
	High Energy Physics and Nuclear Physics	HEN	English	1987
	High Energy Physics and Nuclear Physics	PHE	Chinese	1977
Atomic Energy Science and Technology		CST	Chinese	1959
Journal of Nuclear and Radiochemistry		HFH	Chinese	1979
Nuclear Physics Review		CNPR	Chinese	1984
Nuclear Techniques		NTC	Chinese	1978
Nuclear Science and Techniques		CNST	English	1989

		CPL	English	1984
Chinese Physics Letters				
Acta Physica Sinica		ASI	English	1933
Chinese Physics B		CPB	English	2008
	Chinese Physics	CP	English	1992
	Acta Physica Sinica (Overseas Edition)	ASI/OE	English	2000
Communication of Nuclear Data Progress		CNDP	English	1989
Chinese Journal of Physics		CHP	English	1963
Chinese Journal of Nuclear Physics		CNP	English	1979

In 1985, IAEA-CP and CNDC held a working meeting about compilation in EXFOR at Huangshan Mountian, China. Some charged particle EXFOR entries were transmitted to IAEA for NRDC communication at this meeting as shown in **Table 2**.The first entry S0001 was compiled by Prof. Youxiang Zhuang. Compilation of neutron entries was started in1989, and the first entry 32501was compiled by Prof. Qichang Liang.

Table 2: CNDC provided charged particle EXFOR entries firstly

Entry	1st Author	Reference	Entry	1st Author	Reference
S0001	Li Zhichang+	J,CST,11,229,1977	S0009	Sun Hancheng+	J,CST,15,185,1981
S0002	Liang Qichang+	J,CST,11,10,1977	S0010	Ma Weiyi+	J,CNP,2,239,1980
S0003	Mao Zhenlin+	C,72LANZH,3,1972	S0012	X.Long	R,NST-001,1985
S0004	Yuan Rongfang+,	J,CNP,3,155,1981	S0014	Tao Zhenlan+	J,CNP,3,242,1981
S0005	Jiang Chenglie+	C,72LANZH,3,1972	S0015	Tao Zhenlan+	J,CST,18,506,1984
S0006	Sun Hancheng+	J,CST,18,329,1984	S0016	Zhu Fuying+	J,CNP,5,166,1983

S0007	Yan Chen+	J,CNP,2,137,1980	S0017	Cai Dunjiu+	W,JIANG,1985

Presently, we have a small group to attend EXFOR compilation work. The group consists of five participants, Prof. Zhigang Ge is the director, Dr. Jimin Wang and Dr. Xi Tao and Dr. Lile Liu are responsible for compiling, and Dr. Yongli Jin is responsible for developing computer software. Each compiler responds to scan 3 journals, and collect the scanning results of all responsible journals. Assignment of neutron and charged particle tasks are discussed in group meetings. After that, upload the information such as the assigned entry No., paper in pdf, author, publication date, delayed date, the compiler and the processing of compilation to our EXFOR compilation managed Website (Fig. 1).

Fig. 1. EXFOR compilation managed Website

Since 2009, CNDC has compiled 175 EXFOR entries as shown in Fig. 2, which included 78neutron and 97 charged particle entries. We can find recently the charged particle induced reaction measurements become more and more. There also remain a lot of charge particle papers in earlier issues of "High Energy Physics and Nuclear Physics" and "Chinese Nuclear Physics" to be compiled in the future.

In 2017, 23 entries have been compiled and 8 entries have been updated up to 27 September. 12 entries were accepted by NDS, and other entries are under checking and correcting, which included 17 neutron and 6 charged particle or heavy-ion induced reactions. We still have more than 39 articles under compiling and 5 entries under checking.

Since 2014, N.Otsuka from IAEA/NDS comes to visit CNDC every year, and concentrates a week for compiling, checking and correcting with our group. That is an efficiency way for EXFOR compilation work. In 2017, during our collaborations, we finalized 12 EXFOR entries and fixed the problem in entry 30997.
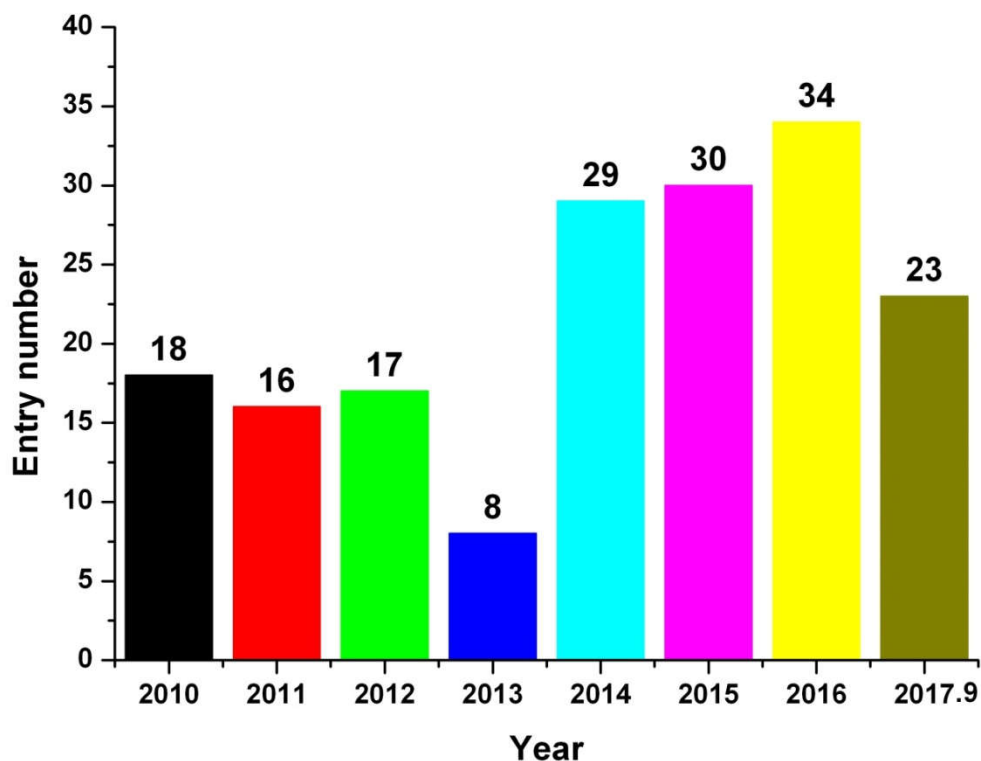
Fig. 2. Compiled EXFOR entries of each year

3. EXFOR Compilation tools

For more than 30 years, CNDC makes great efforts to EXFOR compilation and development of relevant software. In 1993, the ERES code [4] was developed for EXFOR compilation, but now it has been replaced by others.

Since 1997, CNDC devotes to develop software for digitization. The first version of digitization software GDGraph [5] used for reading the numerical data from an image file was developed and released in 2000. It was written using VC++ language. Five years later, much feedback information and bugs of this software were collected. The 2nd version of GDGraph was released in2006, in which the whole software was re-written using Perl computer language to obtain more comfortable conditions for programming and updating. The versions of 3.0, 4.0, 5.0 and 5.1 were released in2011, 2012, 2013 and 2016, respectively. Zoom in the active axis point with magnify glass function was shown in Fig. 3.

Nuclear data plotting software NDPlot was developed by Dr. Yongli Jin in 2017 for upgrading code TT. The code TT is the window plotting software and released in 2002. The features of NDPlot are introduced in this proceeding by Dr. Yongli Jin at another report.
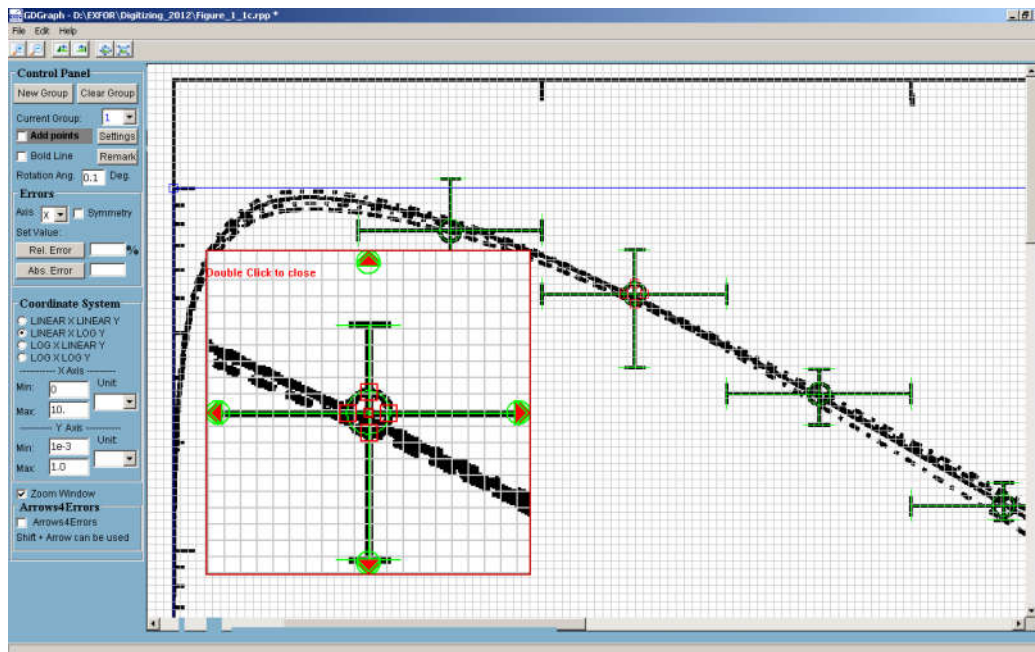
Fig. 3. Magnify glass function

4. Nuclear Data Service

CNDC provides the nuclear data service in China for different institutes, schools or other requirements. CNDC joined the developing of Chinese basic database and established a "The Database of Nuclear Physics" Website (Fig. 4) including experimental data (EXFOR), evaluated data, nuclear structure and decay data, astrophysical data and nuclear data for medical applications for online retrieving and plotting, and the Website is "www.nuclear.csdb.cn".

CNDC also established the mirror site [6] of IAEA-NDS on 31 August, 2013, which Website is "www-nds.ciae.ac.cn". The database of this mirror site is updated with IAEA-NDS Website at the same time. Up to now, the contents of mirror site include EXFOR database and evaluation database, and the contents will be enriched in the future.

Fig. 4. Homepage of "The Database of Nuclear Physics"

5. Conclusion

The needs for experimental nuclear reaction data are always growing. CNDC response to scan, collect and compile the measurements and its information which were carried out by Chinese researchers, measured in China and published in Chinese journals, and related data published in Chinese. Presently, CNDC has a small group to attend EXFOR compilation and relevant code development, and construct an EXFOR compilation managed Website for EXFOR compilation organization. CNDC provides the nuclear data service in China. CNDC will continue to collaborate with NRDC on EXFOR compilation, software development, data evaluation, etc.

References

[1] N.Otsuka et al.,"Towards a More Complete and Accurate Experimental Nuclear Reaction Data Library(EXFOR): International Collaboration Between Nuclear Reaction Data Centres (NRDC)", Nuclear Data Sheets,Vol.120, (2014) pp.272-276.

[2] https://www-nds.iaea.org/nrdc/

[3] N.Otsuka (ed.), IAEA Report IAEA-NDS-207(Rev.2011/01), IAEA, Vienna, Austria (2011).

[4] Li Shubing, Liang Qichang, Liu Tingjin, ERES A PC Program for Nuclear Data Compilation in EXFOR Format, IAEA-NDS-151, (1994).

[5] GDGraph 5.1 Manual, a tool for digitization of graph image, prepared by JIN Yongli and CHEN Guochang, IAEA-NDS-216, (2016).

[6] Chen Guochang, Wang Jimin, Tao Xi, Zhuang Youxiang, Ge Zhigang, "Recent EXFOR Compilation in CNDC", INDC(CPR)-062, (2016) pp.81-85.

Some Possibilities of Radioisotope Production in Low Energy Accelerators and Small Sized Reactors

Ch.Saikhanbayar[1*], G.Khuukhenkhuu[1] and G. Munkh-Erdene[2]

[1]*Nuclear Research Center, National University of Mongolia, Ulaanbaatar, Mongolia*

[2]*Executive Office of the Nuclear Energy Commission, Ulaanbaatar, Mongolia*

A comparative analysis for some possibilities of medical radioisotope production in the low energy electron accelerator, cyclotron, and small sized reactors is carried out to choose, in future, a suitable installation for medical purpose in Mongolia.

1. Introduction

Radioisotopes are widely used in medicine, industry, scientific research, and many other fields. In medicine, for example, radioisotopes are utilized to provide diagnostic information about the functioning of a person`s specific organs, or to treat them, and for sterilization of medical equipment.

Nuclear medicine first became recognized in 1946 when Sam Seidlin in the *Journal of the American Medical Association* reported on the success of radioactive iodine (I-131) in treating a patient with advanced thyroid cancer [1]. By the 1950s, the clinical use of nuclear medicine had become widespread as researchers increased their understanding of detecting radioactivity and using radionuclides to monitor biochemical processes. In Mongolia, nuclear medicine first introduced in 1975 when nuclear medicine department is first established in the First State Central hospital. Nuclear medicine department has been responsible for providing diagnostic procedures and radioisotope therapy to patients. The number of diagnostic procedures and radioisotope therapy have been increasing every year in Mongolia.

Medical radioisotopes are produced on nuclear reactors and accelerators. Mongolia, which has neither reactor, nor enough intensive accelerator to produce radioisotopes, imports these ones from other producer country. Many difficulties occur while radioisotopes are imported. Most radioisotopes, which are used in medicine, have

---

short half-lives. So, they will be lost quantity of radioactivity due to radioactive decay during transportation. Also, transportation cost is high and sometimes may occur delays in delivery system.

In this work, we carried out a comparative analysis for some possibilities of radioisotope production in the low energy electron accelerator, cyclotron, and small sized reactors to choose, in future, a suitable installation for medical purpose in Mongolia.

2. Medical radioisotope production methods

In the nuclear medicine department, ^{99}Mo-^{99m}Tc and ^{131}I isotopes are currently used and imported frequently from Korean Samyoung Unitech Co. Ltd (see Table 1). Actual cost of $500 mCi$ technetium generator is 900\$. But it requires additional 900\$ for transportation from Korea to Mongolia. This is an example of high cost transportation.

Table 1: Information of radioisotopes used in the Nuclear medicine department, First State Central Hospital, Mongolia.

Isotope	Medical Use	Dose, mCi	Period to buy	Cost, \$	Provider
^{99m}Tc	For diagnostic procedure	500	Once in every two weeks	1800	Samyoung Unitech Co. Ltd
^{131}I	For radioisotope therapy	800	Once in 2 months	2500	

Most short-lived isotope ^{99m}Tc ($T_{1/2} = 6h$) is derived from decay of parent isotope^{99}Mo, which is accounting for about 80% of all nuclear medicine procedures worldwide [2]. Because the half-life of ^{99}Mo is about 66 hours, chemical processing, storage and shipment of ^{99}Mo can be extended by an order of magnitude compared to the direct production of ^{99m}Tc.

Two commercial and proven methods to produce^{99}Mo isotopes there are: via fission reaction of ^{235}U in nuclear reactor, which produces ^{99}Mo and other medically important isotopes such as ^{131}I and ^{133}Xe, and the neutron capture reaction of ^{98}Mo to produce ^{99}Mo in nuclear reactor. Over 95% of the ^{99}Mo is produced by the fission of ^{235}U targets in nuclear reactor worldwide [3]. Two types of the ^{235}U targets there are in this production method, which are highly enriched uranium (HEU, isotopic abundance

of ^{235}U is $\geq 20\%$) and low enriched uranium (LEU, isotopic abundance of ^{235}U is $< 20\%$) targets. Nowadays, almost all of the major ^{99}Mo producers utilize HEU targets. The specific activity of ^{99}Mo obtained from HEU targets is very high compared to LEU or other possible methods. This obtainable high specific activity makes this uranium fission technology the leading method of ^{99}Mo production. Disadvantage of this method is, for example, that irradiated targets contain not only ^{99}Mo, but highly radioactive isotopes from fission fragments, also. Because of this, chemical processing is very complex and must be operated inside large and heavily radiation shielded building. During irradiation about 5% of the ^{235}U in the targets are typically consumed. Thus, a large amount of HEU is left in the waste after chemical processing. This HEU could be recovered for reuse, but currently no producer has active plan to do [4].

^{99}Mo production via neutron activation method using the ^{98}Mo(n,ɣ)^{99}Mo reaction is the second proven technology without using the uranium-235 target. The thermal neutron cross section of the ^{98}Mo(n,ɣ)^{99}Mo reaction is only about $0.13 barn$ compared to fission cross section of ^{235}U, which is about $584 barn$ [2]. Because of the low reaction cross section, production of low specific activities of ^{99}Mo can be obtained.^{99}Mo production based on this method is being carried out in several countries (India, Kazakhstan, Uzbekistan, Vietnam, Russia, China and etc.) to supply small scale production for domestic use. In this method natural molybdenum trioxide (MoO$_3$) powder target is commonly used. Natural abundance of ^{98}Mo isotope is 24.13%. The enriched ^{98}Mo target would produce 4-5 times higher ^{99}Mo compared to the natural^{98}Mo target. Because of molybdenum enrichment is much expensive, there is tendency to utilize natural Mo targets. Chemical processing in irradiated target is relatively simple and also no high-level radioactive waste is formed thorough this method.

In 2009, the temporary shutdown of two main producer reactors caused a global shortage of ^{99}Mo. Since the 2009 shortage there has been interest in new ways to produce ^{99}Mo-^{99m}Tc [5]. There are several potential methods for the production of ^{99}Mo and ^{99m}Tc from accelerators. But recently, two of the accelerator based methods are being studied and considered largely by scientists, committee and major radioisotope producers. The direct production of ^{99m}Tc using cyclotron is one of the proposed alternatives that utilized the ^{100}Mo(p,2n) ^{99m}Tc reaction on highly ^{100}Mo-enriched target material. Cyclotrons are mostly used to produce proton-rich medical radioisotopes, the most are ^{18}F, ^{15}O, ^{11}C and ^{13}N. Through this method direct^{99m}Tc is produced, because of only $6h$ half-life of ^{99m}Tc, distribution to another country is difficult. Cyclotron production of ^{99m}Tc is possible to provide a suitable

amount of activity to supply most local and regional needs. Cyclotron-produced ^{99m}Tc is currently undergoing clinical trials and it is anticipated that this method will be used in clinical applications within the next few years [6].Another method based on the accelerator is the use of the ^{100}Mo(ɣ,n)^{99}Mo reaction with^{100}Mo target. The photonuclear reaction method was described by many scientist [7-9]. However, this method is still on the stage of laboratory research.

3. Formulae and results

3.1. Theoretical formulae for activity estimation

When a nuclide, that is being produced in an accelerator or nuclear reactor, is radioactive, it will further decay to its daughter nucleus. Thus, the decay rate can be written in the following form:

$$\frac{dN}{dt} = Y - \lambda N ,$$ (1)

Where Y is the reaction yield, λ is the radioactive decay constant ($\lambda = \ln 2 / T_{1/2}$;$T_{1/2}$ is the half-life of current isotope), and N is the number of produced radioactive nuclei. Solution of (1) can be written in following form:

$$N = \frac{Y}{\lambda}(1 - e^{-\lambda t}) .$$ (2)

Expression (2) is the number of radioactive nuclei at the end of the irradiation. Thus, the activity is presented by:

$$A = \lambda N = Y(1 - e^{-\lambda t}) .$$ (3)

The number of target nuclei is being decreased during irradiation. Change of this reduction depends on long irradiation time, high particle flux and reaction cross section. If target material is irradiated in high flux nuclear reactor, then this change must be considered in the following way. The number of produced radioactive nuclei due to neutron induced reaction in high flux nuclear reactor is described by:

$$\frac{dN}{dt} = \sigma \cdot \phi \cdot (N_0 - N) .$$ (4)

Here: N_0 is the number of target nuclei, σ is the reaction cross section, and ϕ is the flux of bombarding particle.

To find solution of the equation (4) following conditions must be considered. When irradiation time is $t = 0$, the number of produced radioactive nuclei $N = 0$, and when $t \to \infty$, the number of produced radioactive nuclei would be $N \to N_0$. In this case the solution of (4) is given by [10]:

$$N = N_0 \cdot (1 - e^{-\sigma \cdot \phi \cdot t}). \tag{5}$$

In our case we can consider $N_0 = const$, because of irradiation is carried out in the small sized nuclear reactor for not so long time. Then the reaction yield is described as:

$$Y = N_0 \cdot \sigma \cdot \phi. \tag{6}$$

In this case the activity of produced radioactive nuclei (3) is expressed as following:

$$A = Y(1 - e^{-\lambda t}) = N_0 \cdot \sigma \cdot \phi \cdot (1 - e^{-\lambda t}). \tag{7}$$

When spectrum of gamma-quanta or particle projectiles is continuum the reaction yield is determined as [11]:

$$Y = N_0 \cdot \int_{E_{th}}^{E_{max}} \sigma(E) \cdot \phi(E, E_{max}) dE. \tag{8}$$

Here: E_{max} is the maximum energy of gamma-quanta or particle, and E_{th} is the reaction threshold energy.

In this case formula (3) is rewritten as:

$$A = N_0 \cdot (1 - e^{-\lambda t}) \cdot \int_{E_{th}}^{E_{max}} \sigma(E) \cdot \phi(E, E_{max}) dE. \tag{9}$$

The number of target nuclei can be expressed as:

$$N_0 = \frac{N_A \cdot m}{M} \cdot \theta. \tag{10}$$

Here: N_A is the Avogadro's number, m is the mass of target material, M is the molecular mass, and θ is the isotopic abundance of target nuclei.

Using these formulae, the estimations of ^{99}Mo production should be calculated in the following subsection.

3.2. Estimation of ^{99}Mo production rate in small sized reactor

As an example, estimation of ^{99}Mo production via the neutron capture ^{98}Mo(n,γ)^{99}Mo reaction will be calculated for $500kW$ nuclear research reactor. According to information about producing ^{99}Mo in nuclear reactor, suitable time of 7 days irradiation was chosen. Target material is MoO$_3$ powder with purity $> 99\%$. Thermal neutron flux is $2 \cdot 10^{13}$ n/(cm^2·s) [12]. Some important data for calculation are given in Table 2.

Table 2: Data for calculation.

Producing isotope	Half-life, (h) [13]	Target material (mass)	$\sigma (barn)$ [2]	Irradiation time, t	$\phi(\dfrac{n}{cm^2 \cdot s})$
^{99}Mo	65.94	MoO$_3$ ($100g$)	0.13	7 days	$2 \cdot 10^{13}$

For irradiation in the reactor the activity of produced radioactive nuclei is calculated by equation (7). First of all, the number of target nuclei can be found by (10):

$$N_0 = \frac{N_A \cdot m}{M} \cdot \theta = 1.01 \cdot 10^{23}.$$

Here: $m = 66.7g$ is the pure molybdenum mass from $100g$ powder target. $M = 95.96g / mole$ is the molecular mass of molybdenum. $\theta = 0.2413$ is the natural abundance of ^{98}Mo target nuclei.

The activity of ^{99}Mo is calculated using the data from Table 2 and N_0 by formula (7):

$$A = N_0 \cdot \sigma \cdot \phi \cdot (1 - e^{-\lambda t}) = 2.2 \cdot 10^{11} Bq \approx 6Ci.$$

Here: $N_0 = 1.01 \cdot 10^{23}$, $\sigma = 0.13 \cdot 10^{-24} cm^2$, $\phi = 2 \cdot 10^{13} n / cm^2 \cdot s$, $\lambda = \ln 2 / T_{1/2}$,

$T_{1/2} = 65.94h$ and $t = 7 \cdot 24 = 168h$.

It means that at the end of the irradiation the activity of ^{99}Mo from $100g$ MoO$_3$ target material was determined as $A \approx 6Ci$.

To check our calculation method the following calculation was made using the IAEA TECDOC [13] information. In $100MW$ DHRUVA reactor with neutron flux of $1.6 \cdot 10^{14} n / cm^2 \cdot s$ MoO$_3$ powder material ($90g$ -$120g$) was irradiated in 1 week and yield of ^{99}Mo at the end of the irradiation was $40Ci$. The yield of ^{99}Mo was calculated by formula (7) using these data:

$$A = N_0 \cdot \sigma \cdot \phi \cdot (1 - e^{-\lambda t}) = 1.74 \cdot 10^{12} Bq \approx 47Ci.$$

This value of activity is satisfactorily in agreement with the given data of $40Ci$. It means that our formulae can be used to determine the activity of produced radioactive nuclei.

By repeating above calculation, let's determine ^{99}Mo production rate using about 95% enriched MoO$_3$ target material. In this case the number of target nuclei is:

$$N_0 = \frac{N_A \cdot m}{M} \cdot \theta \approx 4 \cdot 10^{23}.$$

Here: $\theta = 0.95$.

^{99}Mo production rate can be determined by (7) using the data from Table 2 and N_0. Due to enrichment in target material, only the number of target nuclei was changed. The values of other quantities are the same as in previous estimation. Then, activity of produced ^{99}Mo is:

$$A = N_0 \cdot \sigma \cdot \phi \cdot (1 - e^{-\lambda t}) = 8.6 \cdot 10^{11} Bq \approx 23Ci.$$

According to above two calculations, it is seen that the activity of produced ^{99}Mo can be increased by $23 / 6 \approx 4$ times if enriched target material is used. In some references [14] it was informed that by using targets made from enriched ^{98}Mo increases activity by 4-8 times depending on neutron flux.

In the nuclear medicine department, $500mCi$ ($0.5Ci$) ^{99}Mo-^{99m}Tc generator is utilized to provide around 100 diagnostic procedures within 2 weeks. $6Ci$ and $23Ci$ activities of ^{99}Mo can be utilized to provide around 1200 and 4600 diagnostic procedures, respectively.

3.3. Estimation of ^{99}Mo production rate in 24 MeV electron accelerator

We will carry out estimation using the data of bremsstrahlung gamma-rays produced, as an example, by electron accelerator MT-25 at the Flerov Laboratory of Nuclear Reactions, Joint Institute for Nuclear Research in Russia. When spectrum of gamma-quanta is continuum (for bremsstrahlung sources) the reaction yield is determined by formula (8). To simplify the calculation, we will use the following approximation:

$$\int_{E_{th}}^{E_{max}} \sigma(E) \cdot \phi(E, E_{max}) dE = \overline{\sigma} \cdot \phi_\gamma .$$

Here: $\overline{\sigma}$ is the average reaction cross section, and ϕ_γ is the bremsstrahlung gamma-rays flux.

Average reaction cross section $\overline{\sigma}$ is determined as:

$$\overline{\sigma} = \frac{1}{E_{max} - E_{th}} \int_{E_{th}}^{E_{max}} \sigma(E) dE = \frac{1}{E_{max} - E_{th}} \cdot \sigma_{int}$$

Here: σ_{int} is the integrated cross section.

For ^{100}Mo(ɣ,n)^{99}Mo reaction integrated cross section is given as $811 MeV \cdot mbarn$ [15]. Thus, average reaction cross section $\overline{\sigma}$ is:

$$\overline{\sigma} = \frac{1}{E_{max} - E_{th}} \cdot \sigma_{int} = 51.6 mbarn .$$

Here: $E_{max} = 24 MeV$, and $E_{th} = 8.29 MeV$.

Then, formula (9) was rewritten in the following form:

$$A = N_0 \cdot \overline{\sigma} \cdot \phi_\gamma \cdot (1 - e^{-\lambda t}) . \tag{11}$$

In reference [16], the bremsstrahlung flux was determined as $\phi_\gamma = 5.54 \cdot 10^{13} \gamma / cm^2 \cdot s$ at maximum energy of $24 MeV$.

Natural $100g$ Mo foil target (9.6% ^{100}Mo) and enriched $100g$ ^{100}MoO$_3$ (95% ^{100}Mo) powder target were used for calculation. For natural Mo foil target, the number of

target nuclei is:

$$N_0 = \frac{N_A \cdot m}{M} \cdot \theta = 6.02 \cdot 10^{22} .$$

For enriched MoO$_3$ powder target, the number of target nuclei is:

$$N_0 = \frac{N_A \cdot m}{M} \cdot \theta = 4 \cdot 10^{23} .$$

The activity of produced ^{99}Mo was determined by formula (11) for natural Mo foil target in 12 hours irradiation:

$$A = N_0 \cdot \overline{\sigma} \cdot \phi_\gamma \cdot (1 - e^{-\lambda t}) = 2 \cdot 10^{10} \approx 0.6 Ci .$$

Here: $N_0 = 6.02 \cdot 10^{22} , \overline{\sigma} = 51.6 \cdot 10^{-27} cm^2 , \phi_\gamma = 5.54 \cdot 10^{13} \gamma / cm^2 \cdot s , T_{1/2} = 65.94h$, and $t = 12h$.

For enriched MoO$_3$ powder target the activity of produced ^{99}Mo was determined by formula (11) in 12 hours irradiation:

$$A = N_0 \cdot \overline{\sigma} \cdot \phi_\gamma \cdot (1 - e^{-\lambda t}) = 1.4 \cdot 10^{11} Bq \approx 3.8 Ci .$$

The $0.6 Ci$ and $3.8 Ci$ activities of ^{99}Mo can be utilized to provide around 120 and 760 diagnostic procedures, respectively.

3.4. Estimation of direct ^{99m}Tc production rate in cyclotron

The following data ($18 MeV$ protons, $250 \mu A$, $6h$ irradiation) obtained on the cyclotron was used for calculating the activity of ^{99m}Tc according to [17]. ^{100}Mo(p,2n)^{99m}Tc reaction cross section is about $220 mbarn$ at $18 MeV$ proton energy [6]. $18 MeV$ $3.4 \cdot 10^{19}$ protons were generated in cyclotron during $6h$ irradiation at $250 \mu A$. In reference [17] the diameter of enriched $1.5g$ ^{100}Mo disk was given $17 mm$. Then, using above data, the proton flux is determined as:

$$\phi = \frac{N_p}{t \cdot S} = 6.9 \cdot 10^{14} \frac{p}{cm^2 \cdot s}$$

Here: $N_P = 3.4 \cdot 10^{19}$, $t = 21600 s$, and $S = 2.27 cm^2$.

The number of target nuclei in enriched 1.5g ^{100}Mo disk was determined by formula (10):

$$N_0 = \frac{N_A \cdot m}{M} \cdot \theta = 8.9 \cdot 10^{21}.$$

The activity of direct produced ^{99m}Tc was determined by:

$$A = N_0 \cdot \sigma \cdot \phi \cdot (1 - e^{-\lambda t}) = 6.8 \cdot 10^{11} Bq \approx 18.4 Ci.$$

Here: $N_0 = 8.9 \cdot 10^{21}$, $\sigma = 220 \cdot 10^{-27} cm^2$, $\phi = 6.9 \cdot 10^{14} p/cm^2 \cdot s$, $T_{1/2} = 6h$, and $t = 6h$.

This quantity of ^{99m}Tc can be utilized to provide around 600 diagnostic procedures.

4. Discussion and conclusions

We carried out the estimations of ^{99}Mo and ^{99m}Tc production rate in $500 kW$ nuclear reactor, $24 MeV$ electron accelerator and $18 MeV$ cyclotron. Depending on target enrichment the ^{99}Mo production rate was estimated $6 Ci$ and $23 Ci$ in $500 kW$ nuclear reactor, $0.6 Ci$ and $3.8 Ci$ in $24 MeV$ electron accelerator, and $18.4 Ci$ in $18 MeV$ cyclotron respectively. Our current supply of ^{99}Mo-^{99m}Tc generator is 2 generators of each $500 mCi$ in 1 month. According to this information, current supply can be produced $0.6 Ci$ in two $24h$ irradiation in electron accelerator. But accelerator production methods are still on the stage of laboratory research. Nowadays, ^{99}Mo production via neutron activation method in the small sized nuclear reactor is only suitable method for domestic use in Mongolia.

References

[1] Dr. Ananya Mandal, History of nuclear medicine. https://www.news-medical.net/health/History-of-Nuclear-Medicine.aspx.

[2] IAEA Nuclear energy series No. NF-T-5.4, Non-HEU production technologies for molybdenum-99 and technetium-99m, Vienna (2013), p.1.

[3] Production and supply of molybdenum-99. https://www.iaea.org/About/Policy/GC/GC54/GC54InfDocuments/English/gc54inf-3-att7_en.pdf.

[4] Medical Isotope Production Without Highly Enriched Uranium, Committee on Medical Isotope Production Without Highly Enriched Uranium and National Research Council(2009),p.29.

[5] Carl Ross *et al*. *La Physique au CANADA*. vol.66, No.1, (2010) p.19.

[6] IAEA Radioisotopes and Radiopharmaceuticals Reports No.2, Cyclotron based production of technetium-99m, Vienna (2017), p.8.

[7] A.V. Sabel'nikov *et al*., *Radiochem*. vol.48, No.2, (2006), p.191.

[8] Y. Danon, R. Block, and J. Harvey, *Trans. Am. Nucl. Soc.* vol.103, (2010), p.1081.

[9] P. Tkac, D. A. Rotsch, M. A. Brown, V. Makarashvili, and G. F. Vandegrift, in *Proceedings of the 2015 Mo-99 Topical Meeting, Boston, Massachusetts,* (2015).

[10] G. Khuukhenkhuu and M. Odsuren, Fast neutron induced nuclear reaction cross section, Munkhiin Useg Group Co.L. Press, Ulaanbaatar (2010), p.141.

[11] Bezshyyko O.A., Golinka-Bezshyyko L.O., Kadenko I.M. *et al*.Proc. of the 2-nd Int. Conf. "Current Problems in Nuclear Physics and Atomic Energy" (June 9 - 15, Kyiv, Ukraine, 2008), vol.I. (2009), p.252.

[12] Le Van So, Proceedings of the International Symposium on Nuclear Research Reactors-Operation, Utilization and Trends(2004), p.1.

[13] IAEA-TECDOC-1340, Manual for reactor produced radioisotopes, Vienna (2003), p.141.

[14] TECHNICAL REPORTS SERIES No. 478, Feasibility of producing molybdenum-99 on a small scale using fission of low enriched uranium or neutron activation of natural molybdenum, IAEA Vienna (2015), p.98.

[15] A.V. Varlamov *et al*. INDC(NDS)-394, (1999), p.17.

[16] Tran Duc Theip *et al*. Письма в ЭЧАЯ.vol.2, No.4 (127), (2005), p.53.

[17] P. Schaffer *et al*.*Physics Procedia,*vol.66, (2015),p.383.

Resonance States in the Simple Schematic Two-Body Model

D.Dolzodmaa[1], G.Khuukhenkhuu[1], K.Katō[2], S.Davaa[1], M.Odsuren[1]

[1]*School of Engineering and Applied Sciences and Nuclear Research Center, National University of Mongolia, Ulaanbaatar 210646, Mongolia*
[2]*Nuclear Reaction Data Centre, Faculty of Science, Hokkaido University, Sapporo 060-0810, Japan*

1. Introduction

During the last several decades resonance problems have covered an important and crucial research area in nuclear physics. Recently, it has attracted much attention that the complex scaling method (CSM) [1-2] is successfully utilized for description of many-body resonant states in light and middle mass nuclei. Although many problems have been solved so far, but further researches are required still.

In this study, the complex scaling method is applied to a simple schematic two-body model [3] and its reliability is confirmed. For this purpose, several resonance states of $J^\pi = 0^+$ and 1^- partial waves are investigated using the simple schematic potential.

2. Complex Scaling Method

The CSM has been proposed to solve the resonance states in the similar way as bound state problems. In the CSM, the distance of the relative coordinate is rotated as $r \longrightarrow re^{i\theta}$ in the complex coordinate planeby introducing a real parameter θ. Therefore, the *Schrödinger* equation

$$\widehat{H}|\Psi\rangle = E|\Psi\rangle \tag{1}$$

is rewritten as

$$\widehat{H}(\theta)|\Psi^\theta\rangle = E^\theta|\Psi^\theta\rangle, \tag{2}$$

where $\widehat{H}(\theta)$ and Ψ^θ are the complex scaled Hamiltonian and the wave function, respectively. $U(\theta)$ operates on a function Ψ, that is,

$$\Psi^\theta = U(\theta)\Psi(r) = e^{\frac{3}{2}i\theta}\Psi(re^{i\theta}). \tag{3}$$

The eigenvalues and eigenstates are obtained by solving the complex scaled

Schrödinger equation Eq.(2). The eigenvalues of resonance states are found as $E^\theta = E_r - i\Gamma_r/2$, where E_r is resonance energy and Γ_r-width of the resonant state. More detailed explanation of the CSM is given in Refs.[1, 2]. The complex scaled Hamiltonian of inter cluster motion is given by

$$\hat{H}(\theta) = U(\theta)\hat{H}U^{-1}(\theta). \tag{4}$$

3. Results and Discussions

The Hamiltonian of the present model is given as

$$H = -\frac{\hbar^2}{2\mu}\nabla^2 + V(r), \tag{5}$$

where

$$V(r) = -8.0\exp(-0.16r^2) + 4.0\exp(-0.04r^2). \tag{6}$$

For simplicity, we put $\frac{\hbar^2}{\mu} = 1$ (MeV fm^2). This potential introduced in Ref. [3] has an attractive pocket in a short range but a repulsive barrier at a large distance. Putting Eq.(6) in Eq.(5), we solve the *Schrödinger* equation (Eq.(2)).To solve the Eq. (2), we employ the Gaussian basis functions given as

$$u_i(\hat{r}) = N_l(b_i)r^l \exp\left(-\frac{1}{2b_i^2}r^2\right)Y_{lm}(\hat{r}), \tag{7}$$

where the range parameters are given by a geometric progression as $b_i = b_0\gamma^{i-1}$, $i = 1,2,\dots,N$.

In this calculation, we apply $N = 20$ and employ the optimal values of b_0 and γ to obtain stationary resonance solutions.

In Tables 1 and 2, we show numerical values of the calculated bound and resonant states for the $J^\pi = 0^+$ and 1^- wavesrespectively, and compare to the results (left) that takes from the Ref. [4].
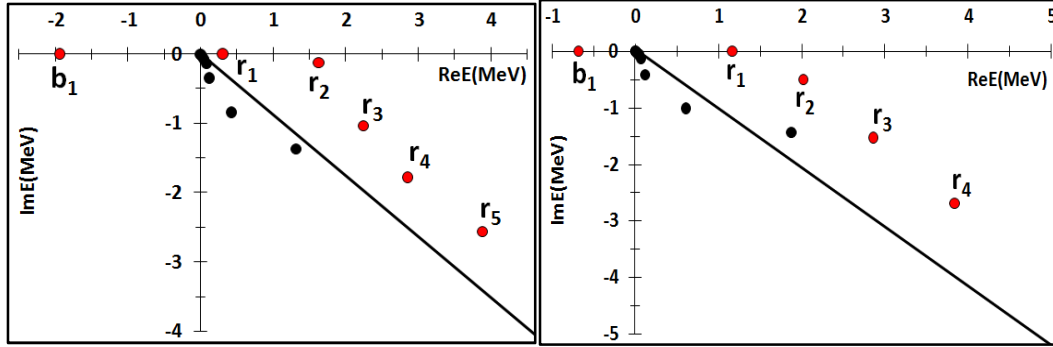
Fig. 1. Distribution of energy eigenvalues of the $J^{\pi} = 0^+$ wave. Symbols (b_1) and (r_1, r_2, r_3, r_4, r_5) represent bound and resonance solutions, respectively. We here employ scaling angle $\theta = 15^0$. The solid line from the origin indicates the so-called 2θ line describing the branch cut.

Fig. 2. Distribution of energy eigenvalues of the $J^{\pi} = 1^-$ wave. Symbols (b_1) and (r_1, r_2, r_3, r_4) represent bound and resonance solutions, respectively. We here employ scaling angle $\theta = 15^0$. The solid line from the origin indicates the so-called 2θ line describing the branch cut.

Table 1: Bound and resonance states energies with decay widths calculated for the $J^{\pi} = 0^+$ wave.

0^+ wave*		0^+ wave	
E(MeV)	State	E(MeV)	State
-1.928	Bound	-1.928	Bound
$0.310-i10^{-6}$	Resonance	$0.310-i10^{-6}$	Resonance
$1.632-i0.123$	Resonance	$1.633-i0.123$	Resonance
$2.249-i1.040$	Resonance	$2.249-i1.075$	Resonance
$2.854-i2.570$	Resonance	$2.850-i1.800$	Resonance
		$3.875-i2.575$	Resonance

*From previous data [4]

70

Table 2: Bound and resonance energies with decay widths calculated for the $J^\pi = 1^-$ state.

1^- wave*		1^- wave	
E(MeV)	State	E(MeV)	State
-0.675	Bound	-0.675	Bound
1.171-i0.005	Resonance	1.171-i0.005	Resonance
2.031-i0.489	Resonance	2.018-i0.493	Resonance
2.832-i1.199	Resonance	2.830-i1.510	Resonance
3.934-i1.788	Resonance	3.655-i2.500	Resonance

*From previous data [4]

It can be seen that from Tables 1 and 2, two calculated results are similar to each other.

Summary

In this study, we employed the simple potential model which gives a bound and several resonance states for $J^\pi = 0^+$ and 1^- waves. Present calculated results are compared with the previous calculated result and we obtained both results are similar to each other.

References

[1] Y.K.Ho, Phys. Rep. **99**, (1983), 1.
[2] T.Myo, Y. Kikuchi, H. Masui, K.Katō, Prog. Part. Nucl.Phys. **79**, (2014), 1
[3] A. Csótó, B. Gyarmati, A. T. Kruppa, K. F. Pál, and N. Moiseyev,Phys. Rev. A **41**, (1990), 3469
[4] M. Odsuren, K. Kato, M. Aikawa, Nucl. Data Sheets **120**, (2014), 126

Alpha Cluster Formation Probability in (n,α) Reaction Induced by Fast Neutrons

G.Khuukhenkhuu[1], M.Odsuren[1,2], B.Batchimeg[1] and J.Munkhsaikhan[1]

[1]*Nuclear Research Center, National University of Mongolia, Ulaanbaatar, Mongolia*

[2]*School of Engineering and Applied Sciences, National University of Mongolia, Ulaanbaatar, Mongolia*

Alpha-clustering in nuclei is one of the important subjects for nuclear structure and reaction study. Many authors investigated the α-clustering effect for a long time using the different methods and theoretical approaches to this problem. However, solid theoretical explanation of the α-clustering in nuclei has not formed yet. In this work we suggest three methods to estimate α-clustering probability for fast neutron induced (n,α) reaction. The statistical model and knock-on mechanism are used in our calculations. Our results are compared with values of the α-clustering factor obtained by other authors.

1. Introduction

The alpha clustering in nuclei, one of the important subjects in the nuclear structure and reaction study [1], has been studied for a long time. Also, study of the α-cluster formation probability, Φ_α, in the fast neutron induced (n,α) reaction is of interest for the nuclear energy application, for example, it is important to estimate helium production, nuclear heating and transmutations in the structural materials of nuclear fusion and fission reactors. One of the many attempts to investigate this phenomena is the evaluation of the α-cluster formation probability, which was calculated by many authors using the different methods. Bonnetti and Milazzo-Colli [2] found the α-cluster formation factor using the preformed alpha particle model. W.M.Seif *et al.* [3] obtained the clustering probability by the ratio of the half-life, calculated by density dependent cluster model, to the experimental one. Popov *et al.* [4-6] have obtained the clustering factors from the experimental data of (n,α) reactions for resonance neutrons. Saad M. Saleh Ahmed [7] calculated the α-cluster formation

probability using the energy dependent formula derived from the formulation of clusterization states representation and the hypothesized cluster-formation model. Unfortunately, consistent and common opinion for theoretical explanation of the α-clustering in nuclei up to now is no available.

In this work, using the statistical model and knock-on mechanism, we suggest three methods to estimate α-clustering probability for fast neutron induced (n,α) reaction:

- Normalization of the theoretical (n,α) cross section to experimental data;
- Comparison of (n,α) and (n,p) cross sections;
- Calculation of α-clustering probability using the (n,α) cross sections and the total neutron cross sections for the ^{4}He.

In Section II, we have briefly explained the theoretical bases of study. In Section III, we give the obtained results and discussions, where the comparison of our result with the values obtained by other authors are done. Finally, in Section IV, conclusions are given.

2. Theoretical bases of study
2.1. Normalization of the theoretical (n,α) cross section to experimental data

In the framework of the statistical model, the fast neutron induced (n,α) reaction cross section can be expressed [8] as follows:

$$\sigma^{th}(n,\alpha) = C\pi(R + \lambda_n)^2 \exp\left(-K\frac{N-Z+0.5}{A}\right), \tag{1}$$

where

$$C = 2\exp\frac{1}{\Theta}\left(-3\alpha + \beta\left[A^{2/3} - (A-3)^{2/3}\right] + \gamma\left(\frac{Z^2}{A^{1/3}} - \frac{(Z-2)^2}{(A-3)^{1/3}}\right)\varepsilon_\alpha - V_\alpha\right)$$

and

$$K = \frac{2\xi}{\Theta}.$$

Here: $R = r_0 A^{1/3}$ is the target nucleus radius ($r_0 = 1.3 \cdot 10^{-13} cm$); λ_n is the wavelength of the incident neutrons divided by 2π; A, N and Z are the nucleon, neutron and proton numbers in the target nucleus, respectively; $\alpha, \beta, \gamma, \xi$ are the Weizsäcker's constants; ε_α is the internal binding energy of α-particle: $\varepsilon_\alpha =$

28.2MeV; V_α is the daughter nucleus Coulomb potential for α-particle [9]; $\theta = kT$ is the thermodynamic temperature, where k is the Boltzmann constant and T is the absolute temperature.
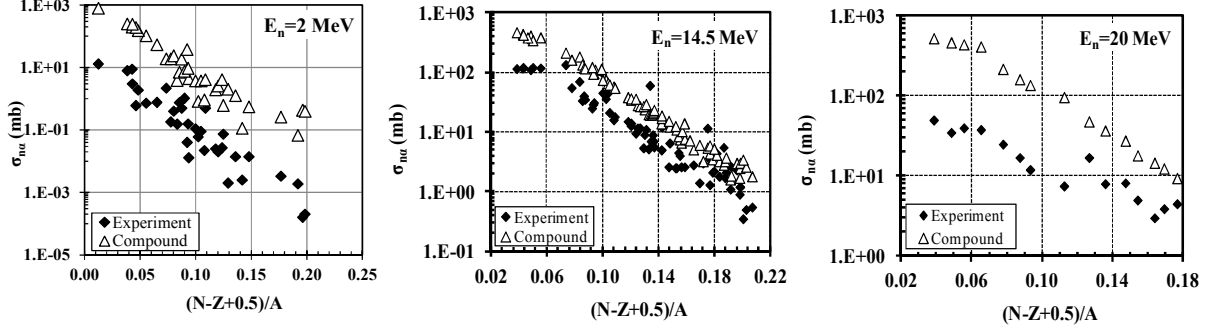
Fig. 1. Comparison of theoretical (n,α) cross sections with experimental data at neutron energies of 2, 14.5 and 20 MeV.

To obtain the formula (1), we used Weisskopf-Ewing evaporation model [10], constant nuclear temperature approximation [11], and Weizsäker's formula [12] for binding energy. However, as shown in Fig.1, it was seen that the theoretical (n,α) cross sections calculated by statistical model formulae was higher than the experimental one. So, it was assumed that these results for (n,α) cross sections are possibly caused by α-clustering effect which was not considered in (1). Therefore, if the clustering effect will be taken into account in (n,α) cross section formula, (1) can be rewritten in the following form:

$$\sigma^{th}(n,\alpha) \cdot \Phi_\alpha = C\pi(R + \lambda_n)^2 \Phi_\alpha \exp\left(-K\frac{N-Z+0.5}{A}\right) = \sigma^{exp}(n,\alpha). \qquad (2)$$

From (2) we can find α-cluster formation probability by ratio of the experimental (n,α) cross section to the theoretical one as:

$$\Phi_\alpha = \frac{\sigma^{exp}(n,\alpha)}{\sigma^{th}(n,\alpha)}. \qquad (3)$$

This formula was used in our first method to obtain the α-cluster formation probability.

2.2. Comparison of (n,α) and (n,p) cross sections

According to Bohr postulate of compound mechanism, the fast neutron induced (n,α) reaction cross section can be written in the following form:

$$\sigma(n,\alpha) = \sigma_c(n)W_\alpha. \tag{4}$$

Here $\sigma_c(n)$ is the compound nucleus formation cross section and W_α is the probability of α-decay of the compound nucleus:

$$W_\alpha = \frac{\Gamma_\alpha}{\Gamma}. \tag{5}$$

On the other hand, by analogy with the formula of (n,α) reaction, the proton emission reaction cross section can be also written as:

$$\sigma(n,p) = \sigma_c(n)\left(\frac{\Gamma_p}{\Gamma}\right). \tag{6}$$

The alpha- and proton-widths of level can be written using the Weisskopf formula [11] and taking into account the α-clustering and p-clustering probabilities as follows:

$$\Gamma_\alpha = \Phi_\alpha \frac{D}{2\pi} T_\alpha \text{ and } \Gamma_p = \Phi_p \frac{D}{2\pi} T_p. \tag{7}$$

Here T_α and T_p are the alpha and proton transmission factors; D is the level spacing.

Then, from formulas (4) - (7) can be obtained following ratio:

$$\frac{\sigma(n,\alpha)}{\sigma(n,p)} = \frac{\Phi_\alpha}{\Phi_p} \cdot \frac{T_\alpha}{T_p} \ .$$

If we assume for proton-clustering probability $\Phi_p = 1$, then the α clustering factor for (n,α) reaction can be expressed by

$$\Phi_\alpha = \left(\frac{T_p}{T_\alpha}\right)\frac{\sigma(n,\alpha)}{\sigma(n,p)}. \tag{8}$$

The formula (8) was used in our second method for determination of the α-cluster formation probability.

75

2.3. Calculation of α-clustering probability using the (n,α) cross sections and the total neutron cross sections for the ^{4}He.

The last method suggested in this work is based on the knock-on mechanism. By analogy of the compound model (4), we assume that the (n,α) cross section can be expressed as two stages process:

$$\sigma(n,\alpha) = \Phi_\alpha \sigma_n^{tot}(^4\text{He}). \tag{9}$$

Here, the (n,α) cross section can be defined by the multiplication of alpha cluster formation probability on the surface of nuclei and total neutron cross section of ^{4}He.

From (9) we can find the *α*-cluster formation factor as

$$\Phi_\alpha = \frac{\sigma^{exp}(n,\alpha)}{\sigma_n^{tot}(^4\text{He})}. \tag{10}$$

For the evaluation of the alpha cluster formation factor, the (n,α) cross section and total neutron cross section of ^{4}He data were extracted from the EXFOR [13].

3. Results and Discussion

3.1. Normalization of the theoretical (n,a) cross section to experimental data
Taking into account the alpha cluster formation probability in the (n,α) cross section, we determined Φ_α, normalizing the theoretical (n,α) cross section to experimental data, which are shown in Fig.2 for $E_n = 2, 14.5, 20$MeV, as examples.
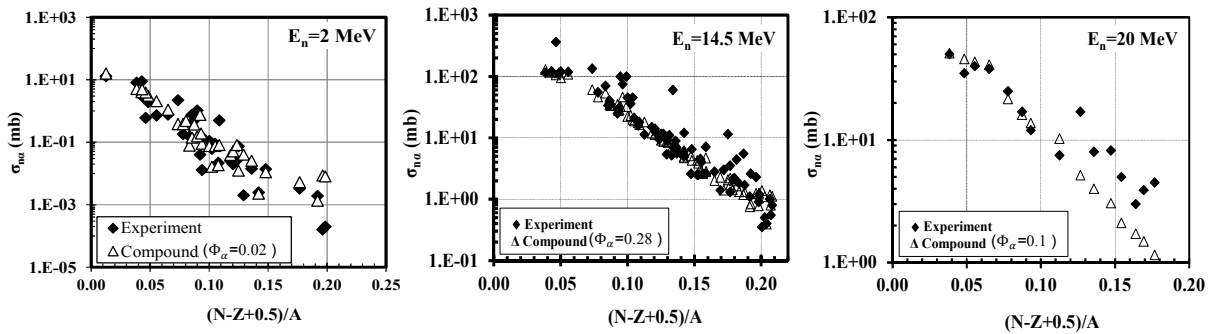

Fig. 2. The normalized theoretical (n,α) cross sections and experimental data at neutron energies of 2, 14.5 and 20 MeV. The values of Φ_α are given in brackets.

Some discrepancy in Fig. 2 between the theoretical and experimental cross sections at

20MeV for the asymmetry parameter (N-Z+0.5)/A>0.12 is, perhaps, caused by contributions from the pre-equilibrium and direct mechanisms to the (n,α) cross sections.

The values of the α-clustering factor, Φ_α, obtained by the normalization of the theoretical cross sections to the experimental ones are given in Appendix 1 for neutron energy of 2 to 20 MeV.

The dependence of the α-clustering factor, Φ_α, on the neutron energy E_n is shown in Fig. 3. It is seen that Φ_α is increasedin the region of $E_n=2\div8$ MeV and is constant around $E_n=8\div13$ MeV. From the $E_n=14.5$ MeV the Φ_α factor is decreased.
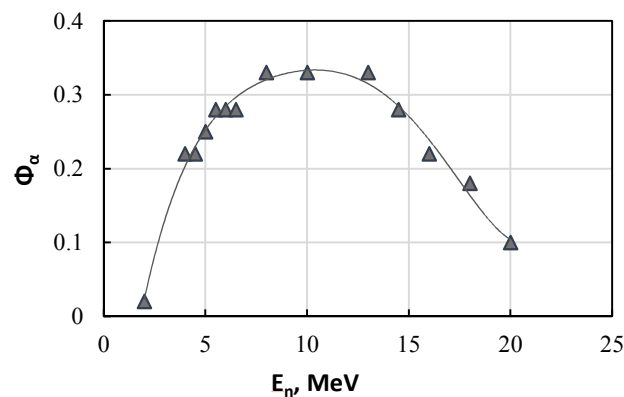
Fig. 3. The neutron energy dependence of Φ_α obtained by the normalization of the theoretical (n,α) cross section to experimental one.

3.2. Comparison of (n,α) and (n,p) cross sections

The α-cluster formation factors obtained by the second method are given in Appendix 2. The Φ_α factors were determined at the 4,5 and 6 MeV neutron energy for some medium-mass nuclei, where (n,α) and (n,p) cross sections of the same isotopes are available. The T_α and T_p transmission factors were calculated by a code written in a Matlab. The experimental (n,α) and (n,p) reactions cross sections data were obtained from [13].

77
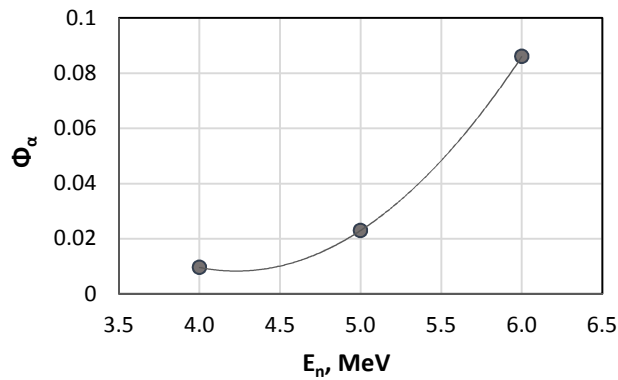
Fig. 4. The neutron energy dependence of Φ_α obtained by comparison of (n,α) and (n,p) cross sections

From the obtained results, as shown in Fig.4, it was observed that for this neutron energy range the alpha-cluster formation probability is increased depending on the neutron energy.

3.3. Calculation of α–cluster formation probability using the (n, α) cross sections and the total neutron cross sections for the ^{4}He.

The results obtained by our last method are given in Appendix 3. We have calculated the alpha cluster formation probability, Φ_α, for 19 isotopes for neutron energy range of $E_n = 1 \div 20$ MeV.
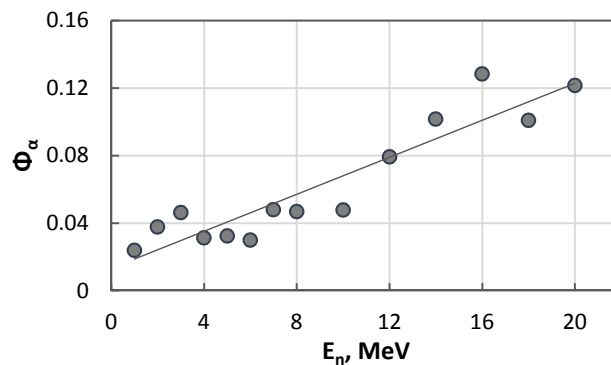
Fig. 5. The neutron energy dependence of Φ_α obtained using the (n,α) cross sections and the total neutron cross sections for the ^{4}He

78

From the obtained results, as shown in Fig.5, it was observed that the cluster formation factors have tendency that is on an average grew depending on the E_n.

3.4. Comparison of our results with the α-clustering factor values obtained by other authors.

In the framework of this study we obtained the cluster formation factors for the (n,α) reaction at the different neutron energy. We have compared our results for E_n =4, 5 and 6 MeV with the values obtained by other authors, which aregiven in Appendix 4.Results obtained by the first method were close to the values obtained by Bonetti and Milazzo-Colli [2], Popov *et al.*[4-6], Saad M. Saleh Ahmed[7], T.T.Ibrahim *et al.*[14], and Buck *et al.*[15].The alpha-formation probability calculated by our second and third methods were close to each other. The differences between the obtained values were, perhaps, caused by the different approaches of suggested methods of the study. All our results were in agreement with the α-clustering factors obtained by Shuqing Guo *et al.* [16]. It is, also, seen that our results were appreciably different from the values calculated by Kadmensky and Furman [17]. Therefore, to obtain more detailed information about α-cluster formation probability, it is desirable to develop the suggested methods in further investigations. It should be noted that results of study in [7], [14-16] were obtained for α-decay.

4. Conclusions

1. In the framework of the statistical model and knock-on mechanism, we calculated the α-particle formation factor using the following three different types of approaches: 1) normalization of the theoretical (n,α) cross section to experimental data; 2) comparison of (n,α) cross section with (n,p) one; 3) calculation of α–clustering probability using the (n,α) cross sections and the total neutron cross sections for the ^{4}He.

2. Our results calculated by the first method was close to the values of Bonetti and Milazzo-Colli [2], Popov *et al.* [4-6], Saad M. Saleh Ahmed [7], T.T.Ibrahim*et al* [14] and Buck *et al*. [15]. The cluster formation factors obtained by the second and third methods were close to each other, while the one calculated by first method was different from others. We assume that the discrepancy between the values may be related to the different approaches of suggested methods. All of our calculated results were in agreement with α-clustering factors obtained by Shuqing Guo *et al.* [16] and appreciably different from the values calculated by Kadmensky and Furman [17].

References

[1] P.E.Hodgson, Alpha-clustering in Nuclei, Chapter 23 of "The Uncertainty Principle and Foundations of Quantum Mechanics". Editor: W.C.Price and S.S.Chissick, New York, John Wiley, (1977), p.485.

[2] R.Bonetti and L.Milazzo-Colli, Phys. Lett. B, v.49, N1, (1974), p.17.

[3] W.M.Seif *et al.*, Phys Rev. C, v.84, (2011), 064608.

[4] Yu.Popov *et al*., Yad. Fiz., v.13, N5, (1971), p.913.

[5] Yu.Popov and V.I.Furman, In book:III School of Neutron Physics, JINR, (1978), Dubna, p.390.

[6] N.P.Balabanov *et al*., Physics of Elementary Particles and Atomic Nuclei, v.21, N2, (1990) p.317.

[7] S.M. Saleh Ahmed, Alpha-cluster preformation factor within cluster-formation model for odd-a and odd–odd heavy nuclei, submitted to Nucl. Phys. A (2017).

[8] G.Khuukhenkhuu *et al*., Physics of Elementary Particles and Atomic Nuclei, Letters, v.11, N.6 (190), (2014), p.1159.

[9] D.G.Gardner and Yu-Wen Yu, Nucl. Phys., v.60, N1, (1964), p.49.

[10] V.F.Weisskopf and D.H.Ewing, Phys. Rev., v.57, N6, (1940), p.472.

[11] J.M.Blatt and V.F.Weisskopf, Theoretical Nuclear Physics, New York, John Wiley and Sons, (1952).

[12] C.F.Weizsaker, Z.Phys. A, v.96, N7-8, (1935), p.431.

[13] http://www-nds.iaea.org/exfor/exfor.htm.

[14] T.T.Ibrahim and S.M.Wyngaardt, J. Phys. G: Nucl. Part. Phys., v.41, (2014) 055111.

[15] Buck *et al*., Phys. Rev. C, v.45, (1992) p.2247.

[16] ShuqingGuo *et al*., Nuclear Physics A, v.934, (2015) p.110.

[17] S.G.Kadmensky and V.I.Furman, Physics of Elementary Particles and Atomic Nuclei, v.6, part 2, (1975), p.469 (in Russian).

Appendix 1: Method I: The Φ_α cluster formation probability obtained by normalization of the theoretical (n,α) cross section to experimental data for different neutron energy

E_n, MeV	2	4	4.5	5	5.5	6	6.5	8	10	13	14.5	16	18	20
$<\Phi_\alpha>$	0.02	0.22	0.22	0.25	0.28	0.28	0.28	0.33	0.33	0.33	0.28	0.22	0.18	0.1

Appendix 2: Method II: The Φ_α cluster formation probability obtained by the comparison of (n,α) cross section with (n,p) one

E_n, MeV	Isotope	σ(n,p), barn	σ(n,α), barn	T_p	T_α	Φ_α	$<\Phi_\alpha>$
4	^{54}Fe	0.276	8E-4	0.004	5.32E-04	0.021	0.0096
	^{58}Ni	0.352	0.0102	3.5E-3	0.056	0.002	
	^{63}Cu	0.075	3E-4	0.005	1.5E-3	0.013	
	^{64}Zn	0.133	0.059	8.00E-04	0.162	0.002	
5	^{41}K	0.014	0.003	2.06E-02	0.12	0.032	0.023
	^{54}Fe	0.3	0.003	0.038	0.014	0.025	
	^{58}Ni	0.509	0.047	0.03	0.38	0.007	
	^{59}Co	0.008	1.3E-4	0.004	0.002	0.038	
	^{63}Cu	0.073	0.001	0.039	0.025	0.028	
	^{64}Zn	0.181	0.079	9.9E-3	0.84	0.005	
6	^{41}K	0.014	0.008	0.165	0.92	0.097	0.086
	^{54}Fe	0.465	0.008	0.18	0.15	0.021	
	^{55}Mn	0.006	9E-4	9.9E-3	0.009	0.169	
	^{59}Co	0.015	0.001	0.036	0.032	0.085	
	^{63}Cu	0.089	0.006	0.17	0.21	0.057	

Appendix 3: Method III: The Φ_α cluster formation probability obtained using the (n,α) cross sections and the total neutron cross sections for the ^{4}He.

E_n, MeV	$\sigma_n^{tot}(^4\text{He})$	Isotope	σ(n,α), barn	Φ_α	$<\Phi_\alpha>$	E_n, MeV	$\sigma_n^{tot}(^4\text{He})$	Isotope	σ(n,α), barn	Φ_α	$<\Phi_\alpha>$
1	6.31	^{6}Li	0.252	0.039	0.024	7	1.78	^{6}Li	0.056	0.032	0.048
		^{10}B	0.198	0.031				^{10}B	0.055	0.031	
		^{14}N	0.002	3.2E-4				^{14}N	0.203	0.114	
2	4.09	^{6}Li	0.244	0.059	0.038			^{16}O	0.086	0.048	
		^{10}B	0.346	0.085				^{39}K	0.155	0.087	
		^{14}N	0.027	0.007				^{40}Ca	0.208	0.117	
		^{20}Ne	0.001	3E-4				^{52}Cr	0.002	0.001	
3	2.79	^{6}Li	0.183	0.066	0.046			^{54}Fe	0.009	0.005	
		^{10}B	0.175	0.063				^{58}Ni	0.071	0.039	
		^{14}N	0.215	0.077				^{63}Cu	0.0095	0.005	
		^{20}Ne	0.014	0.005		8	1.71	^{6}Li	0.045	0.027	0.047
		^{40}Ca	0.059	0.021				^{16}O	0.065	0.038	
4	2.51	^{6}Li	0.095	0.038	0.031			^{39}K	0.161	0.094	
		^{10}B	0.243	0.097				^{40}Ca	0.193	0.113	
		^{14}N	0.365	0.146				^{54}Fe	4.01E-2	0.023	
		^{16}O	0.058	0.023				^{56}Fe	6.3E-3	0.004	
		^{39}K	0.101	4.03E-2				^{58}Ni	0.113	0.066	
		^{54}Fe	0.001	3E-4				^{63}Cu	0.018	1.03E-2	
		^{58}Ni	1.02E-2	0.004		10	1.45	^{16}O	0.138	0.095	0.048
		^{63}Cu	3E-4	1.1E-4				^{54}Fe	0.041	0.028	
		^{64}Zn	0.059	0.024				^{63}Cu	0.029	2.02E-2	
		^{67}Zn	0.007	0.003		12	1.25	^{6}Li	0.032	0.026	0.079
		^{95}Mo	7E-4	3E-4				^{16}O	0.224	0.178	
		^{143}Nd	1.2E-4	4.79E-5				^{63}Cu	0.042	0.034	
5	2.18	^{6}Li	0.089	0.041	0.038	14	1.09	^{6}Li	0.029	0.026	0.102
		^{10}B	0.169	0.077				^{16}O	0.295	0.271	
		^{14}N	0.186	0.085				^{20}Ne	0.274	0.251	
		^{39}K	0.138	0.063				^{39}K	0.084	0.077	
		^{40}Ca	0.199	0.091				^{40}Ca	0.138	0.127	
		^{54}Fe	0.004	0.002				^{54}Fe	0.083	0.076	
		^{58}Ni	0.047	0.022				^{63}Cu	0.047	0.043	

E_n, MeV	$\sigma_n^{tot}(^4He)$	Isotope	$\sigma(n,\alpha)$, barn	Φ_α	$<\Phi_\alpha>$	E_n, MeV	$\sigma_n^{tot}(^4He)$	Isotope	$\sigma(n,\alpha)$, barn	Φ_α	$<\Phi_\alpha>$
5	2.18	^{63}Cu	0.001	6E-4	0.038	14	1.09	^{64}Zn	0.036	0.033	0.102
		^{64}Zn	0.079	0.036				^{144}Sm	0.011	10.09E-3	
		^{95}Mo	0.001	6E-4		16	0.97	^{6}Li	0.022	0.023	0.128
		^{143}Nd	2E-4	9.6E-5				^{16}O	0.36	0.373	
		^{147}Sm	2E-4	1.1E-4				^{54}Fe	0.082	0.085	
		^{149}Sm	1.00E-5	4.6E-6				^{63}Cu	0.032	0.033	
6	2.05	^{6}Li	0.071	0.035	0.029	18	0.86	^{6}Li	0.019	0.022	0.101
		^{14}N	0.144	7.02E-2				^{16}O	0.24	0.278	
		^{39}K	0.154	0.075				^{54}Fe	0.072	0.083	
		^{40}Ca	0.198	0.097				^{63}Cu	0.018	0.021	
		^{58}Ni	0.075	0.037		20	0.78	^{16}O	0.215	0.276	0.122
		^{63}Cu	0.006	0.003				^{39}K	0.057	0.073	
		^{64}Zn	0.076	0.037				^{63}Cu	0.012	0.015	
		^{67}Zn	0.008	0.004							
		^{95}Mo	0.002	8E-4							
		^{143}Nd	3E-4	1.5E-4							
		^{147}Sm	3E-4	1.4E-4							
		^{149}Sm	1E-4	5E-5							

Appendix 4: Comparison of our results with the α-clustering factor values obtained by other authors.

E_n, MeV	Φ_α			Bonetti and Milazzo-Colli [2]	Popov *et al.* [4-6]	SaadM.Saleh Ahmed [7]	T.T.Ibrahim *et al.* [14]	Buck *et al.* [15]	Shuqing Guo *et al.* [16]	Kadmensky and Furman [17]
	Method I	Method II	Method III							
4	0.22	0.0096	0.031	0.01÷0.7 <0.25>	<0.19>	$Pee{\sim}0.183$ $Peo{\sim}0.168$ $Poe{\sim}0.144$ $Poo{\sim}0.133$ (343 nuclei)	$Pee \sim 0.83 \pm 0.25$ $Peo\sim 0.65 \pm 0.17$ $Poe \sim 0.68 \pm 0.53$ $Poo \sim 0.55 \pm 0.35$ (65 SHI)	$Pee{\sim}1$ $Peo{\sim}0.6$ $Poe{\sim}0.6$	$Pee{\sim}0.002$ $÷0.6$ (158e-e nuclei)	$7 \cdot 10^{-4}$ favoured $3 \cdot 10^{-5}$ Semi-favoured $8 \cdot 10^{-7}$ unfavoured
5	0.25	0.023	0.038							
6	0.28	0.086	0.029							
$<\Phi_\alpha>$	<0.25>	<0.039>	<0.033>							

Note:* ee- even- even nuclei, eo- even-odd nuclei, oe- odd-even nuclei, oo-odd-odd nuclei, SHI-Super heavy isotopes.

Dynamics of Two-Cluster Systems and Structures of Light Nuclei

A.D. Duisenbay.[1], V.S. Vasilevsky[2], K. Kato[3], V.O. Kurmangaliyeva[1], N. Kalzhigitov[1], N. Takibayev[1]

[1]*Al-Farabi KazakhNationalUniversity, Almaty, Kazakhstan*

[2]*Bogolyubov InstituteforTheoreticalPhysics, Kiev, Ukraine*

[3]*Hokkaido University, Sapporo, Japan*

The properties and the dynamic structure of the light nuclei ^{5}He, ^{5}Li, ^{6}Li, ^{7}Li, ^{7}Be, and ^{8}Be are considered within the framework of two-cluster microscopic models [1-3]. The research was aimed at the development and studies of the two-cluster microscopic models and their ability to give a complete description of the physical characteristics of the light nuclear systems [1].

It was also important to distinguish and predict the features of the new states in the excitation spectrum of these light nuclei.

It was demonstrated that the developed model gives a satisfactory agreement of the calculated characteristics of these light nuclei with the experimental data. This gives a possibility to use the method for determination of new excited and resonance states [1-3].

The cross sections and phases of elastic scattering in the framework of the resonating group method have been studied in detail and calculated.

The calculations have been carried out and general the features revealed for the considered group of light nuclei represented in the form of the two-cluster systems: α + p, α + d, α + t, α + ^{3}He, α + α.

Theoretical calculations of the elastic scattering processes, ground and resonance states were performed using the Hasegawa-Nagata potential, which is often used in various microscopic models [4].

The cluster fragmentation gives us an opportunity to investigate the dominant binary channel and to determine bound energy, excited levels of the system and scattering resonances in the positive energy region. It gives us a possibility to consider the scattering process of two fragments. For example, the elastic scattering of two clusters or the elastic scattering of a nucleon on an alpha particle: n + α → n + α (^{5}He),   p +

$\alpha \rightarrow p + \alpha$ (^{5}Li), $d + \alpha \rightarrow d + \alpha$ (^{6}Li),   etc.

Theoretical basis and the calculations within the frame of the algebraic version of the dynamics for the two cluster subsystems can be found in [1, 5, 6].

Analytical methods of analysis on a complex energy plane are given in [7 - 9].

Continuous Spectrum States

Considering a continuity spectrum of elastic scattering, the calculations are obtained for the phase shifts, partial and total cross sections for elastic scattering of the clusters. The calculations were provided for the resonance state parameters and for the   wave functions.

To verify the two-cluster model, let us consider the experimental information about the considered nuclei. Figure 1 demonstrates the importance of the two body partition or clusterization of the selected nuclei. In this figure we display the experimental energy of the ground state (from Refs. [9, 10]) measured from the lowest two-cluster threshold. The nuclei ^{6}Li, ^{7}Li, ^{7}Be are presented by the bound states, while the nuclei ^{5}He, ^{5}Li and ^{8}Be are presented by the lowest resonance states, which are usually treated as their ground states [9].

As we see, the nuclei ^{6}Li, ^{7}Li, ^{7}Be can be easily split into two fragments (clusters) as their binding energy is less than 2.5 MeV, and other nuclei ^{5}He, ^{5}Li and ^{8}Be as resonance states in the two-cluster continuum. These facts unambiguously indicate the importance of a two-cluster fragmentation in the considered nuclei.

Relative positions of the main two-cluster decay thresholds are seen in Fig. 2. As in the previous Figure, the energy of the second two-cluster threshold is reckoned from the first dominant threshold. Fig. 2 demonstrates that for the nuclei ^{5}He, ^{5}Li, ^{6}Li and ^{8}Be, the second binary channel lies far away from the first one (more than 14 MeV), and one can assume that the influence of the second binary channel on the low energy spectrum would be negligibly small. This Figure justifies the use of a single-channel approximation for the ^{5}He, ^{5}Li, ^{6}Li and ^{8}Be.

Somehow different situation is observed in ^{7}Li and ^{7}Be, where the second binary channel is separated only by 4.78 and 4.02 MeV, respectively, from the first binary channel. In this case, we can rely on the bound and continuous spectrum states below the energy of the second binary channel, where it has, as we believe, small influence on the obtained results.

Omitting the theoretical calculations (see, for example [1]), we give some results of calculations and quantitative estimates.

Resonance States

The resonance states are very interesting phenomena in two- and many-cluster continuum. Present model allows us to study the so-called shape resonance states, i.e. the resonance states created by the Coulomb or/and centrifugal barriers. These resonances lie close to the two-cluster decay threshold. Some of these resonances belong to the rotational spectra. We are going to study in detail parameters of resonance states and analyze their wave functions.

As we consider two pairs of mirror nuclei, namely ^{5}He and ^{5}Li, ^{7}Li and ^{7}Be, we would investigate the effects of the Coulomb interaction on energy and width of the resonance states in these nuclei. Table I presents the parameters of the narrow resonance states. In fact, this Table includes three very narrow resonance states with the total width Γ varying from 1 to 17 keV. The later represent the ground state of ^{5}He and ^{5}Li, nuclei that have no bound states.

Table I: Parameters of the most narrow resonance states in light nuclei.

Nucleus	J^π	E, MeV,	Γ, MeV	E, MeV	Γ, MeV
^{5}He	$3/2^-$	0.782	0.679	-	-
^{5}Li	$3/2^-$	1.598	1.316	2.78 ± 0.03	3.83 ± 0.03
^{6}Li	3^-	0.716	0.017	-	-
^{7}Li	$7/2^-$	0.741	0.001	2.78 ± 0.03	3.83 ± 0.03
^{7}Be	$7/2^-$	1.716	0.012	-	-
^{8}Be	0^+	0.0932	$12.98 \cdot 10^{-6}$	0.0918	$(5{:}57 \pm 0{:}25) \cdot 10^{-6}$

Let us consider the wave functions of the selected resonance states. In Figure 2 we display the wave functions of the narrow resonance states ^{5}He, ^{5}Li, ^{6}Li, ^{7}Li and ^{7}Be, with the quantum numbers indicated in Table I.

Wave functions are represented in coordinate space and thus they depend on distance between clusters r. Main feature of these resonances is that their wave functions are concentrated at small distances, where interaction between cluster is very strong.

To demonstrate how the parameters of the resonance states depend on the shape of a

nucleon-nucleon potential, we selected the nucleus ^{8}Be and made additional calculations by involving the Minnesota potential (MP) [11] and the Volkov potential N2 (VP) [12]. As for the MHNP, we selected the oscillator length b to minimize the energy of an alpha particle, the exchange parameter u of the MP; the Majorana parameter m of the VP is chosen to reproduce energy of the 0^+ resonance state in ^{8}Be.

Table II: Parameters of broad resonance states in ^{5}He, ^{5}Li, ^{6}Li, ^{7}Li, ^{7}Be, ^{8}Be.

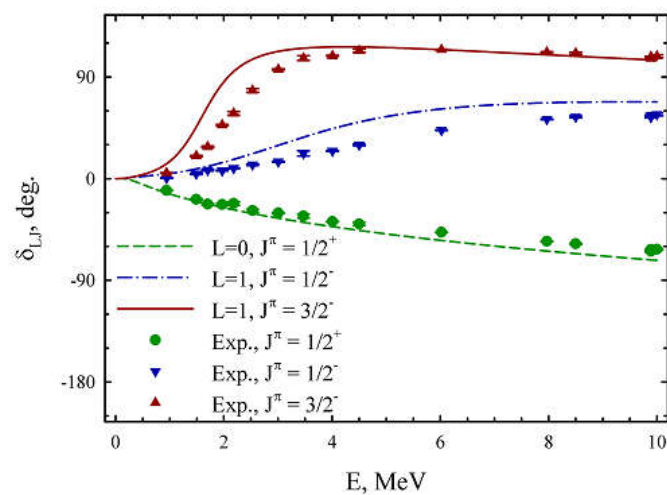| Nucleus	J^π	E, MeV	Γ, MeV	E, MeV	Γ, MeV
^{5}He	$1/2^-$	2.117	5.957	2.068	5.57
^{5}Li	$1/2^-$	2.996	7.297	3.18	6.60
^{6}Li	2^+	3.019	0.999	2.838±0.022	1.30±0.10
	1^+	4.056	2.331	4.176±0.050	1.5±0.20
^{7}Li	$5/2^-$	5.417	2.118	4.137	0.918
^{7}Be	$5/2^-$	6.398	2.025	5.143±0.10	1.2
^{8}Be	2^+	2.831	1.194	3.122±0.01	1.513±0.015
	4^+	10.73	1.925	11.442±0.15	3.50

Fig. 1. Theoretical and experimental phase shifts for the elastic α + p scattering.

The optimal parameters for the MP are b = 1.285 fm, u = 0.9276, and for the VP they are equal to b = 1.376 fm, m = 0.6011. Results of these calculations are presented in Table II. Energy of the resonance states is determined with respect to the α + α threshold energy. In Table II we also compare the results of our calculations with the available experimental data [10].

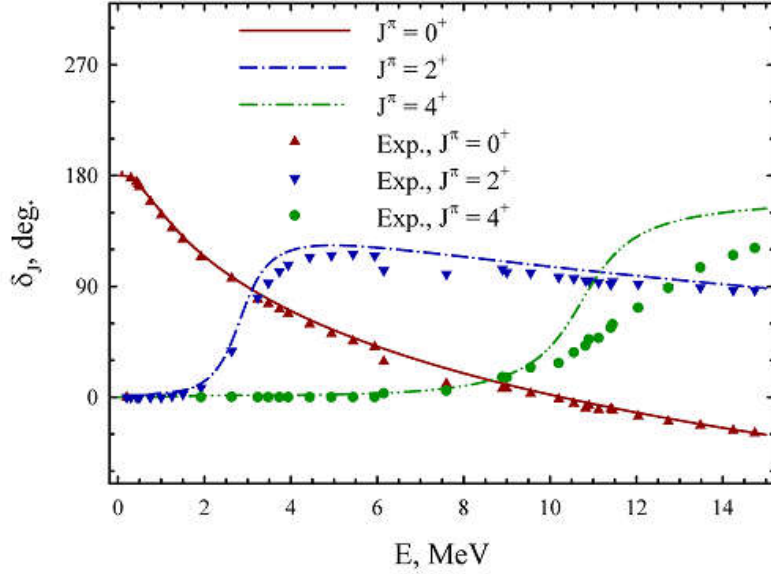**Fig. 2.** Phase shifts of the elastic α + α scattering, calculated within the present two-cluster model and compared with the corresponding experimental data.

Conclusions

We have considered the bound and resonance states in the p-shells of the lightest nuclei ^{5}He, ^{5}Li, ^{6}Li, ^{7}Li, ^{7}Be, and ^{8}Be. The Resonating Group Method was used to describe the discrete and continuous spectrum states. These nuclei were considered as the two-cluster systems with the dominant two-cluster configurations. The effective semi-realistic Hasegawa-Nagata potential was employed as a nucleon-nucleon interaction. The Majorana exchange parameter was slightly modified to reproduce the ground state energy. Continuous spectrum of the negative and positive parity states was calculated with such a value of the Majorana parameter.

Energy and width of resonance states were calculated and compared with available experimental data. It was shown that our model describes fairly well the resonance structure of nuclei ^{5}He, ^{5}Li, ^{6}Li, ^{7}Li, ^{7}Be and ^{8}Be [1-3, 7, 8, 13 - 15].

References

[1] V.S. Vasilevsky, K. Kato, V. Kurmangaliyeva, A.D. Duisenbay, N. Kalzhigitov, N. Takibayev, "Investigation of discrete and continuous spectrum states in two-cluster systems", 2017-10-11, 62pp., Monograph CIPhys-3.pdf, http://hdl.handle.net/2115/67294. Hokkaido University, Sapporo, Japan, (2017).

[2] V. S. Vasilevsky, Yu. A. Lashko_, G. F. Filippov, "Two- and three-cluster decays of light nuclei with the hyperspherical harmonics", 38 pp., arXiv:1706.04127v1 [nucl-th], (2017).

[3] V. S. Vasilevsky, N. Zh. Takibayev, and A. D. Duisenbay, "Microscopic description of ^{8}Li and ^{8}B nuclei within three-cluster model," Ukr. J. Phys., vol. 62, no. 6, (2017), pp.461- 472.

[4] A. Hasegawa and S. Nagata, "Ground state of ^{6}Li", Prog. Theor. Phys., vol. 45, (1971), pp.1786 -1807.

[5] C. Beck, ed., Clusters in Nuclei, Volume 3, vol. 875 of Lecture Notes in Physics, Berlin Springer Verlag, (2014).

[6] H. Horiuchi, K. Ikeda, and K. Kato, "Recent Developments in Nuclear Cluster Physics", Prog. Theor. Phys. Suppl., vol. 192, (2012), pp.1-238.

[7] Y. Lashko, G. Filippov, and V. Vasilevsky, "Dynamics of two-cluster systems in phase space", Nucl. Phys. A, vol. 941, (2015), pp.121 - 144.

[8] K. Kato, V. S. Vasilevsky, and N. Z. Takibayev, "Nuclear Cluster Dynamics in Nucleo-Synthesis in Neutron Stars", in Book "Neutron Stars. Physics, Properties and Dynamics", ed. N. Takibayev and K. Boshkayev, ch. 6, New-York: Nova Science Publishers, Inc., (2017), pp.173-226.

[9] D. R. Tilley, C. M. Cheves, J. L. Godwin, G. M. Hale, H. M. Hofmann, J. H. Kelley, C. G. Sheu, and H. R. Weller, "Energy levels of light nuclei A=5, 6, 7," Nucl. Phys. A, vol. 708, (2002), pp.3 -163.

[10] D. R. Tilley, J. H. Kelley, J. L. Godwin, D. J. Millener, J. E. Purcell, C. G. Sheu, and H. R. Weller, "Energy levels of light nuclei A=8, 9, 10", Nucl. Phys. A, vol. 745, (2004), pp.155 - 362.

[11] D. R. Thompson, M. LeMere, and Y. C. Tang, "Systematic investigation of scattering problems with the resonating-group method," Nucl. Phys., vol. A286, no. 1, (1977), pp.53 - 66.

[12] A. B. Volkov, "Equilibrum deformation calculation of the ground state energies of 1p shell nuclei", Nucl. Phys., vol. 74, (1965), pp.33 - 58.

[13] A. V. Nesterov, V. S. Vasilevsky, T. P. Kovalenko, "Effect of cluster polarization on the spectrum of the ^{7}Li nucleus and on the reaction ^{6}Li(n;^{3}

H)^{4}He", Phys. Atom. Nucl. 72 (2009),pp.1450 - 1464.
doi:10.1134/S1063778809090051.

[14] V. S. Vasilevsky, N. Z. Takibayev, and A. D. Duisenbay, "Inuence of the cluster polarization on spectrum and reactions in mirror ^{8}Li and ^{8}B nuclei", in The III International Workshop "Nuclear Physics and Astrophysics", April 14-16, vol. 3, Almaty, Kazakhstan, Phys. Sci. Technol., (2016), pp.24 - 29.

[15] V. S. Vasilevsky, F. Arickx, J. Broeckhove, and T. P. Kovalenko, "A microscopic three cluster model with nuclear polarization applied to the resonances of ^{7}Be and the reaction ^{6}Li(p;^{3} He)^{4}He", Nucl. Phys. A, vol. 824, (2009), pp.37 - 57.

Recent EXFOR Compilation Status in India and Estimation of Uncertainty Propagation in Efficiency

Vidya Devi

Institute of Engineering and Technology, Bhaddal, Ropar, Punjab, INDIA

vidyathakur@yahoo.co.in

Nuclear Reaction data have been crucial resource in nuclear technology, e.g. fission, fusion energy, and medical diagnostics as well as science, e.g. nuclear physics, astrophysics and nuclear chemistry etc. There is strong need to compile Experimental data in a database and make it accessible to nuclear data users all over the world. EXFOR database is one of such nuclear reaction databases maintained by International Network of Nuclear Reaction data Centre (NRDC) under the auspices of International Atomic Energy Agency (IAEA). This report summarizes the review of compilation status in India. In this report we will also briefly present some methods such as Unscented Transform technique and Monte Carlo method for the determination of the Uncertainty propagation. We generate and present the covariance information by taking into account various attributes influencing the uncertainties and also the correlations between them.

Successful contribution of INDIA to the EXFOR entries:

In India, EXFOR compilation on a regular basis has been started since 2006. EXFOR compilation in INDIA is the outcome of the initiative and efforts undertaken by Nuclear Data Physics Centre of India (NDPCI).
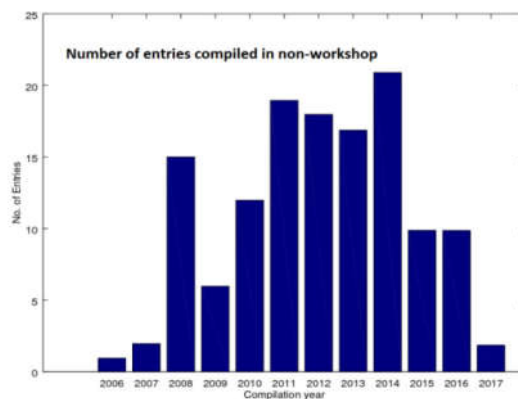

Fig. 1. Status of number of entries compiled in non-workshop.

Compilation was done by Voluntary compilers and through EXFOR theme meetings. Since the past few years, EXFOR compilation has also been done by Universities through funds given by NDPCI-BRNS. All EXFOR compilations were done under the supervision of NDS, IAEA (Previously with the help of Dr. O. Schwerer, Dr. S. Dunaeva and currently with Dr. N. Otsuka). Fig. 1 shows the status of compilation of number of entries other than EXFOR workshops.

Fig. 2 shows the number of papers compiled in different DAE-BRNS workshop on EXFOR during 2006 to 2017.
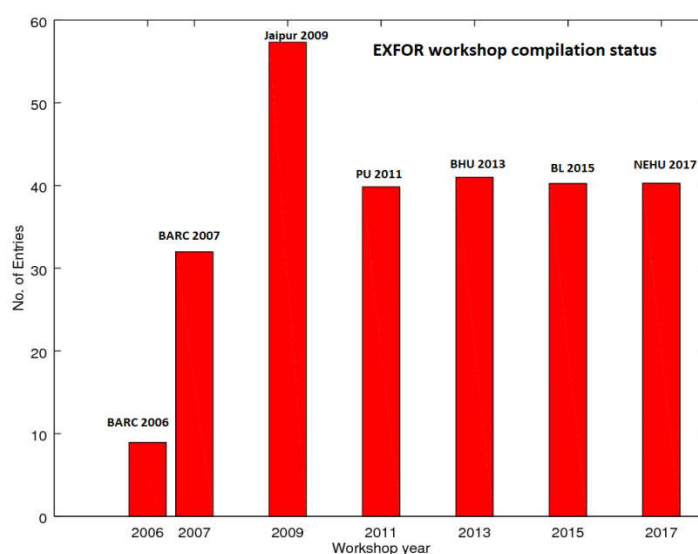

Fig. 2. Status of number of entries compiled in workshop.

Journal Survey of Indian Published Paper:

We participated in the Journal survey of Indian published paper and results were also checked against the EXFOR database summarized as Memo and distributed to other centres (see Annexure 1 & 2).

In April 2014, NDPCI scanned Pramana (PRM) Vols. 2 to 5 and Indian J. Pure and Applied Phys. (IPA) Vol. 21 to 41, and created two new entries (D6216 and D6217) accordingly. As continuation in 2016, NDPCI scanned PRM Vol. 6 to 63 and IPA Vol.1 to 20. A list of articles for creation or revision of EXFOR entries by NDPCI and NNDC is appended in the Memo Memo CP-D/839 (**Completeness checking for**

articles published in PRM and IPA).

Annexure 1. Articles published in Pramana (PRM) Vol. 1 and 6 to 63, and Ind. J. Pure and Applied Phys. (IPA) Vol. 1 to 20 and missing in EXFOR

Completeness checking for articles published in PRM and IPA
(Vidya, N. Otsuka, 2016-07-15, Memo CP-D/910)

In April 2014, NDPCI scanned Pramana (PRM) Vols. 2 to 5 and Indian J. Pure and Applied Phys. (IPA) Vol. 21 to 41, and created two new entries (D6216 and D6217) accordingly. As continuation, NDPCI scanned PRM Vol. 1 and 6 to 63, and IPA Vol. 1 to 20. A list of articles for creation or revision of EXFOR entries by NDPCI and NNDC is appended to the this memo.

Two articles not in the list but for revision of existing entries:

- S.Kailas+,J,PRM,7,6,1976 reports averaged cross sections, for which original experimental works are compiled in EXFOR D6017, D6059, D6085, D6095. NDPCI is going to add the 1976 article under REL-REF of these entries.

- M.Ismail+,J,PRM,51,743,1998 reports "fusion cross sections", which are sums of (α,n), (α,2n) and (α,3n) cross sections in EXFOR F0068 and O1266. The 1998 article is for addition under REL-REF by CNPD and NEA DB.

Addition to this working paper:

1. Namely NDPCI has completed scanning of PRM Vol.1 (1973) to 63 (2004) and IPA Vol.1 (1963) -41 (2003).

2. The Ismail's 1988 article has been already added under O1266 of REL-REF (TRANS.O058).

Article	1st author	Lab.	Proj.	Quant.	Source	EXFOR	Centre	Remark
J,IPA,2,364,1964	M.K.Saxena	3INDTAT	cp	TTD	Table		NDPCI	Relative data
J,IPA,8,108,1970	M.K.Saxena	3INDTAT	cp	TTD	Curve		NDPCI	Relative data
J,IPA,10,200,1972	M.L.Srivastava	3INDTAT	cp	TTD	Curve		NDPCI	Relative data
J,IPA,10,567,1972	M.L.Srivastava	3INDTAT	cp	TTD	Curve		NDPCI	Relative data
J,PRM,12,653,1979	C.R.Ramaswamy	3INDTRM	cp	DA	Curve		NDPCI	
J,PRM,18,205,1982	S.C.L.Sharma	3INDITK	n	FY	Curve		NDPCI	

J,PRM,35,439,1990	S.Kailas	1USAWAU	cp	DAE	Curve		NNDC	
J,PRM,37,425,1991	G.R.Pansare	3INDPOO	n	CS	Table		NDPCI	Two data points in 31412.
J,PRM,38,291,1992	M.Dasgupta	3INDTRM	hi	CS	Table	D6113	NDPCI	for revision. Delete D6141 (from same experimental work).
J,PRM,39,85,1992	R.K.Jain	3INDVEC	cp	CS	Table		NDPCI	
J,PRM,41,151,1993	R.K.Sheline	1USAFSU	cp	DAP	Table		NNDC	
J,PRM,45,519,1995	R.K.Jain	3INDVEC	cp	CS	Table		NDPCI	
J,PRM,49,515,1997	R.K.Jain	3INDBHU	n	CS	Table	31424	NDS	for revision (addition of ref.; same data in text)
J,PRM,53,513,1999	M.Dasgupta	3AULCBR	cp	CS	Curve	A0719	CNPD	for revision (addition of ref. only; part of compiled data in figs)
J,PRM,53,541,1999	T.Madhusoodhanan	3INDNSD	cp	DAA	Curve		NDPCI	
J,PRM,61,507,2003	B.S.Nara Singh	3INDTRM	hi	DAP	Curve		NDPCI	

Annexure 2. Assessment of the old neutron articles missing in EXFOR.

Nuclear Data Section

International Atomic Energy Agency

P.O.Box 100, A-1400 Vienna, Austria

<u>Memo CP-D/839</u>

Subject: EXFOR completeness for neutron data from India

1. Data in absolute unit (to be compiled by NDPCI)

Reference	Year	Author	Quantity	Remark

J,IJP,28,396	1954	Nandi+	CS	Cross section ratio
J,IJP,30,80	1956	Saha+	CS	
J,IPA,12,640	1974	Rama Prasad+	CS	
J,JIN,31,1217	1969	Prakash+	KE	
J,JIN,34,2685	1972	Prakash+	KE	
J,JRN,82,263	1984	Nair+	FY	in compilation (33048)
J,JRN,91,291	1985	Tomar+	FY	in compilation (33049)
J,JRN,125,85	1988	Ramaswami+	FY	in compilation (33050)
J,NIM,205,145	1983	Ajitanand+	KE	
J,NP,55,127	1964	Koul.	DA	
J,NP,83,407	1966	Bharathi+	DA	in compilation (33061)
J,NP/A,133,625	1969	Ajitanand	FY	
J,NP/A,213,35	1973	Murty+	CS	Some data are in EXFOR
J,NP/A,235,307	1974	Alam+	CS	
J,NP/A,346,473	1980	Choudhury+	KE	
J,NP/A,355,13	1981	Sharma+	KE	
J,NP/A,502,307	1989	Manohar+	FY	Conf. Proc.
J,PHY,28,1011	1962	Machwe	DA	
J,PR,131,283	1963	Kapoor+	MFQ	PFNS
J,PR,166,1190	1968	Kapoor+	FY	X-ray
J,PR,177,1776	1969	Kapoor+	FY	X-ray
J,PR/C,21,1411	1980	Datta+	FY	
J,PR/C,51,3127	1995	Samant+	NU	
J,PRM,24,131	1985	Sharma+	DA	

Reference	Year	Author	Quantity	Remark
J,PS,24,935	1981	Srinivasa Rao+	CS	
J,RCA,31,65	1982	Raghuraman+	FY	
J,RCA,35,15	1984	Srivastava+	FY	
J,RCA,46,177	1989	Bhargava+	FY	

2. Data in arbitrary unit

Reference	Year	Author	Quantity	Remark
J,PR,129,1350	1963	Ramanna+	DA	
J,IJP,30,99	1956	Patro+	CS	
J,NP,25,136	1961	Ramanna+	DA	
J,NP,27,166	1961	Kondaiah+	DA	
J,NP,41,435	1963	Sen.	DA	
J,NP,65,635	1965	Chatterjee	DA	
J,PR,133,B598	1964	Kapoor+	DA	

Estimation of uncertainty propagation in efficiency:

Understanding the structure of the atomic nucleus and developing a technology from the gained knowledge requires the experimental data and its uncertainties. We mostly require physical quantities that cannot be directly measured and have to be calculated from variables that can be experimentally determined by using their functional dependence on each other [1].

We have to propagate the uncertainties of known variables to find the uncertainties of unknown variables. We will discuss two methodologies:

1. Deterministic approach (Sandwich formula of error propagation)
2. Stochastic approach (Monte Carlo method and Unscented Transform Method).

Deterministic approach (Sandwich formula):

The Sandwich formula for error propagation is first order sensitivity analysis method. Consider an independent variable vector x of order n, and dependent variable vector y of order m. Let $y = f(x)$, then the mean value of y is given as $\bar{y} \approx f(\bar{x})$ and the covariance matrix for Sandwich formula is [2-3]

$$C_y \approx H_x C_x H_X^T \tag{1}$$

Here C_x is $n \times n$ covariance matrix of x, C_y is $m \times m$ covariance matrix of y and H_x is the sensitivity matrix with elements

$$H_{xij} = \left(\frac{\partial f_i}{\partial x_j} \right) \quad (i = 1, 2, ..., n)$$

This method works quite well for functions with small nonlinearity and small uncertainties. As the nonlinearity increases it produces unsatisfactory results. Higher order terms of Taylor expansion can be involved in calculations to have more accurate results. This can be achieved by using stochastic method (Monte Carlo method). In this method an $m \times m$ covariance matrix can be approximated by a sum of matrices, each corresponding to a distinct uncertainty attribute [4].

Monte Carlo Method:

Higher order terms of Taylor expansion can be involved in calculations to have more accurate results. This can be achieved by using stochastic method (Monte Carlo method or unscented transformation method).

Let x be the n-dimensional vector of primary variables and V_x be covariance matrix. This method involves producing a large number of X_k, $k = 1, 2, ... K$, vectors by randomly varying each component X_i of x in accordance with the probability function $P(X_i)$ governing them.

For each vector (X_k), m values of elements of vector y are calculated. Hence we get large collection of vectors of derived variables from which sample means are calculated as

$$\langle y_i \rangle_K = \frac{\left(\sum_{K=1}^{K} y_{ik} \right)}{K}, i = 1, 2, ...m.$$

Sample variance and covariance are given as

$$\left(v_{yik}\right)_K = \frac{\sum_{K=1}^{K} y_{ik}}{K} - \langle y_i \rangle_K \langle y_j \rangle_K \tag{2}$$

where $i, j = 1, 2, \dots, n, m$.

Unscented Transform Method:

It is difficult to transform a probability density function(PDF) through a general nonlinear function that is why uncertainty propagation is also difficult. Unscented Transform method (UT) is based on two principles;

it is easy to perform a nonlinear transformation on a single point, and, it is easy to find a set of individual points in state space whose sample PDF approximates the true PDF of a state vector [1]. Consider a primary variable vector x with mean $\bar{x}$ and covariance P. If we find a set of deterministic vectors called sigma points whose ensemble means and covariance are same as that of x. Then using these sigma points, on the known nonlinear functional relationship to obtain transformed vectors, we can calculate mean and covariance of transformed vectors.

Let X be $n \times 1$ vector with mean $\bar{X}$ and covariance P. We choose $2n$ sigma points $X^{(i)}$ as follow:

$$X^{(i)} = \bar{X} + \bar{X}^{(i)}, \quad i = 1, 2, \dots, 2n \tag{3}$$

where $\widetilde{X}^{(i)} = \left(\sqrt{nP}\right)_i^P$ and $\widetilde{X}^{(n+1)} = -\left(\sqrt{nP}\right)_i^T$, for $i = 1, 2, \dots, n$. Here $\sqrt{nP}$ can be calculated using Cholesky factorization. Using these sigma points, we can calculate $2n$ transformed vectors (y). The mean and covariance are given by the formula

$$\bar{Y} = \sum_{i=1}^{2n} W^{(i)} Y^{(i)} \tag{5}$$

$$C = \sum_{i=1}^{2n} W^{(i)} \left(y^{(i)} - \bar{y}\right)\left(y^{(i)} - \bar{y}\right)^T \tag{6}$$

$W^{(i)} = 1/2n, \quad i = 1, 2, \dots, 2n$ are weight coefficients. In this experiment the efficiency of the detector is determined at six different energies of the calibration source ^{152}Eu.

98

The number of counts (C) and gamma abundances (α) are taken from [4] (Table I).

The activity (A_0) of the source at the time of its manufacturing was 7767.67 ± 155.35.

The time elapsed (t) between manufacturing and the experiment date was 9.893 years, half-life (T) of ^{152}Eu is 13.537 ± 0.006 years. The efficiency (ε) is given as [4-5]:

$$\varepsilon = \frac{C}{\alpha A_0 \, e^{\left(\frac{-0.693}{T}t\right)}}$$

The efficiencies calculated using Sandwich (SA), Monte Carlo (MC) and Unscented Transform (UT) methods are given in Table 1.

Table 1: The efficiencies calculated using Sandwich (SA), Monte Carlo (MC) and Unscented Transform (UT) methods

Energy (keV)	SA Method $\varepsilon(\Delta\varepsilon)(10^{-2})$	MC Method $\varepsilon(\Delta\varepsilon)(10^{-2})$	UT Method $\varepsilon(\Delta\varepsilon)(10^{-2})$
244.675	3.3262(0.0903)	3.3274(0.0904)	3.3275(0.0906)
411.116	1.9954(0.1236)	1.9963(0.1236)	1.9962(0.1237)
867.378	0.9042(0.0563)	0.9054(0.0562)	0.09046(0.0563)
964.079	0.8563(0.0236)	0.8567(0.0237)	0.8567(0.0238)
1112.074	0.7817(0.0220)	0.7820(0.0221)	0.7820(0.0221)
1299.140	0.7459(0.0676)	0.7462(0.0677)	0.7462(0.0676)

Table 2: Covariance matrix $(\times 10^{-7})$ using Sandwich, Monte Carlo and Unscented Transform method

Sandwich Method	Monte Carlo Method	Unscented Transform Method
8.145	*8.172*	*8.218*
2.655 15.26	2.646 15.26	2.699 15.29
1.203 0.722 3.165	1.206 0.710 3.161	1.223 0.734 3.171
1.139 0.684 0.31 0.559	1.146 0.686 0.309 0.560	1.158 0.695 0.315 0.564
1.04 0.624 0.283 0.268 0.486	1.047 0.624 0.284 0.269 0.487	1.057 0.634 0.287 0.272 0.487
0.992 0.595 0.27 0.256 0.233 4.567	0.997 0.586 0.267 0.256 0.234 4.589	1.009 0.605 0.274 0.260 0.237 4.571

Future Plan:

1) To prepare a quick manual to help Indian EXFOR users this document include all home rules of compilation of EXFOR that are not in EXFOR manual. Participation in regular compilation activities.
2) Praticipation in other NDPCI assigned work such as Journal survey, removing the duplication of entry.
3) Participation in the neutron and proton induced reaction cross-sections experiments to be held at BARC, Mumbai.

References

[1] D. Simon, Optimal State Estimation, John Wiley & sons, 2006.
[2] H. Kadvekar, A Preliminary Examination of the Application of Unscented Transformation Technique to Error Propagation in Nonlinear Cases of Nuclear Data Science, Nuclear Science and Engineering, (2016), 183.
[3] D. L. Smith, N. Otuka, Experimental Nuclear Reaction Data Uncertainties: Basic Concept and Documentation, Nuclear Data Sheets 113, (2012), 3006-3053.
[4] B. S. Shivashankar, S. Ganesan et.al, Measurement and Covariance Analysis of Reaction Cross Sections for ^{58}Ni(n,p)^{58}Co Relative to Cross Section for Formation of ^{97}Zr Fission Product in Neutron-Induced Fission of ^{232}Th and ^{238}U at Effective Neutron Energies E_n =5.89,10.11and 15.87 MeV, Nuclear Science and Engineering, (2015), 179.
[5] Y. Shanthi Sheela, H. Naik, K. Manjunatha Prasad, S. Ganesan and S.V. Suryanarayana, Detailed data sets related to covariance analysis of the measurement of cross section of ^{59}Co(n,g) ^{60}Co reaction relative to the cross section of ^{115}In(n,g)^{116}In, Internal report, STATISTICS/DAE-BRNS/2017.

Analysis of (n,α) Reaction Total Cross-Sections at 14.8 MeV Using the Exciton Model Approaches

Ts.Zolbadral and G.Khuukhenkhuu

Nuclear Research Center, National University of Mongolia, Ulaanbaatar, Mongolia

In this work, we analyzed known integral (n,α) cross sections at 14.8 MeV for some isotopes using the different versions of the exciton model to compare obtained results. Main discussions are focused on the comparison between the results of Ribansky and Oblozinsky's "Coalescence Model", Iwamoto-Harada's "Pick up Model" and, TALYS-1.8 and PRECO6 codes in which the Kalbach's "Direct model" is used.

1. Introduction

In the framework of the pre-equilibrium mechanism of the nuclear reactions, using the exciton model many approaches such as Milazzo-Colli and Bonetti's "pre-formed α-particle model" [1], Ribanskyand Oblozinsky's "Coalescence Model" [2], Iwamoto-Harada's "Pick up Model" [3], and the Kalbach's "Direct model" [4,5] were suggested and developed to consider the complex particles in either the entrance or exit channels. In our previews work, these approaches excluding "pre-formed model" were clearly considered[6] for explanation of known experimental energy spectra (differential cross sections) for outgoing α-particles from (n,α) and (p,α) reactions in the energy range of 14.8 to 60 MeV using the one-component and the closed-form expression.

Bonetti and Milazzo-Colli introduced a pre-formation factor, "*f*", into the expression for α-particle emission rate in the exciton model. However, this approach wascriticized by Wu and Chang [7] and Iwamoto-Harada [3]. Wu and Chang considered the following drawbacks: first, the competition between nucleons and complex particles is omitted in the processes of nuclear equilibration and particle emission; and second, concerning the particle-hole state density with a mixture of nucleons and α-particle, as well as, the nuclear transition rates resulting from the

two-body residual interactions between a pair of nucleons or a nucleon and an α-particle are ambiguous. By relating to this work, J.J.Hogan [8] deduced the number of alpha clusters, which should exist in the ground level of the target nucleus, as well as, this value was considered as the increasing function of mass number such as 2.1 for Ti to 7.8 for Th. The Iwamoto-Harada doubted that it is much larger than that anticipated from microscopic calculations and it is hard to believe that so many alphas exist in the actual nucleus.

Wu and Chang improved the Ribansky and Oblozinsky's "Coalescence Model" and presented an empirical estimation of the cluster formation probability, γ_x, by comparing theoretical calculation with experimental data. They carried out some attempts that considering the cluster formation probability, γ_x, is a function of target mass number and the state density for complex particles, g_x, is constant and equals to g/4 for alpha particle, as first was suggested in [1]. They assumed that $g_x(E_x)$ is an energy dependent which was, only, estimated for high energy case of proton induced reaction. Their improvements were successful in reproducing the spectral shape for (p,x)reactions. However, their model is strongly criticized by Kalbach, in papers [4,5]. Also, the Iwamoto-Harada critically considered that the assumption of constant formation probability is unphysical. So, they introduced the pickup process by nucleons, where both bound and unbound nucleons are involved in the reaction and calculated the α-particle formation factor, $F_{lm}(\varepsilon_x)$, from the overlap integral of wave functions for the α particle and four nucleons near the nuclear surface. This formation factor is a function of ejectile's energy, ε_x. But they used a root-mean-square (rms) approximation where no correlations existed between the coordinates in the phase space which consequently leads to a systematically larger nuclear surface region [9,10].

Finally, the Kalbach's "Direct model" have been suggested and developed in the PRECO-6 code [11]. Also, this model is used in the TALYS code. There is one unclear issue in this model that any formation factor of the ejectile complex particle is not considered and only uses the mass number of the ejectile in the expression of the emission rate. Then contributions of some direct model such as nucleon transfer (NT), and knock-out (KO) are calculated, in addition. The concept without the formation factor is perhaps doubtful for us because the alpha particle from the reaction can be referred only the 4 nucleons which is excited upper than Fermi-level.

Main purpose of this study is to compare between Ribansky and Oblozinsky's "Coalescence Model", Iwamoto-Harada's "Pick up Model" and Kalbach's "Direct Model" as well as to advance a better approximation of the complex particles exciton

model calculations for the spectra of the α-particles and the integrated total (n,α) cross-section for E_{inc}= 14.8 MeV neutrons.

2. Outline of the Exciton Model

In the framework of the pre-equilibrium mechanism the exciton model assumes that the nuclear reaction to proceed via a sequence of relatively simple states characterized by their the exciton number. In the spin-independent formulation of the exciton model the energy spectrum of the emitted particles is expressed as following:

$$\frac{d\sigma}{d\varepsilon_k} = \sigma_C \sum_n \tau_n W_n\,(n, E, \varepsilon_k), \tag{1}$$

where $W_n(n, E, \varepsilon_k)$ is the particle emission rate from an n-exciton state (n = p + h) of excitation energy E to continuum; ε_k is the energy of the ejectile of type "k"; and σ_C is the cross section of creation of the composite system; τ_n is the time spent in an n-exciton state.

The particle (nucleon) emission rate to a final open channel characterized by an emitted nucleon with energy between ε_{nuc} and $\varepsilon_{nuc} + d\varepsilon_{nuc}$ is given by

$$W_n(n, E, \varepsilon_{nuc}) = \frac{2s_{nuc}+1}{\pi^2 \hbar^3} \mu_{nuc} \varepsilon_{nuc} \frac{\omega(p-1,h,U)}{\omega(p,h,E)} \sigma_{INV}(\varepsilon_{nuc}), \tag{2}$$

where μ_{nuc} and s_{nuc} are the ejectile particle reduced mass and spin, respectively; $U = E - B_{nuc} - \varepsilon_{nuc}$ is the excitation energy of residual nucleus which is produced in an $(n - 1)$ exciton state; $\omega(p, h, E)$ is the particle-hole state density; and $\sigma_{INV}(\varepsilon_i)$ is the inverse cross section, which can be replaced by the optical model cross section representing the capture of a projectile i by the nucleus in its ground state. We used a simple expression, which has been guided by comparisons with measured non-elastic cross sections [11].

3. Complex Particle Emission Rate

In the simplest case, the complex particles emission rate can be written formally in exactly the same way as for nucleons, just by replacing the exciton number of the residual nucleus $(p - 1, h)$ by $(p - p_x, h)$, where it assumes that the complex particles x is formed by p_x of the total of p excited particles.

3.1. Ribansky and Oblozinsky Coalescence Model

In order to reduce the disagreement between the results of experimental data and theoretical approaches of simple exciton model, Cline multiplied the emission rates sensibly by the energy-independent factor $p_x!$. The new factor $p_x!$ could not be derived as a physical meaning. Therefore, Ribansky and Oblozinsky replaced this artificial factor by

$$\gamma_x \frac{\omega(p_x, 0, \varepsilon_x + B_x)}{g_x} \quad , \tag{4}$$

which has straightforward physical interpretation: γ_x is the x-particle formation probability, which expresses the fact that these excitons really makeup the complex particles x and its second part is simply the number of configurations of the p_x excitons forming the complex particles, so that their product is the number of complex particles of given type with proper energy. This approach led to both reasonable absolute values and for some complex particles even rather good spectra shapes. The full expression for the particle emission rate is now obtain

$$W_n(n, E, \varepsilon_x) = \frac{2s_x + 1}{\pi^2 \hbar^3} \mu_x \varepsilon_x \sigma_{INV}(\varepsilon_x) \frac{\omega(p - p_x, h, U)}{\omega(p, h, E)} \times \gamma_x \frac{\omega(p_x, 0, \varepsilon_x + B_x)}{g_x}. \tag{5}$$

This γ_x parameter is to be gotten from the way to fit into the data. From the comparison of theoretical calculation with experimental data was observed the dependence of $\gamma_x \approx \frac{1}{A^m}$ in the above mass 27, with $m \approx \frac{4}{3}$ for α. As the Wu and Chang's improvement of the Ribansky and Oblozinsky's "Coalescence Model", the state density for complex particles, g_x, is constant and equals to g/4 for alpha particle. It means that the magnitude of differential cross-section can be directly grown up 4 times.

3.2. Iwamoto-Harada Coalescence (Pickup) Model

In the Iwamoto-Harada model the complex particles emission rate is given by

$$W_n(n, E, \varepsilon_x) = \frac{2s_x + 1}{\pi^2 \hbar^3} \mu_x \varepsilon_x \sigma_{INV}(\varepsilon_x) F_{lm}(\varepsilon_x) \frac{\omega^*(p - l, h, U)}{\omega(p, h, E)}. \tag{6}$$

The symbol $F_{lm}(\varepsilon_x)$ stands complex particles formation factors, which are calculated from the overlap integral between the wave functions of complex particles and the constituting nucleons. Those factors were composed of l particles above the Fermi level and m particles below.

3.3. Kalbach's Direct Model

It is however well-known that for nuclear reactions involving projectiles and ejectiles with different particle numbers, mechanisms like stripping, pick-up, break-up and knock-out play an important role and these direct-like reactions are not covered by the exciton model. Therefore, Kalbach developed a phenomenological contribution for these mechanisms. In total, the pre-equilibrium cross section for these reactions is given by the sum of the exciton model (EM), nucleon transfer (NT) and knock-out (KO) contributions:

$$\frac{d\sigma_k^{PE}}{d\varepsilon_k} = \frac{d\sigma_k^{EM}}{d\varepsilon_k} + \frac{d\sigma_k^{NT}}{d\varepsilon_k} + \frac{d\sigma_k^{KO}}{d\varepsilon_k} \ . \tag{7}$$

In the Kalbach's direct reaction mechanism for the exciton model, the complex particles emission rate is expressed by

$$W_x(n, E, \varepsilon_x) = \frac{2s_x+1}{\pi^2\hbar^3}\mu_x\varepsilon_x \frac{\omega(p-A_x,h,U)}{\omega(p,h,E)}\sigma_{INV}(\varepsilon_x), \tag{8}$$

where A_x is mass number of emitting complex particles.

4. Calculation

We considered the integral cross-section as integrated by the energy of ejectile particle from the expression of the differential cross sections for outgoing α-particles from (n,α) reaction:

$$\sigma_{tot} = \int_0^{\varepsilon_{max}} \frac{d\sigma}{d\varepsilon_x}d\varepsilon_x. \tag{9}$$

Because of the experimental results are regarded as the sum of the all reaction mechanisms, it is inadequate to compare with only the net pre-equilibrium results. Therefore, we additionally calculated the contribution of the equilibrium process into the integrated cross-section.

The equilibrium calculations are performed using a simple Weisskopf-Ewing evaporation formula as in [12]. The particle emission rates are given by

$$W_x(E, \varepsilon_x) = \frac{2s_x+1}{\pi^2\hbar^3}\mu_x\varepsilon_x\sigma_x(\varepsilon_x)\frac{\omega(U)}{\omega(E)}. \tag{10}$$

This has the same form as the pre-equilibrium emission rates and the variables have the same meaning, but here the state densities are characterized only by the excitation energy of the nucleus. The state density in the numerator is evaluated in the residual

nucleus formed by emission of a particle of type *x*, while the state density in the denominator is valuated for the emitting nucleus.

The equation for this state density is

$$\omega_T(E) = t^{-1}\exp(E/t),$$ (11)

Where *t* is the constant nuclear temperature is determined as:

$$t = \left(\sqrt{(a_0/E_{eff})} - 1.25/E_{eff} \right)^{-1}.$$ (12)

The effective excitation energy E_{eff} is given by

$$E_{eff} = (2.5 + 150/A) \quad \text{MeV.}$$ (13)

For such calculations, the single particle state density is given by

$$g = \frac{A}{15} \ (\text{MeV}^{-1}),$$ (14)

where *A* is the target nucleus mass number.

The calculations by TALYS-1.8[13] and PRECO-6[11] codes with the default parameters were executed.

5. Results and Discussions

5.1. *Spectrum of the α-particles from (n, α) reaction*

Our calculations for the spectra of the α-particles and the integrated total cross-section were carried out for (n, α) reaction with E_{inc}= 14.8 MeV neutrons on the ^{54}Fe, ^{58}Ni, ^{60}Ni, ^{63}Cu and ^{65}Cu isotopes. Results of these calculations for the spectra of the α-particles in comparison with experimental data taken from Ref. [14,15] are given in the "a" and "b" of Figs.1÷5.

Figs.1÷5. "a" show total results of the compound, pre-equilibrium and direct mechanisms of the TALYS-1.8 and PRECO6 codes in comparison with the experimental data. In addition, in these Figs, net Equilibrium, marked as "EQ" and sum results of the Equilibrium and Ribansky and Oblozinsky's Coalescence model, marked as "EQ+RO" and Iwamoto-Harada's Pick-up model, marked as "EQ+IH". Simultaneously, in the Figs. 1÷5. "b", comparisons of calculated results by net pre-equilibrium mechanism and experimental data are shown.

It is seen from Figs.1÷5. "a" that for (n,α) reactions on the considering isotopes with

E_{inc}= 14.8 MeV neutrons, the TALYS-1.8 code calculated and summation results of calculation, marked as EQ+RO and EQ+IH, are satisfactorily in agreement with experimental spectra of α-particles above the 8 MeV. However, total results, calculated by PRECO6 code with default parameter, are a little higher than the experimental spectra of α-particles.
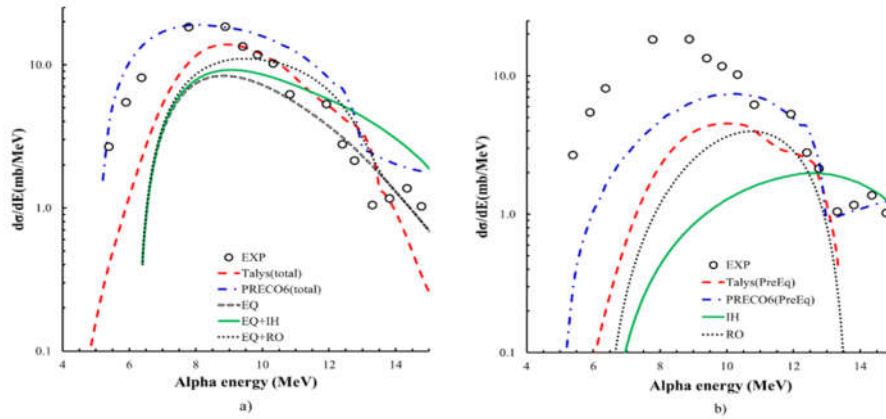
Fig. 1. Comparison of the calculated energy spectra of the ^{54}Fe(n,α)^{51}Cr reaction at E_{inc}=14.8 MeV with the experimental data from Ref[15]. a) The total spectra, including compound mechanism. b) net pre-equilibrium results of the calculations.
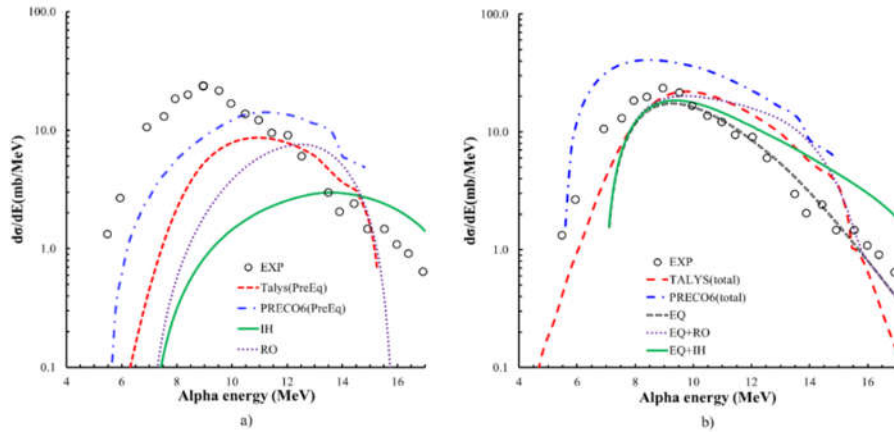
Fig. 2. The same as in Fig.1 for the ^{58}Ni(n,α)^{55}Fe reaction.
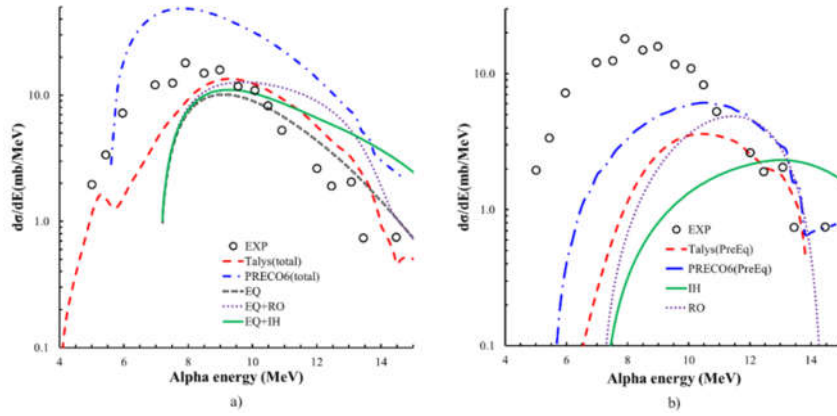
Fig. 3. The same as in FIG.1 for the ^{60}Ni(n,α)^{57}Fe reaction
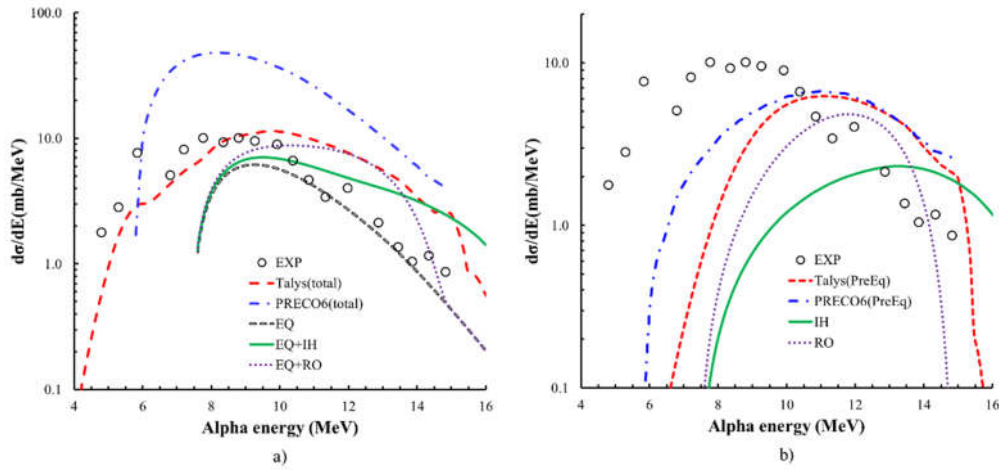
Fig. 4. The same as in Fig.1 for the ^{63}Cu(n,α)^{60}Co reaction
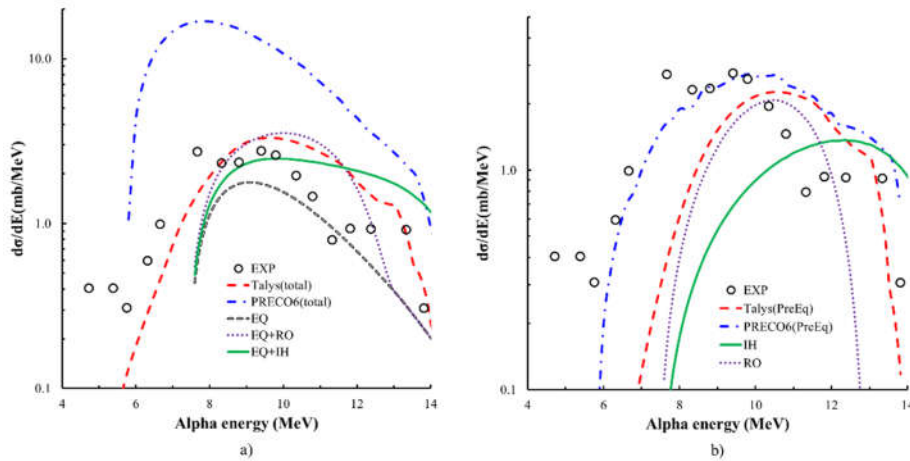
Fig. 5. The same as in FIG.1 for the ^{65}Cu(n,α)^{62}Co reaction

Figs.1÷5. "b" show that results calculated by approaches of net pre-equilibrium mechanism are in agreement with experimental data, excluding the Iwamoto-Harada's

model. As the calculation by the Iwamoto-Harada's Pick-up model, it was observed a tendency which the maximum value of α spectrum slightly moved into higher energy side in this region. It would be explained with relating to the α-particle formation factor, $F_{lm}(\varepsilon_x)$,which has a function form of ejectile's energy.

5.2. Total cross-sections of (n, α) reaction

The integrated (total) cross-sections are given in Appendix 1. In this table S.M.Grimes's results are found by energy integrating the expression for fitting curvature of values in Ref[14]. Other experimental data were utilized from the EXFOR [15].

Results calculated by TALYS-1.8 code, EQ+RO and EQ+IH are generally in agreement with the experimental data excluding ^{54}Fe(n,α)^{51}Cr reaction, as well as, these values are in close each other as both compound and preequilibrium mechanisms. But, these results are a little lower than the experimental data for the total cross-section of ^{54}Fe(n,α)^{51}Cr reaction.

For all considering reactions, results calculated by PRECO6 codes are relatively greater than the experimental data and results calculated by TALYS-1.8 code, EQ+RO and EQ+IH.

6. Conclusions

- Iwamoto-Harada, Ribansky-Oblozinsky and Kalbach's approaches for complex particle emission in the exciton model were considered for the spectra of the α-particles and the integrated total cross-section of (n, α) reaction with E_{inc}= 14.8 MeV neutrons on the ^{54}Fe, ^{58}Ni, ^{60}Ni, ^{63}Cu and ^{65}Cu isotopes.

- Results calculated by the PRECO6 codes with the default parameters are relatively greater than the results calculated using the Ribansky-Oblozinsky and Iwamoto-Harada models and TALYS-1.8 code, and experimental data.

- Results calculated by the Iwamoto-Harada, the Ribansky-Oblozinsky and TALYS-1.8 code are in agreement with experimental data for considering isotopes excluding ^{54}Fe(n,α)^{51}Cr reaction.

References

[1] R.Bonetti and L.Milazzo-colli, Phys. Lett., B49, (1974), p.17.

[2] I.Ribansky and P.Oblozinsky, Phys. Lett., B45, (1973),p.318.

[3] A.Iwamoto and K.Harada, Phys. Rev., C26, (1982),p.1821.

[4] C.Kalbach, Phys. Rev., C19, (1979),p.1547.

[5] C.Kalbach, Z.Phys., A283, (1977),p.401.

[6] Ts.Zolbadral and G.Khuukhenkhuu, Proceeding of International Conference on Contemporary Physics, ICCP-VI, 7-10 June, Ulaanbaatar, (2016),p.540.

[7] J.R.Wu and C.C.Chang, Phys. Rev., C17, (1978),p.1540.

[8] J.J.Hogan, Z. Phys., A 295, (1980),p.169.

[9] K.Sato, A.Iwamoto and K.Harada, Phys. Rev., C28, (1983),p.1527.

[10] S.Kunieda et.al, Phys. Rev., C85, (2012),p.054602.

[11] C.K.Walker, Triangle Universities Nuclear Laboratory, Duke University, User's Manual for PRECO-2006: "Exciton Model Preequilibrium Code with Direct Reactions," 2006 (unpublished).

[12] K. H. Narasimha Murthy, A. Chatterjee, and S. K. Gupta, "Proc. Int'l Conf. on Nucl. Cross Sections for Technology," Knoxville TN, 1979, NBS Spec. Pub. 594, p.793; A. Chatterjee, K. H. N. Murthy and S. K. Gupta, Pramana 16,(1981),p.391.

[13] A. Koning, S. Hilaire, and S. Goriely, "User Manual of TALYS-1.8" (Nuclear Research and Consultancy Group, Petten, The Netherlands, 2015).

[14] S.M.Grimes and R.C.Haight, Phys. Rev., C19, (1979),p.2127.

[15] https://www-nds.iaea.org/exfor/exfor.htm

Appendix 1: Comparison of calculated (n,α) reaction total cross-sections at 14.8 MeV with experimental data.

^{54}Fe(n,α)^{51}Cr						
σ (mbarn)	TALYS-1.8	PRECO-6	Ref[3]	Ref[5]	EXFOR[15]	Fitting[14]
Preequilibrium	18.7	37.2	11.2	15.1		
Compound	39.6	69.7	40.3	40.3		
Direct	2.0	-	-	-		
Total	60.3	106.9	51.5	55.4	96±3.5 88±5.7	79.0
^{58}Ni(n,α)^{55}Fe						
Preequilibrium	42.3	77.3	19.7	33.7		
Compound	65.6	160.6	79.0	79.0		
Direct	0.2	-	-	-		
Total	108.1	237.9	98.7	112.7	125±10.5 105±7	97.1
^{60}Ni(n,α)^{57}Fe						
Preequilibrium	15.3	28.7	13.3	18.9		
Compound	45.3	198.5	43.4	43.4		
Direct	0.4	–	–	–		
Total	61	227.2	56.7	62.3	56±2 43±2	72.3
^{63}Cu(n,α)^{60}Co						
Preequilibrium	30.7	37.9	14.3	19.2		
Compound	34.7	199.5	25.1	25.1		
Direct	0.05	–	–	–		
Total	65.4	237.4	39.4	44.3	46.6±1.7 42.3 ±1.2	61.3
^{65}Cu(n,α)^{62}Co						
Preequilibrium	9.1	13.6	6.4	6.5		
Compound	5.5	61.4	6.8	6.8		
Direct	0.3	–	–	–		
Total	14.9	75.0	13.2	13.3	8.1±0.6 8.9±1.3	8.7

Systematical Analysis of Photonuclear Reaction Data

G.Khuukhenkhuu[1], M.Odsuren[1,2,†], B.Regzedmaa[2] and Ts. Bilguun[2]

[1]*Nuclear Research Center, National University of Mongolia, Ulaanbaatar, Mongolia*

[2]*School of Engineering and Applied Sciences, National University of Mongolia, Ulaanbaatar, Mongolia*

Systematical analysis of photo-nuclear reaction experimental data is important to understand the nuclear reaction mechanism and a role of the electromagnetic interaction in nuclei. From the beginning of the photonuclear reaction study some attempts of such systematics were carried out using the different theoretical approaches and were obtained several regular behaviors in the giant resonance parameters. But, up to now common opinion and unified viewpoint for these obtained systematical regularities are no available. The purpose of this work is the systematical analysis of known contemporary experimental data of the photonuclear reactions using the dipole vibration approach and hydrodynamic model.

1. Introduction

Gamma- rays are an electromagnetic wave in which the magnetic and electric fields are perpendicular to each other and propagate together to the same direction. The protons have an electrical charge and will interact with the electric field. The protons and neutrons have magnetic moments, but the magnetic force is usually weak, so we don't consider it. The protons in a nucleus are accelerated in one direction by electric field associated with passing photons. The neutrons are unaffected by the field, but they move in the direction opposite to that - of the protons and the center of mass of the nucleus remains stationary and momentum is conserved. When the next phase of the photon arrives, the proton and neutron move to opposite from the previous. This motion of nucleons in the nucleus is called the dipole vibration. We assume that wavelength of the gamma rays is large with respect to the diameter of a nucleus. As a result of this assumption, the electric field associated with gamma ray is nearly uniform across the nucleus. This approach to the photonuclear reaction is called the electric dipole approximation or long wave-length limit. When the frequency of the oscillating electric field associated with the gamma rays matches the resonance

frequency of the mode of the nucleus, will be the giant resonance phenomenon and are ejected protons, p, neutrons, n, or heavier particles from nuclei. This effect is called a photonuclear reaction.

Since 1934, when the photonuclear reaction was discovered by Chadwick and Goldhaber [1], many experimental data were obtained and they have been collected at the different research laboratories. The experimental data compiled in the EXFOR system supported by the IAEA [2]. Systematical analysis of photonuclear reaction experimental data is important to understand the nuclear reaction mechanism and a role of the electromagnetic interaction in nuclei. From the beginning of the photo-nuclear reaction study many attempts of such systematics were carried out using the different theoretical approaches and were obtained some regular behaviors in the main giant resonance parameters (see, for example, [3-9]). But, up to now common opinion and unified viewpoint for these obtained systematical regularities are no available.

The purpose of this work is the systematical analysis of known contemporary experimental data of the photonuclear reactions using the dipole vibration approach and hydrodynamic model.

2. The Main Parameters of the Photonuclear Reaction

The shape of the photonuclear reaction cross section is usually described by the, so-called, Lorentzian curve [10, 11] (see Fig. 1):

$$\sigma(E\gamma) = \sigma_m \frac{(\Gamma^2 E_\gamma^2)}{(E_m^2 - E_\gamma^2)^2 + \Gamma^2 E_\gamma^2} \qquad (1)$$

Here: $E\gamma$ is the energy of the incident photons; σ_m is the maximum cross section; E_m is the gamma-ray energy at the maximum cross section; $\sigma_m/2$ is the half of the maximum cross section; Γ is the full width at the half maximum. In Fig. 1 E_{th} is the threshold energy of the photonuclear reaction and Δ is the energy interval between the E_{th} and according to $\sigma_m/2$ energy.

So, these above mentioned quantities are the Lorentz parameters or the main parameters of the photonuclear reaction which will be considered in this work.
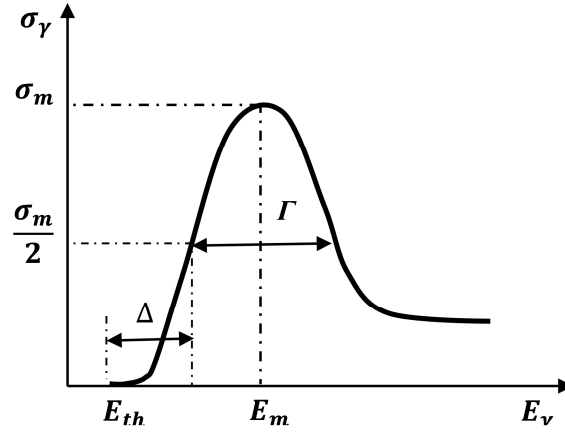
Fig. 1. Schematic dependence of the photonuclear reaction cross section on the gamma-ray energy (Lorentz curve).

3. Theoretical Approaches

3.1. Dipole Vibration Model

Interaction of the electromagnetic radiation with nucleus can be considered using the perturbation theory the Hamiltonian of which is expressed as [8]:

$$H = H_0 + V(r, t), \qquad (2)$$

where H_0 is the unperturbed operator of a system:

$$H_0 = \frac{\hat{p}^2}{2m} + U. \qquad (3)$$

Here: U is the nuclear potential energy operator.

The perturbation operator for the photonuclear reaction can be written as follows:

$$V(r, t) = V(r)e^{i\omega t} + V(r)e^{-i\omega t} = V^{+(r,t)} + V^{-(r,t)} \qquad (4)$$

In the case of the perturbation independent of time, $V(r)$, the transition probability rate between the excited and initial states is determined by:

$$W = \frac{2\pi}{\hbar} |\langle f|V(r)|i\rangle|^2 \rho_f(E_f) = \frac{2\pi}{\hbar} \left| \int \psi^*_f V(r)\psi_i d\tau \right|^2 \rho_f(E_f). \qquad (5)$$

Here: ψ_i is the initial target-nucleus wave function; ψ^*_f is the complex conjugate wave function of the final state; $\rho_f(E_f)$ is the density of the final state (dN/dE). We use the classic electrodynamic Hamiltonian:

$$H = \sum_{\alpha=1}^{A} \left[\frac{1}{2m_\alpha} \left(p_\alpha - \frac{e_\alpha}{c} \mathcal{A} \right)^2 + e_\alpha \varphi \right] + U. \tag{6}$$

Here: α is the nucleon number; e_α is the charge of the α-th nucleon; c is the light velocity; φ is the scalar potential and $\mathcal{A}$ is the vector potential of the electromagnetic wave, which can be written in the following form:

$$\mathcal{A} = 2\mathcal{A}_0 \varepsilon \cos(kr - \omega t). \tag{7}$$

Here: ε is the unit vector; k is the wave number; ω is the angular frequency; $\mathcal{A}_0$ is the amplitude of the vector potential. It can be chosen that $\varphi = 0$.

Then, the time independent perturbation operator can be written in the form:

$$V(r) = -\frac{1}{c} \mathcal{A}_0 \sum_{\alpha=1}^{A} \frac{e_\alpha}{m_\alpha} e^{ikr} p_\alpha . \tag{8}$$

When the long wave-length limit is used, from (5) and (8) the matrix element is expressed by:

$$\langle f|V(r)|i\rangle_{\varepsilon 1} = -\frac{1}{c} \mathcal{A}_0 \sum_{\alpha=1}^{A} \frac{e_\alpha}{m_\alpha} \langle f|p_\alpha|i\rangle . \tag{9}$$

Using the transformation from the momentum representation to coordinate representation, the matrix element is obtained by:

$$\langle f|V(r)|i\rangle_{\varepsilon 1} = \frac{\mathcal{A}_0}{i\hbar c} \left(E_f - E_i \right) \langle f| \sum_\alpha e_\alpha r_\alpha |i\rangle. \tag{10}$$

If we introduce the dipole moment

$$D = \sum_\alpha e_\alpha r_\alpha, \tag{11}$$

from (5) and (10) the transition probability can be rewritten as:

$$W = \frac{2\pi}{\hbar} \left| \frac{\mathcal{A}_0}{i\hbar c} \left(E_f - E_i \right) \langle f|D|i\rangle \right|^2 \rho_f(E_f) . \tag{12}$$

Then, the photonuclear reaction cross section is obtained as following:

$$\sigma = \frac{\overline{W}}{\Phi_\gamma} = \frac{\overline{W}}{c} = \frac{2\pi}{\hbar c} |< f|V(r)|i >|^2 \rho_f(E_f) . \tag{13}$$

The integral cross section for discrete energy spectrum can be written in the form:

$$\int \sigma_{\varepsilon 1} dE = \frac{4\pi^2}{c} \sum_f \omega_{fi} |\langle f|D_z|i\rangle|^2 = \frac{2\pi^2 e^2 \hbar}{cM} \sum_f F_{fi} . \tag{14}$$

Here: F_{fi} is the oscillator strength per unit energy in the final state, one is determined

115

by the Thomas-Reiche-Kuhn's sum rule [11,12]:

$$\sum_f F_{fi} = Z .$$ (15)

If we use, so-called, conception of the effective charge for protons (eN/A) and neutrons $(-eZ/A)$, in the case of dipole vibration approximation the integral cross section for photon absorption is expressed by following well known formula:

$$\int_0^\infty \sigma_{\varepsilon 1}\, dE = \frac{2\pi^2}{mc}\sum_\alpha \varepsilon_\alpha^2 = \frac{2\pi^2}{mc}\left[Z\frac{e^2 N^2}{A^2} + N\frac{e^2 Z^2}{A^2}\right] = 60\frac{NZ}{A} MeV\, mb .$$ (16)

Here we used the summed oscillator strength as following:

$$\sum_f F_{fi} = \frac{NZ}{A} .$$ (17)

The formula (16) will be used in our systematical analysis of the photon absorption integral cross sections.

3.2. The Hydrodynamic Model

Simple collective models, namely hydrodynamic models [14-16], are widely used to explain experimental results of the photonuclear reactions. Migdal [14] first suggested the compressible fluids model for protons and neutrons motion inside of nucleus. This model was developed by Steinwedel, Jensen [15] and Danos [16]. Goldhaber and Teller [17] proposed incompressible fluids model for protons and neutrons.

3.2.1. The Incompressible Fluids Model

According to Goldhaber and Teller's model [17] the protons and neutrons in nucleus assumed as two inter-penetrating incompressible fluids (see Fig. 2).
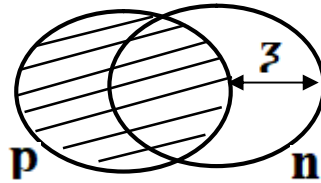
Fig. 2. The dipole vibration of the incompressible protons and neutrons fluids.

For small displacements, $\mathfrak{z} \ll R$ (R is the nuclear radius), of proton and neutron fluids inside nucleus it may be assumed that according to Hooke's law the displacement and force are proportional to each other and the motion is a harmonic. In this case the frequency of the harmonic motion is given by

116

$$\omega_m = \sqrt{\frac{k}{m}}, \tag{18}$$

where k is the coefficient of elasticity, and m is the nucleus mass.

If, it is assumed, that the elastic force is the surface tension, can be then written following relation:

$$k \sim S \sim R^2 \sim A^{-\frac{2}{3}}, \tag{19}$$

where S is the nuclear surface area. On the other hand, the mass of the nucleus is proportional to the volume as:

$$m \sim V \sim R^3 \sim A^{-1}. \tag{20}$$

So, the energy for the harmonic vibration of nucleus can be from (18), (19) and (20) expressed by:

$$E_m = \hbar\omega_m = \hbar\sqrt{\frac{k}{m}} = const A^{-\frac{1}{6}} \text{ MeV}. \tag{21}$$

The constant in (21) can be determined following the Goldhaber and Teller's assumption [17].

Then, the formula (21) can be rewritten in the form [8]:

$$E_m = 45 A^{-\frac{1}{6}} \, MeV \,. \tag{22}$$

3.2.2. *The Compressible Fluids Model*

In the case of the compressible fluids for protons and neutrons the energy at the maximum cross section can be, also, estimated using the formula (18) for harmonic oscillator. If we assume that restoring force is proportional to the distance which a nucleon must cover from one end to the other end of the nucleus:

$$F \sim k \sim R \sim A^{\frac{1}{3}}. \tag{23}$$

Then, by analogy with the incompressible fluids, from (20), (21) and (23) can be estimated E_m as follows:

$$E_m = \hbar\sqrt{\frac{k}{m}} \sim \sqrt{\frac{R}{R^3}} = const A^{-\frac{1}{3}} \, MeV \,. \tag{24}$$

The constant in (24) was found to be different for various approaches and usually used [8, 13] value of ~75:

$$E_m = 75A^{-\frac{1}{3}} \, MeV \, . \tag{25}$$

4. Results of Analysis and Discussion

4.1. The Integrated Absorption Cross Section

The dependence of the integral absorption cross section of photons on the mass number of the target nuclei is shown in Fig. 3.

It is seen from Fig. 3 that the dipole vibration model formula (16) gives good agreement with modern renewed experimental data. It should be noted that some discrepancies between the calculated by (16) values and old experimental data [8, 9] were observed for heavy nuclei (A≳150).
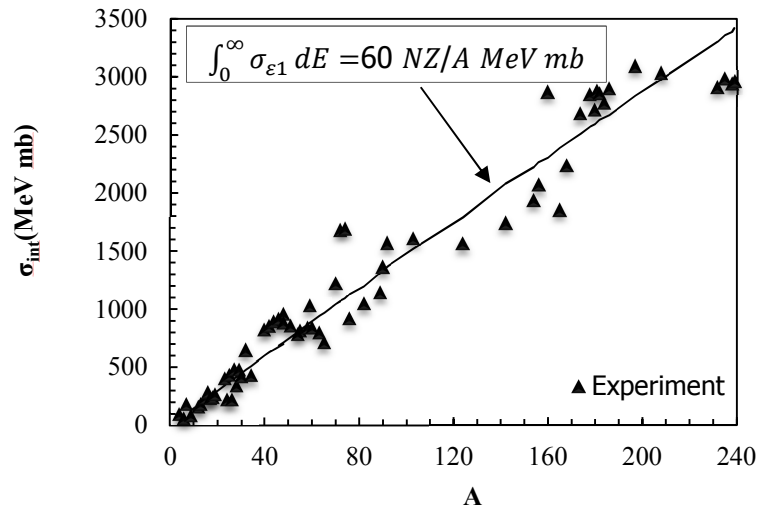
Fig. 3. The dependence of the integral cross section of photons on the mass number of target nuclei.

4.2. The Energy at the Maximum Cross Section

The dependence of photon energy at the maximum cross section on mass number of the target nuclei (see Fig. 4) shows that theoretical curve by formula (25) is satisfactorily in agreement with experimental data for heavy nuclei.
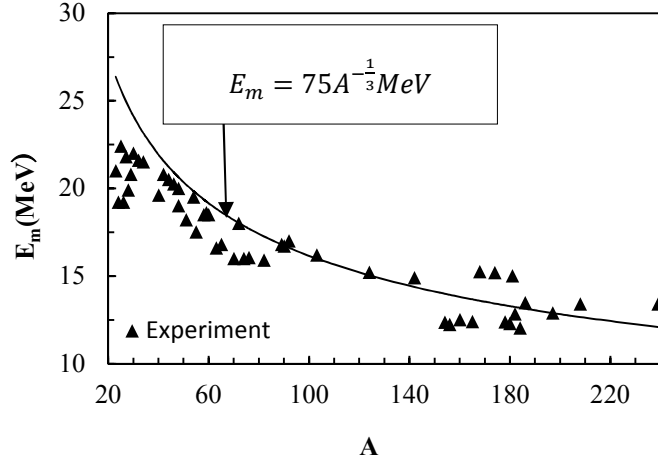
Fig. 4. The dependence of the photon energy at the maximum cross section on mass number of the target nuclei.

The formula (22) for the incompressible fluids gives overestimated values of the photon energy, E_m, at the maximum cross section (Fig. 5). At the same time, the coefficient in formula (22) was found to be 34.88 by fitting of theoretical curve to experimental data. It is seen from here that satisfactory agreement between the theoretical and experimental values was obtained for light and medium mass target nuclei. But, for heavy nuclei conspicuous discrepancy of the theoretical curve with experimental data was observed.

Thus, it can be concluded that the formula (25) gives acceptable results for heavy target nuclei and the formula (22) describes satisfactorily the dependence of E_m on the mass number A for light and medium mass nuclei.

These facts give the idea to assume that the photonuclear reaction is perhaps described by the hybrid model of the compressible and incompressible fluids. Using this hypothesis, Berman and Fultz [11] suggested the following formula for E_m:

$$E_m = 31.2A^{-\frac{1}{3}} + 20.6A^{-\frac{1}{6}} MeV \tag{26}$$

Results calculated by formula (26) are in good agreement with the experimental data (Fig. 6).
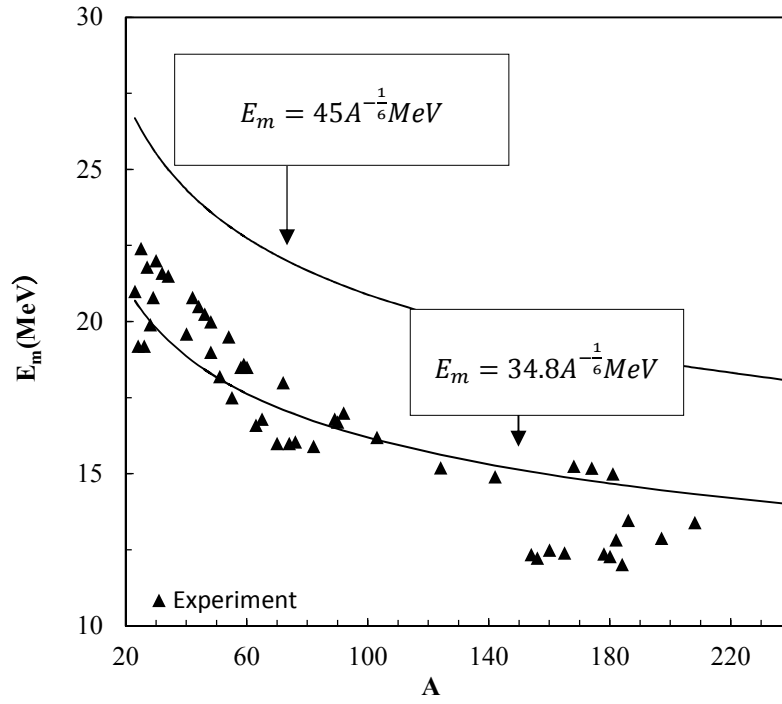
Fig. 5. The same as in Fig. 4 for incompressible fluids.
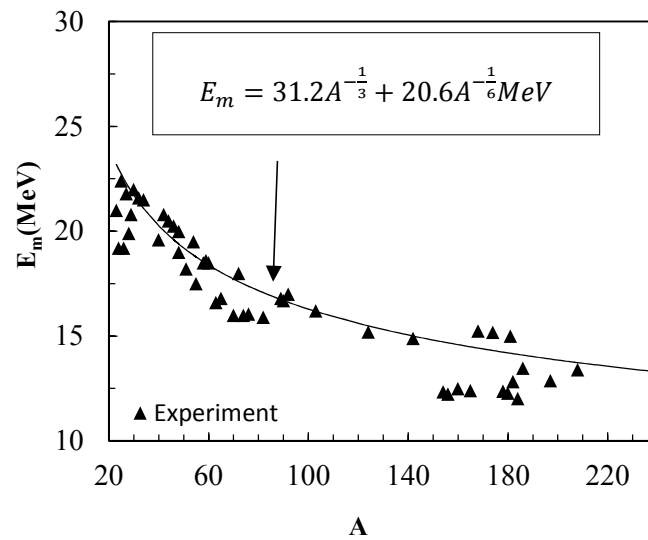
Fig. 6. The same as in Fig. 4 for the hybrid model of the compressible and incompressible fluids.

5. Conclusions

1. The formula for the photon absorption integral cross section was derived using the dipole vibration approximation. It was shown that the formula describes satisfactorily the renewed contemporary experimental data for the photon absorption integral cross section.

2. In the framework of the hydrodynamic model, the formulae for the photon energy at the maximum cross section for compressible and incompressible fluids were deduced. It was shown that the incompressible fluid model formula gives acceptable results for heavy target nuclei and at the same time calculated values by the compressible fluid model formula are in agreement with experimental data for light and medium mass nuclei, only.

3. It can be concluded that results calculated by formula using the hybrid model of the compressible and incompressible fluids were in conformity with the contemporary experimental data for the photon energy at the maximum cross sections.

References

[1] J. Chadwick, M. Goldhaber, Nature, v.134, 1934, p.237

[2] https://www-nds.iaea.org/exfor/exfor.htm

[3] J. Heidmann, H.A.Bethe, Phys. Rev., v.84, 1951, p.274

[4] E.V. Weinstock, J. Halpern, Phys. Rev., v.94, 1954, p.1651

[5] J. Goldemberg, J. Leite Lopes, Phys. Rev., v.99, 1955, p.1053

[6] R. Nathans, J. Halpern, Phys. Rev., v.93, 1954, 437

[7] R. Nathans, J. Halpern, Phys. Rev., v.92, 1953, p.207

[8] Б.С. Ишханов, И.М. Капитонов, Взаймодействие электромагнитного излучения с атомными ядрами. изд. МГУ, 1979, Москва

[9] nuclphys.sinp.msu.ru/el/lec/

[10] Ch. Selebade, H.P. Weise, G.J. Lutz, Photon Activation Analysis, Walter de Gruyter, Berlin. New York, 1988

[11] B.L.Berman, S.C.Fultz, Rev.Mod.Phys., v.47 , 1975, p.713

[12] J.S.Levinger, H.A.Bethe, Phys. Rev., v.78, 1950, p.115

[13] J.S.Levinger, Nuclear Photo-Disintegration, Oxford University Press, 1960

[14] A.B. Migdal, JETF., v.15, 1945, p.81

[15] J.H.D. Jensen, H. Steinwedel, Zs.Naturforsch., 5a, 1950, p.413

[16] M. Danos, Nucl.Phys., v.5, 1958, p.23

[17] M. Goldhaber, E.Teller, Phys. Rev., v.74, 1948, p.1046

List of Participants

	№	Title, Name	Affiliation	Email
	1	Prof. Masayuki AIKAWA	Professor, Faculty of Science, Hokkaido University, Japan	aikawa@sci.hokudai.ac.jp
	2	Ms Duisenbay AKNUR	Department of Theoretical and Nuclear Physics, Al-Farabi Kazakh National University, Kazakhstan	aknurka_93@mail.ru
	3	Ms Battur BATCHIMEG	Junior researcher, Nuclear Data Division, Nuclear Research Center, NUM, Mongolia	babu.tr4@gmail.com
	4	Dr. Damba BAATARKHUU	Senior researcher, Nuclear Data Division, Nuclear Research Center, NUM, Mongolia	ddd.baatarkhuu@gmail.com
	5	Prof. Suren DAVAA	Senior Officer, Nuclear Energy Commission, Mongolia	ts.suren.davaa@gmail.com
	6	Dr. Vidya DEVI	Institute of Engineering and Technology, Bhaddal, District Ropar, Punjab India	vidyathakur@yahoo.co.in

	7	Ms Dashdondog DOLZODMAA	Student, School of Engineering and Applied Sciences, NUM, Mongolia	dolzodmaa1004@yahoo.com
	8	Dr. Tsedenbalkir ENKHBAT	Director, Nuclear Research Center, NUM, Mongolia	enkhbat@gmail.com
	9	Dr. Dagvadorj ICHINKHORLOO	Research fellow, Nuclear Reaction Data Center, Hokkaido University, Japan	ichinkhorloo@nucl.sci.hokudai.ac.jp
	10	Dr. Yongli JIN	China Nuclear Data Center, China Institute of Atomic Energy, China	jyl@ciae.ac.cn
	11	Prof. Gonchigdorj KHUUKHENKHUU	Head, Nuclear Data Division, Nuclear Research Center, NUM, Mongolia	g_khuukhenkhuu@yahoo.com
	12	Prof. Masaaki KIMURA	Head, Nuclear Reaction Data Centre and Nuclear Theory Laboratory, Faculty of Science, Hokkaido University, Japan	masaaki@nucl.sci.hokudai.ac.jp

	13	Dr. Naohiko OTSUKA	Nuclear Data Section, IAEA, Austria	n.otsuka@iaea.org
	14	Dr. Myagmarjav ODSUREN	Associate Professor, School of Engineering and Applied Sciences, NUM, Mongolia	odsuren@seas.num.edu.mn
	15	Ms Batsukh REGZEDMAA	Student, School of Engineering and Applied Sciences, NUM, Mongolia	regzedmaa4411@gmail.com
	16	Mr Chinzorig SAIKHANBAYAR	Researcher, Nuclear Data Division, Nuclear Research Center, NUM, Mongolia	saikhanaa.ok@gmail.com
	17	Dr. Xi TAO	China Nuclear Data Center, China Institute of Atomic Energy, China	taoxixishi@ciae.ac.cn taoxixishi@163.com
	18	Mr Unenbat UNDRAKH	Junior Researcher, Nuclear Data Division, Nuclear Research Center, NUM, Mongolia	undrakh_1202@yahoo.com
	19	Dr. Kurmangaliyeva VENERA	Department of Theoretical and Nuclear Physics, Al-Farabi Kazakh National University, Kazakhstan	venera_93@gmail.com

	20	Dr. Jimin WANG	China Nuclear Data Center, China Institute of Atomic Energy, China	jmwang@ciae.ac.cn
	21	Dr. Sung-Chul YANG	Korea Atomic Energy Research Institute, Republic of Korea	scyang@kaeri.re.kr
	22	Dr. Timur ZHOLDYBAYEV	The Institute of Nuclear Physics, Kazakhstan	zholdybayev@inp.kz
	23	Mr Tsoodol ZOLBADRAL	Researcher, Nuclear Data Division, Nuclear Research Center, NUM, Mongolia	ts.zolbadral@yahoo.com